Higgs Boson Production in Standard Model Effective Field Theory

---

Dissertation

zur

Erlangung der naturwissenschaftlichen Doktorwürde
(Dr. sc. nat.)

vorgelegt der

Mathematisch-naturwissenschaftlichen Fakultät

der

Universität Zürich

von

Agnieszka Janina Ilnicka

aus

Polen

Promotionskommission

Prof. Dr Massimiliano Grazzini (Vorsitz und Leitung der Dissertation)
PD Dr Michael Spira (Leitung der Dissertation)
Prof. Dr Günther Dissertori
Prof. Dr Thomas Gehrmann

Zürich, 2018

Abstract

The first Run of the LHC led to the discovery of the long-sought Higgs boson, the last missing ingredient in the Standard Model (SM) description of fundamental particles and their interactions. The second LHC Run has allowed first studies of the Higgs boson properties, but no evidence for new particles or dynamics has been reported so far. In the case in which new physics is not directly accessible at the LHC, precise measurements can be the only way to access new physics via small deviations from the SM predictions. The Standard Model Effective Field Theory (SMEFT) offers a consistent approach to quantify such deviations, by introducing new higher dimension operators built of the Standard Model fields. In this thesis we apply this approach to the case of Higgs boson production through gluon fusion and its transverse momentum (p_T) spectrum. We consider the SM Lagrangian with four additional dimension-six operators corresponding to modifications of the top and bottom Yukawa couplings, a point-like Higgs coupling to gluons and a chromomagnetic operator. We present the first analytic computation of the Higgs p_T spectrum including the effect of these dimension-six operators. We implement our results into a numerical program that computes the transverse momentum spectrum of the Higgs boson. The effect of the modifications of the top and bottom Yukawa couplings and of the point-like Higgs coupling to gluons is studied including the resummation of the large logarithmic contributions appearing at small-p_T, thereby providing a uniform prediction of the p_T spectrum from the low-p_T to the high-p_T region. The effect of the chromomagnetic operator is finally investigated. We find that the effective operators, while affecting the total rate within the current uncertainties, may lead to significant distortions in the spectrum. The proper parametrisation and modelling of such effects is increasingly important for experimental analyses in Run 2 of the LHC and beyond.

Zusammenfassung

Der erste Run des LHCs führte zur Entdeckung des lang ersehnten Higgsbosons, dem letzten fehlenden Baustein der Standard-Modell-Beschreibung (SM-Beschreibung) der elementaren Teilchen und Wechselwirkungen. Der zweite LHC-Run erlaubte die ersten Studien der Eigenschaften des Higgsbosons, aber bisher wurde kein Hinweis auf neue Teilchen oder Dynamiken gefunden. Im Fall, dass neue Physik nicht direkt am LHC zugänglich sein sollte, können Präzisionsmessungen der einzige Weg sein, neue Physik in Form von kleinen Abweichungen von den SM-Vorhersagen zu detektieren. Die SM-effektive-Feldtheorie (SMEFT) bietet einen konsistenten Zugang zur Quantifizierung derartiger Abweichungen an, indem neue höher-dimensionale Operatoren eingeführt werden, die aus den Feldern des SMs zusammengesetzt sind. In dieser Arbeit wenden wir diesen Zugang auf die Higgsboson-Produktion über die Gluonfusion und sein Transversalimpuls-Spektrum (p_T-Spektrum) an. Wir betrachten die SM-Lagrangedichte mit vier zusätzlichen Dimension-sechs-Operatoren, die Modifikationen der Top- und Bottom-Yukawakopplungen, eine punktförmige Higgskopplung an Gluonen und einen chromomagnetischen Operator einführen. Wir präsentieren die erste analytische Berechnung des Higgs-p_T-Spektrums unter Einschluß der Effekte dieser Dimension-sechs-Operatoren. Wir implementieren unsere Ergebnisse in einem numerischen Programm, das das p_T-Spektrum des Higgsbosons berechnet. Der Effekt der Modifikationen der Top- und Bottom-Yukawakopplungen und der punktförmigen Higgskopplung an Gluonen wird untersucht unter Berücksichtigung der Resummation großer Logarithmen, die bei kleinen p_T-Werten auftauchen, so dass eine einheitliche Beschreibung des p_T-Spektrums von der Niedrig- bis zur Hoch-p_T-Region erzielt wird. Schliesslich wird der Effekt des chromomagnetischen Operators untersucht. Wir finden, dass der effektive Operator zu signifikanten Verzerrungen des Spektrums führen kann, wobei die totale Rate nur innerhalb der gegenwärtigen Unsicherheiten variiert wird. Die korrekte Parametrisierung und Modellierung dieser Effekte wird zunehmend wichtig sein für die experimentellen Analysen im Run 2 des LHCs und jenseits.

Contents

1 Introduction **11**

2 Standard Model Effective Field Theory (SMEFT) **17**

2.1 Prelude: Standard Model 17

2.2 The quest for a theory of Standard Model deviations 20

2.3 Generalities on Effective Field Theories 23

2.4 The Top-Down approach 26

2.5 The Bottom-Up approach 26

3 Higgs boson production at the LHC **39**

3.1 Generalities on the calculations for hadron colliders 39

3.2 Higgs boson production in the SM 41

3.3 Higgs boson production in the SMEFT 49

4 Higgs boson production via gluon fusion in the SMEFT – analytical results **51**

4.1 The Lagrangian and Feynman rules 51

4.2 Higgs production via gluon fusion 54

4.3 Higgs plus jet production 56

5 Higgs boson transverse momentum spectra in the SMEFT – numerical results **67**

5.1 Higgs Transverse-Momentum Spectra at NLL+NLO 67
5.2 Approximation at NNLL+NNLO 76
5.3 Effects of the chromomagnetic operator at high p_T 78

6 Conclusions and Outlook **81**

Bibliography **105**

Preface

This thesis summarises the research conducted at the University of Zürich, Paul Scherrer Institute and ETH Zürich between September 2014 and March 2018, and is based mostly on the already published papers. In particular the description of the Standard Model Effective Field Theory in the context of Higgs properties measurements in Chapter 2 is based on:

[1] M. Boggia, J. M. Cruz-Martinez, H. Frellesvig, N. Glover, R. Gomez-Ambrosio, G. Gonella, Y. Haddad, A. Ilnicka, S. Jones, Z. Kassabov, F. Krauss, T. Megy, D. Melini, D. Napoletano, G. Passarino, S. Patel, M. Rodriguez-Vazquez, T. Wolf
The HiggsTools Handbook: Concepts and observables for deciphering the Nature of the Higgs Sector
to appear in J. Phys. G, arXiv: 1711.09875

The inclusion of the dimension six operators into the Higgs p_T spectra described in the Chapters 4 and 5 is based on:

[2] M. Grazzini, A. Ilnicka, M. Spira, M. Wiesemann
Modeling BSM effects on the Higgs transverse-momentum spectrum in an EFT approach
JHEP 1703 (2017) 115, arXiv: 1612.00283

[3] M. Grazzini, A. Ilnicka, M. Spira, M. Wiesemann
Effective Field Theory for Higgs properties parametrisation: the transverse momentum spectrum case
Moriond QCD proceedings 2017, arXiv: 1705.05143

[4] M. Grazzini, A. Ilnicka, M. Spira
Higgs boson production at large transverse momentum within SMEFT: analytic results
to appear

Finally, I also worked on the Inert Doublet extension of the SM, during my time in Zürich, which is not a part of this thesis, and which was the basis for the IDM benchmarks provided to the Yellow Report 4:

[5] A. Ilnicka, M. Krawczyk, T. Robens
Inert Doublet Model in light of LHC Run I and astrophysical data
Phys.Rev.D93 (2016) no.5, 055026, arXiv: 1508.01671

[6] de Florian, D *et al.*
Handbook of LHC Higgs Cross Sections: 4. Deciphering the Nature of the Higgs Sector
arXiv: 1610.07922

1

Introduction

The *Standard Model* of particle physics (SM) is the basis of our understanding of the fundamental particles and their interactions. It is a quantum field theory, based on the $SU(3)_C \times SU(2)_L \times U(1)_Y$ gauge symmetry, with fermion fields describing the matter content of the Universe and the gauge bosons describing their interactions. The gauge group can be separated into the strong interaction sector governed by the $SU(3)_C$ symmetry, which describes the interaction of quark and gluons through quantum chromodynamics (QCD), and the $SU(2)_L \times U(1)_Y$ sector describing electroweak (EW) interactions. The weak interaction carriers—denoted as $W^{\pm}$ and Z bosons—are massive, however the naive inclusion of the mass terms into the SM Lagrangian would break its gauge symmetry. As a solution for this problem the *Higgs mechanism* [7–12] was proposed in the mid-60's. Through this mechanism the gauge bosons acquire mass, in a gauge-invariant way, via the interaction with a scalar field with a non-vanishing vacuum expectation value (*vev*). The same scalar, Higgs, field is also responsible for the fermion mass generation via the Yukawa interactions. The Higgs mechanism preserves the full gauge symmetry and renormalizability of the SM [13, 14]. The Higgs mechanism leads to Electroweak Symmetry breaking (EWSB): the $SU(2)_L \times U(1)_Y$ gauge symmetry is reduced to the $U(1)_Q$ symmetry of electromagnetism. Although the SM theory successfully describes the strong, weak and electromagnetic forces, it completely neglects gravity, since its interaction strength is orders of magnitude smaller that those of the three other forces. The formulation and the understanding of the SM took decades of both theoretical and experimental work, and are still one of the main areas of modern physics research.

Currently, the main window allowing us to look into the world of the fundamental particles and interactions is the Large Hadron Collider (LHC). By colliding protons at a centre-of-mass energy of 13 TeV, the LHC is the most energetic collider ever built. One of the main tasks of particle physics nowadays is the most efficient and thorough exploitation of the LHC. This concerns not only the experimentalists who measure and analyse the signals obtained in the LHC experiments, but also theorists, who are supposed to provide the precise predictions and improved tools to be used in the analyses and interpretation of the measurements. The LHC, already during its first Run, proved to have the capacity not only to discover new particles—the long sought Higgs boson [15, 16]—but also to quite precisely measure their properties [17]. The properties of the 125 GeV resonance suggest that it is compatible with the Higgs boson of the SM. The existence of a Higgs boson is a basic prediction of spontaneous symmetry breaking via a scalar sector as

implemented in the SM [7–12] and its discovery gained its postulators the Nobel Prize in Physics in 2013. This discovery ended also the epoch of searches for the particles predicted in the SM.

Although the SM in now complete, in a sense that all the particles it postulates were experimentally detected, it does not mark the end of particle physics. The SM allows to theoretically predict the particle properties to a great precision, thanks to the perturbative framework. Indeed, although the computation of the relevant observables in quantum field theory cannot be carried out exactly, we are able to evaluate them as a series expansion in the coupling constant. The precise measurements accumulated over the years show full consistency with those SM predictions [18], with just some exceptions in the neutrino sector, and few, $\sim 3\sigma$ deviations in the flavour sector. This makes the SM a very successful and precisely tested theory. However the SM is clearly not a complete theory of the Universe, since it does not account for gravity. Additionally it encounters problems already at lower scales: many cosmological phenomena cannot be described within the SM. The astrophysical observations and simulations, revealed that only a small fraction of matter is described through the SM, the rest being the currently unknown *Dark Matter* [19]. Further astrophysical observations revealed that there is a vast amount of *Dark Energy*, the origin of which is unknown. Also, when considering CP violation in the SM, which leads to different production of particles and antiparticles, it is orders of magnitude too small to explain the current dominance of matter over antimatter [20]. The existence of Dark Matter and Energy and the observed baryon asymmetry are just the most crucial problems which cannot be accommodated within the SM, thus calling for its extension.

Another conceptual problem of the SM, when considering it to be a theory valid up to the Planck scale[1], is the *hierarchy problem*. This follows from the existence of a fundamental scalar in the theory, the Higgs field, which is not protected against the radiative corrections originating from physics at high energy scales. While considering quantum corrections to the self-energy of the scalar particle, unlike in the case of fermions or gauge bosons, terms proportional to the square of the cutoff scale appear. By using the Planck scale as a cutoff it is clear that the measured value of Higgs mass around 125 GeV requires *fine-tuned* cancellation between the bare mass and its quantum corrections, which seems to be *unnatural*. This shortcoming of the SM triggered many Beyond the Standard Model (BSM) investigations. The most popular are *supersymmetry*, which postulates a set of new particles, via the extension of the Poincarè group, which will contribute with opposite sign to the quantum corrections to scalar particles, and *composite Higgs models*, which assume that the Higgs scalar is a composite object of high scale strong dynamics. Both these extensions of the SM—and also many others—have an impact on the scalar sector of the theory, and on the properties of the physical Higgs particle, thereby allowing us to test them experimentally.

With the discovery of the Higgs particle in the first Run of the LHC [15, 16], it leaves more than 20 years of planned LHC activity and 3000 fb^{-1} of planned integrated luminosity [21] to measure its properties with considerable precision. The LHC experiments have also a rich programme of searches for new resonances[2], however there is no guarantee that such new particles are within the LHC reach. This emphasises the relevance of a programme of precise measurements of SM particle properties, and especially of measurements of SM deviations. These deviations may become the

[1]The Planck scale $\Lambda_{Planck} \approx 10^{19}$ GeV is a scale at which quantum effects of the gravitational force should become important.

[2]The results of finished analyses are available on the ATLAS and CMS webpages: `atlas.cern` and `cms.cern`.

long standing legacy of the LHC, contributing to the guideline for building BSM models.

To consistently introduce deviations from the SM Higgs sector, explicit models beyond the SM can be directly studied, however considering their number this seems to be highly inefficient. The ongoing debate on and urge for a model independent framework for the interpretation of the LHC data is reflected by the wide discussions presented recently in Refs. [1, 6]. So far the ATLAS and CMS experiments used the so-called κ-framework [22] for the presentation of their measurements [17]. This framework consists in a simple scaling of measured production cross sections and decay rates compared to the best SM predictions. Although very useful in the early days after a Higgs discovery, the κ-framework suffers from limitations, such as entanglement of experimental and theoretical uncertainties or lack of a clear way to extend it beyond the leading order, which call for its extension.

One of the drawbacks of the κ-framework is that it introduces New Physics effects through a naive rescaling of the terms which are already present in the Lagrangian. Moreover, it was primarily built at the level of total rates, and cannot—without further assumptions— account for SM deviations in the kinematical distributions of a Higgs boson. However the kinematic distributions—with the Higgs transverse-momentum (p_T) distribution as one of the most relevant observables—provide an important perspective to study the Higgs boson properties. While the total rate can be very close to the SM value, deviations from the SM in the high-p_T tail can be still large, since the production rate in the high-p_T tail is orders of magnitude smaller than at low p_T. Additionally, high-p_T tails provide a powerful probe to explore much higher energies: $p_T > m_h$. In general, the transverse-momentum spectrum provides more information than the total cross section—since we can study its shape, not only the normalisation—and it allows us to disentangle effects that remain hidden in the total rates. For example, it is the simplest measurement to shed light on the nature of the Higgs coupling to gluons. The fact that the Higgs is a scalar, gives an additional simplification in the modeling of the Higgs p_T-spectrum, due to the factorization of production and decay in the narrow-width approximation.

The LHC experiments reported the first results on the kinematic distributions already with the data accumulated during the Run 1: the ATLAS and CMS collaborations presented the spectra coming from the $\gamma\gamma$, four-leptons (ZZ) and two-leptons two-neutrinos (WW) final states in Refs. [23–26] and Refs. [27–29], respectively. The fully reconstructed decay channels into $\gamma\gamma$ and four-leptons offered a better resolution, and their combined results were reported by ATLAS [25]. In Run 2 these measurements can be extended to a larger range in the transverse momentum with significantly higher statistics and accuracy after accumulating up to $\mathcal{O}(100\ \text{fb}^{-1})$ of luminosity. The first ATLAS papers including data collected at 13 TeV were published recently [30, 31], reporting results for the spectra measured in the four-lepton and diphoton decay channels. The uncertainties of these measurements are still large, usually exceeding the deviations from the SM predictions, but with the data to be accumulated in the future such uncertainties are expected to decrease significantly. Also the use of a boosted analysis would give information about the high-p_T regime of the spectra [32, 33].

The so called *Standard Model Effective Field Theory* (SMEFT) offers a consistent approach to go beyond the κ-framework and to more rigorously quantify deviations from the SM picture. In such an approach the SM Lagrangian is extended by the inclusion of operators of higher dimension (in first approximation dimension six), built from SM fields and suppressed by powers

of the New Physics scale (Λ) [34–37]. This provides a theoretically consistent parametrisation of model-independent effects of high-scale New Physics—which manifest themselves through small deviations from the SM predictions—in a systematic way. The dimension-six operators present in the SMEFT allow various modifications in the Higgs boson interactions, not only a rescaling of those already present in the SM Lagrangian. A significant effort has been recently devoted to supplement the, usually tree-level, tools used in the modelling of LHC data with the effects of appropriate dimension-six SMEFT operators, and it is extensively reviewed in this thesis.

Due to the increasing precision of the LHC measurements, accurate SM predictions are essential to highlight possible deviations from the SM picture and this implies the computation of radiative corrections. This is an area where research is very active, and, for instance, next-to-next-to-next-to leading ($\mathrm{N^3LO}$) corrections in the QCD coupling α_S have been recently obtained for the two main Higgs boson production channels: gluon fusion [38–40] and vector boson fusion [41]. However, the area of perturbative computations within the SMEFT is much less developed, and the precision reached by the LHC experiments will call for theoretical improvements and effects of SMEFT operators beyond leading order [42]. The existence of tools allowing the consistent modelling of Higgs observables in SMEFT is highly relevant, since in this way indirect BSM effects can be directly tested in the experimental analyses.

This is exactly the focus of this thesis. We consider the dominant Higgs boson production channel at the LHC, gluon fusion (GGF) through a heavy-quark loop, and we supplement the corresponding SM predictions with the relevant dimension six operators. The GGF channel accounts for nearly 90% of Higgs particles produced at the LHC, and is also the most important with respect to the kinematic distributions. The dimension-six SMEFT operators which are relevant in this case are: the modification of the heavy-quark Yukawa couplings, a point-like Higgs coupling of the Higgs boson to gluons and a new Higgs-gluon-quark interaction driven by the so called *chromomagnetic* operator. We present the analytical computation of the lowest order Higgs production cross section including the effect of these operators, as well as of the matrix element needed to describe Higgs boson production in association with a hard jet. Additionally, we have implemented the obtained analytical results into a numerical program that computes the transverse momentum spectrum of the Higgs boson by performing a resummation of the large logarithmic terms at small transverse momenta at next-to-leading logarithmic accuracy (NLL). We present predictions which combine the fixed order result valid at large p_T with the low-p_T resummation up to NLL+NLO. Our computation includes the effect of the dimension-six operators modifying the top and bottom Yukawa couplings as well as the point-like Higgs coupling to gluons, on top of the known SM contributions. This allowed us to study the impact of these operators on the whole p_T range. We also obtained approximate NNLL+NNLO SMEFT spectra, using our SMEFT results at NLL+NLO to rescale the state-of-the-art SM predictions at the NNLL+NNLO level. We also studied the impact of the chromomagnetic operator at moderate and high p_T values. Our results show that the effects of the different dimension-six operators manifest themselves in different regions of the spectrum. The framework and the tool we provide here have proved to be of interest in the experimental community. For example, the CMS analysis of the Higgs p_T spectrum obtained from combined $4l$ and 2γ channels [43] aims to set bounds on the Wilson coefficients using the framework presented here.

The thesis is organised as follows. Chapters 2 and 3 provide the theoretical background for the results presented in Chapters 4 and 5. In more details, in Chapter 2 the Standard Model Effective

Field Theory is described as the appropriate tool to account for the SM deviations which will be measured at the LHC. In Chapter 3 the methodology and the recent advances in the calculations of the Higgs cross sections and kinematic distributions at the LHC are discussed. Chapter 4 presents the analytical calculations for the gluon fusion Higgs and Higgs plus jet production in the SMEFT. In the following Chapter 5, these calculations are used to obtain the transverse momentum spectra of the Higgs particle. In particular in Section 5.1 the spectra including the SMEFT operators at the NLL+NLO precision are presented, and they are approximately extended to the NNLL+NNLO level in Section 5.2. Additionally the effects of the chromomagnetic operator are studied in the high p_T range in Section 5.3. Our conclusions are presented in Chapter 6.

2

Standard Model Effective Field Theory (SMEFT)

2.1 Prelude: Standard Model

Even though this chapter is devoted to the Standard Model Effective Field Theory we start by recalling the classical Standard Model, and will set up the conventions used throughout this thesis. The fields of the Standard Model are:

- **gauge bosons** of the gauge symmetries $SU(3)_C$ – 8 gluons G^a_μ , $SU(2)_L$ – 3 bosons W^i_μ and $U(1)_Y$ – boson B_μ — the latter two mix into the physical $W^\pm$ and Z vector bosons and photon A due to the spontaneous symmetry breaking (SSB) of the Higgs potential.

- **quarks** – fermions being triplets of $SU(3)_C$. The left-handed components form a doublet of $SU(2)_L$: $q_L = \begin{pmatrix} u_L \\ d_L \end{pmatrix}$ and right-handed component are singlets of $SU(2)_L$: $u_R,\ d_R$. The electric charge equals $^2/_3$ and $-^1/_3$ for u and d respectively. There exist three families of these fields: $\{u, d\},\ \{c, s\},\ \{t, b\}$.

- **leptons** – fermions being singlets of $SU(3)_C$. The left-handed components form again a doublet of $SU(2)_L$: $l_L = \begin{pmatrix} \nu_L \\ e_L \end{pmatrix}$ and there is just one right-handed components corresponding to the charged lepton: e_R. The ν is electrically neutral, and e carries charge -1. The lepton also come in three families: $\{\nu_e, e\},\ \{\nu_\mu, \mu\},\ \{\nu_\tau, \tau\}$.

- **Higgs field** – scalar complex doublet of $SU(2)_L$ and singlet of $SU(3)_C$, after SSB acquiring the nonzero *vev*: $H(=\varphi) = \begin{pmatrix} \phi^+ \\ \frac{v+i\phi^0+h}{\sqrt{2}} \end{pmatrix} \overset{\text{unitary gauge}}{\longrightarrow} \frac{1}{\sqrt{2}} \begin{pmatrix} 0 \\ v+h \end{pmatrix}$, where the physical particle h is a neutral scalar.

The SM Lagrangian can be briefly written as:

$$\mathcal{L}_{\text{SM}} = \mathcal{L}_{\text{kin. gauge}} + \mathcal{L}_{\text{kin. fermions}} + \mathcal{L}_{\text{Higgs}} + \mathcal{L}_{\text{Yukawa}}. \tag{2.1}$$

The kinetic term of the gauge bosons reads:

$$\mathcal{L}_{\text{kin. gauge}} = -\sum_{V=G,W,B} \frac{1}{4} V^{\alpha,\mu\nu} V^{\alpha}_{\mu\nu}, \tag{2.2}$$

where the field strengths are defined as $V^{\alpha}_{\mu\nu} = \frac{1}{ig_V}\text{Tr}[D^V_\mu, D^V_\nu] = \partial_\mu V^\alpha_\nu - \partial_\nu V^\alpha_\mu - g_V f_V^{\alpha\beta\delta} V^\beta_\mu V^\delta_\nu$ with D^V_μ, $f_V^{\alpha\beta\delta}$ and g_V being the appropriate covariant derivatives, structure and coupling constants: g_S for $SU(3)_C$, g for $SU(2)_L$ and g' for $U(1)_Y$. The generic kinetic term of the fermions reads:

$$\mathcal{L}_{\text{kin. fermions}} = \sum_{f=l_L,q_L,u_R,d_R,e_R} i\bar{f}\not{D} f, \tag{2.3}$$

where the covariant derivative $D_\mu = \partial_\mu + i\sum_V g_V V_\mu$ with $V_\mu = T^a V^a_\mu$ depends on the $SU(3)_C \times SU(2)_L \times U(1)_Y$ representation of the fermion fields, which is displayed in Table 2.1. We write explicitly just the most complicated case of the quark doublet:

$$\bar{q}_L \not{D} q_L = \bar{q}_L \gamma^\mu (\partial_\mu + i g_S \frac{\lambda^a}{2} G^a_\mu + i g \frac{\sigma^j}{2} W^j_\mu + i g' \frac{1}{6} B_\mu) q_L, \tag{2.4}$$

where λ^a and σ^j are the Gell-Mann and Pauli matrices, respectively.

Field	$SU(3)_C$	$SU(2)_L$	$U(1)_Y$
H	1	2	$1/2$
l_L	1	2	$-1/2$
e_R	1	1	-1
q_L	3	2	$1/6$
u_R	3	1	$2/3$
d_R	3	1	$-1/3$

Table 2.1: The gauge representations for the SM fields. A singlet is denoted by 1, a doublet by 2 etc.[1]

Finally we move to the parts of the SM Lagrangian involving the Higgs field and we briefly sketch the generation of masses of gauge bosons and fermions via the SSB. The Higgs part of the Lagrangian reads:

$$\mathcal{L}_{\text{Higgs}} = |D_\mu H|^2 - V(|H|^2) = |D_\mu H|^2 + \mu_H^2 |H|^2 - \lambda |H|^4, \tag{2.5}$$

[1] In the convention used here we have $Q = I_3 + Y$, where Q is a particle's electric charge, I_3 is a third component of isospin and Y is a hypercharge.

and the Higgs potential $V(|H|^2)$ develops the non-vanishing minimum at $\langle H\rangle = \frac{1}{\sqrt{2}}\begin{pmatrix} 0 \\ v \end{pmatrix}$ where $v^2 = \frac{\mu_H^2}{\lambda}$. We will continue the discussion of the other terms using the unitary gauge for simplicity, in which $H = \frac{1}{\sqrt{2}}\begin{pmatrix} 0 \\ v+h \end{pmatrix}$. First, we notice that the Higgs potential written in the unitary gauge has the form:

$$V(h) = \frac{m_h^2}{2}h^2 + \lambda v h^3 + \frac{\lambda}{4}h^4 - \frac{\lambda v^4}{4}, \tag{2.6}$$

where the physical Higgs particle mass is $m_h = 2\mu_H^2 = 2\lambda v^2$ and the trilinear and quartic couplings of the Higgs particle appear. Next, we expand explicitly the kinetic term of the Higgs field:

$$D_\mu H = (\partial_\mu - ig\frac{\sigma^j}{2}W_\mu^j - ig'\frac{1}{2}B_\mu)H \overset{\text{only } vev}{=} \frac{-i}{2\sqrt{2}}\begin{pmatrix} gW_\mu^3 + g'B_\mu & \sqrt{2}W_\mu^+ \\ \sqrt{2}W_\mu^- & -gW_\mu^3 + g'B_\mu \end{pmatrix}\begin{pmatrix} 0 \\ v \end{pmatrix}, \tag{2.7}$$

where $W_\mu^\pm = \frac{1}{\sqrt{2}}(W_\mu^1 \mp iW_\mu^2)$. Then squaring this term we obtain:

$$|D_\mu H|^2 \to \frac{1}{4}g^2v^2W_\mu^-W^{+\mu} + \frac{v^2}{8}(-gW_\mu^3 + g'B_\mu)^2, \tag{2.8}$$

from where we can read off the mass of the $W^\pm$ vector bosons $m_W = \frac{1}{2}gv$, but the term involving W_μ^3 and B_μ requires a rotation into the mass eigenstates:

$$\begin{pmatrix} A_\mu \\ Z_\mu \end{pmatrix} = \begin{pmatrix} \cos(\theta_W) & \sin(\theta_W) \\ -\sin(\theta_W) & \cos(\theta_W) \end{pmatrix}\begin{pmatrix} B_\mu \\ W_\mu^3 \end{pmatrix}, \tag{2.9}$$

where $\cos(\theta_W) = \frac{g}{\sqrt{g^2+g'^2}}$ and $\sin(\theta_W) = \frac{g'}{\sqrt{g^2+g'^2}}$. Rewriting Eq. (2.8) in terms of the rotated fields A_μ and Z_μ we find that the former stays massless and the latter acquires a mass $m_Z = \frac{1}{2}\sqrt{g^2+g'^2}\,v$. From this we infer that the gauge symmetry $SU(2)_L \times U(1)_Y$ of 3+1 massless gauge bosons was broken into the $U(1)_Q$ of a massless photon responsible for the electromagnetic interactions. Let us note also that three degrees of freedom of the Higgs doublet field are absorbed as the longitudinal polarisations of the weak vector bosons[2] leaving h as a leftover physical particle.

Finally we address the Yukawa terms of the interaction between the fermions and the Higgs field:

$$\mathcal{L}_{\text{Yukawa}} = -Y^{ij}\bar{f}^i{}_L H f_R^j + h.c. = -Y_u^{ij}\bar{q}^i{}_L H^c u_R^j - Y_d^{ij}\bar{q}^i{}_L H d_R^j - Y_e^{ij}\bar{l}^i{}_L H e_R^j + h.c., \tag{2.10}$$

where Y^{ij} are in general Yukawa matrices in flavour space and $H^c = i\sigma^2 H^*$. When considering the unitary gauge we get mass matrices of the form:

$$M_X^{ij} = Y_X^{ij}\frac{v}{\sqrt{2}}, \tag{2.11}$$

which however are not diagonal in general, and to diagonalise them we need two hermitian matrices (for every Y_X^{ij}) $m_X = U_X M_X V_X^\dagger$ where $m_X^i = \text{diag}(m_{X_1}, m_{X_2}, m_{X_3})$ for $X = e, d, u$. The unitary

[2]Massless vector bosons have two polarisations while massive have three.

matrices U_X and V_X are also used to rotate the fermions into mass eigenstates (which we show on the example of electrons): ${e'}^i_L = U_e^{ij} e^j_L$ and ${e'}^i_R = V_e^{ij} e^j_R$. Then the diagonalisation leads to:

$$\bar{e}^i_L M_e^{ij} e^j_R = \bar{{e'}}^i_L (U M_e V^\dagger)^{ij} {e'}^j_R = \bar{{e'}}^i_L (U_e U_e^\dagger m_e V_e V_e^\dagger)^{ij} {e'}^j_R = \bar{{e'}}^i_L m_e^i {e'}^i_R. \tag{2.12}$$

The shift between the gauge and mass eigenstates also causes the appearance of the flavour non-diagonal interactions for the quarks in the weak sector[3] governed by the CKM matrix: $V_{CKM} = U_u U_d^\dagger$.

2.2 The quest for a theory of Standard Model deviations

One of the main goals of the LHC was the search for the Higgs boson, which in the Standard Model is a signature of the Electroweak Symmetry Breaking (EWSB) [7–12]. Although the mass of the Higgs boson is a free parameter of the Model, many of its properties are strictly defined as a consequence of the EWSB, i.e. the couplings to fermions and EW bosons should be proportional to their masses or squared masses, respectively. With the discovery of the scalar resonance by CMS and ATLAS in 2012 the paradigm has changed from the discovery phase to the property measurement phase. For the property measurements some common framework needed to be established, and in the first instance the so-called κ *framework* was used [22].

2.2.1 The κ-framework

As an interlude, we recall here the definition and the assumptions lying behind the κ-framework, as proposed in Ref. [22] to parameterise small deviations from the predicted SM Higgs boson couplings and widths (for a recent review see also Ref. [44]). The basic assumptions are:

- The signals observed in the different search channels originate from a single narrow resonance with a mass near 125 GeV.
- The *zero-width approximation* is used, meaning that the total width of the resonance is narrow enough to be negligible with respect to the mass ($\Gamma_h \ll m_h$). In this case, the signal cross section can be decomposed (for all $i \to h \to f$ channels) as

$$\sigma_i \cdot \mathrm{BR}^f = \frac{\sigma_i \cdot \Gamma_f}{\Gamma_h}\,, \tag{2.13}$$

  where σ_i is the production cross section for $i \to h$ with $i = (gg\mathrm{F}, \mathrm{VBF}, Wh, Zh, t\bar{t}h)$ and BR^f is the decay *branching ratio* for $h \to f$ with $f = (ZZ, WW, \gamma\gamma, \tau\tau, bb, \mu\mu)$. Γ_f and Γ_h are the partial and total decay widths of the Higgs boson, respectively.
- For the simplification of the framework the tensor structure of the couplings is assumed to be the same as in the SM predictions, only modifications of coupling strengths are taken into account. This implies that the observed state is assumed to be a CP-even scalar.

[3] They do not appear for the leptons due to the lack of the right-handed neutrinos.

The couplings cannot be directly measured by the experiments and events collected in the detector undergo an unfolding procedure to extract the information from some measurable observable(s). Typically, the measured observable is $\sigma \times \mathrm{BR}$, which is defined within a certain acceptance and with some specific experimental cuts, and this leads to some model dependence. Obviously, it is not possible to fit the experimental data within the context of the SM while treating Higgs couplings as free parameters. Once the value of the Higgs boson mass is specified, the couplings are specified as well. For this reason, it is only possible to test the overall compatibility of the SM with the data. This kind of study can be used to extract or constrain deviations in the measured couplings with respect to the SM ones.

The framework is built in such a way that the predicted SM Higgs cross sections and partial decay widths are dressed with scaling factors κ_j. The cross section σ_i and the partial decay width Γ_f scale with κ_i^2, κ_f^2 when compared to SM predictions.

$$\sigma_i \cdot \mathrm{BR}^f = (\sigma_i \cdot \mathrm{BR}^f)_{\mathrm{SM}} \cdot \frac{\kappa_i^2 \cdot \kappa_f^2}{\kappa_h^2} \,. \tag{2.14}$$

In the SM, all the κ_i are unity by definition and therefore, the best available (i.e. highest possible perturbative order) predictions are recovered. However, when $\kappa_i \neq 1$ higher-order accuracy is in general lost as the factorisation of Eq. (2.14) does not necessarily hold beyond LO.

The κ are sometimes confused with the actual couplings in the Lagrangian. They are the same at tree level, but not the same once radiative corrections are taken into account. As an example we consider the process $gg \to t\bar{t}h(bb)$. At tree level one can say that the squared matrix elements are proportional to the coupling of the interactions:

$$|\mathcal{M}|^2 \propto (c_t c_b)^2 \,, \tag{2.15}$$

where c_i are modifiers of the Yukawa couplings, and then, the total width of the Higgs boson will change due to the modification of couplings: $\Gamma_h \equiv \kappa_h(c_t, c_b)\Gamma_h^{\mathrm{SM}}$, and one would have $\kappa_i = c_t$ and $\kappa_f = c_b$. At higher orders this formula does not hold, as new terms proportional to QCD or EW coupling constants will appear.

Another quantity that can be expressed in this framework and is a common experimental observable, is the *signal strength* μ. Consider a specific process $i \to h \to f$. For the production $(i \to h)$ the signal strength μ is defined as

$$\mu_i = \frac{\sigma_i}{\sigma_{i\mathrm{SM}}} \,, \tag{2.16}$$

whereas, for the decay $(h \to f)$ we have

$$\mu_f = \frac{\mathrm{BR}^f}{\mathrm{BR}^f_{\mathrm{SM}}} \,. \tag{2.17}$$

By definition, in the SM $\mu_i = 1$ and $\mu_f = 1$. The only object that can be measured experimentally is the product of μ_i and μ_f, since it is not possible to separate them without further assumptions. In terms of the κ-framework we obtain the following expression:

$$\mu \equiv \mu_i \mu_f \equiv \frac{\kappa_i^2 \kappa_f^2}{\kappa_h^2} \,. \tag{2.18}$$

Different production processes and decay modes probe different coupling modifiers. Together with the individual modifiers related to the coupling of the Higgs boson to different particles, two *effective* modifiers need to be introduced to describe loop induced processes: the modifier κ_g to describe the GGF production process and κ_γ for the $h \to \gamma\gamma$ decay. This is possible since it is expected that other BSM particles which might be present in the loop do not change the kinematics of the process to first approximation. The study of these processes can therefore be approached by either using effective coupling modifiers, which provide sensitivity to the presence of BSM particles in the loops, or using *resolved* coupling modifiers corresponding to the SM particles, e.g. $\kappa_g^2 = 1.06 \cdot \kappa_t^2 + 0.01 \cdot \kappa_b^2 - 0.07 \cdot \kappa_t \kappa_b$.

This framework, although very useful for the early CMS and ATLAS results [17], comes with shortcomings [1], from which the most severe ones are:

- deep entanglement of experimental and theoretical uncertainties and lack of an easy way to update them with eg. new theoretical calculations
- usability only in the case of total rates with no clear way to extend it to the description of distributions
- lack of a well defined procedure of calculating the κs at NLO, and how to proceed with the κs coming from the loop-induced couplings in the SM.

This suggests that with a larger data sample, which allows more precise measurements, a general update of the framework is needed.

2.2.2 Beyond the κ-framework

The urge of extending the κ-framework and in general the program of the non-resonant, mostly model-independent searches for New Physics in the LHC has resulted in new concepts proposed in the 4th Yellow Report of Higgs Cross Section Working Group [6] and discussed also in Ref. [1]. These are (starting from the *closest* to the experimental viewpoint):

- **Fiducial Cross Sections** [45] are differential cross sections as measured in the fiducial volume of the experiments. They are the most model independent measurements, however they come with a number of limitations, e.g.: an impossibility to combine measurements from the different experiments, a problematic interpretation within the BSM models (needed Monte Carlo allowing to apply many cuts), a prohibition of use of the modern experimental analysis techniques (multi variate analysis, boosted decision trees).
- **Simplified Template Cross Sections (STXS)** [6] (Section III.2) aim on the categorisation of the Higgs events based on the production mode into simplified fiducial volumes, and then on smaller subcategories based on some kinematic variables. This allows with a cost of small theory dependence, to use the advanced experimental techniques. Although the dedicated BSM sensitive *bins* are foreseen, still this approach might be problematic for the interpretation for the BSM phenomenologists to test the models against data.

- **Pseudoobservable (PO)** is a concept, based on the multi-pole expansion of the amplitudes, which proved to work well in the LEP analyses [46,47] and was reintroduced for the description of Higgs decays [48] and production [49]. Although this approach seems to be in closer relation with the well defined theoretical quantities, the need of deconvoluting some effects (eg. parton distributions, showers) will lead to some, not necessarily small, model dependence and extra uncertainties.

- **Standard Model / Higgs Effective Field Theory (EFT)** is a well defined theoretical framework to systematically account for the deviations of the SM. This approach is the most motivated from the theoretical side, however in experimental analysis setting bounds on Wilson coefficients[4] would require noticeable theory input.

Most probably the future LHC results will be expressed in terms of one or several of these frameworks, possibly chained. The utility of the frameworks is actually mostly based on the availability of the tools allowing to perform the calculations at the appropriate accuracy. Thus one of the tasks of phenomenologists should be preparing the appropriate tools which can then be embedded in the experimental analysis.

Note that the model-independent search for New Physics via deviations from the SM is complementary to the direct search for new resonances, and those programs are pursued as an independent experimental analysis. Especially in case when no other resonances, but the Higgs boson of 125 GeV, will be found in the LHC, the measured deviations from the SM may become the only and long lasting compass for the BSM model builders and phenomenologists. This emphasises also the need of a well designed framework for their parametrisation, with the option to update it with the theoretical advances without the need to rerun the full experimental analysis.

The Effective Field Theory approach is especially attractive from the theoretical viewpoint due to its well established link to the UV theory via the decoupling of heavy states, as well as the prescription on how to calculate higher order QCD and EW corrections. As additional advantages, there is a clear hierarchy of the importance of effects and a possibility to link different measurements in this framework, not only from the Higgs physics or even the LHC, but also from the whole field of particle physics. This would allow to obtain hopefully more precise combined results, that will result in a better understanding of the underlying theory. In the following chapter these and more features of the EFT are discussed.

2.3 Generalities on Effective Field Theories

Effective Field Theory is a general framework that can be used in cases when two well separated scales occur in the theory. The requirement that the scale separation is *large* is somehow arbitrary, but it has a key meaning when it comes to the validity of the approach. In general a full theory which can benefit from the EFT approach can be written as:

$$\mathcal{L}_{full} = \mathcal{L}_{low}(\varphi) + \mathcal{L}_{high}(\boldsymbol{\phi}) + \mathcal{L}_{int}(\varphi, \boldsymbol{\phi}) \tag{2.19}$$

[4]Wilson coefficients are the parameters of the EFT Lagrangian, described in later parts of this Chapter.

where φ and $\boldsymbol{\phi}$ are light and heavy fields respectively. While we consider processes on the energy scales corresponding to the light fields' masses, it would be more convenient to have a theory where there are no heavy fields, since they cannot be produced. It is possible to omit the heavy fields using the *top-down* EFT approach but due to the $\mathcal{L}_{int}(\varphi, \boldsymbol{\phi})$ term[5] while integrating out the $\boldsymbol{\phi}$ fields new interactions of the φ fields will appear and they will be of a higher mass dimension than four[6], thereby suppressed by powers of the scale $\Lambda \sim M_{\boldsymbol{\phi}}$:

$$\mathcal{L}_{EFT} = \mathcal{L}_{low}(\varphi) + \sum_j \sum_k \frac{c_k^{(j)}}{\Lambda^j} \mathcal{O}_k^{(j)}(\varphi) \tag{2.20}$$

where the sum over j is infinite, but due to the fact that we consider the process at the scale well below $\Lambda \sim M_{\boldsymbol{\phi}}$ the importance of the power suppressed contributions drop with the increase of j. The $\mathcal{O}_k^{(j)}(\varphi)$ are operators built from the light fields, and $c_k^{(j)}$ are the *Wilson coefficients*, which are related to the full model parameters, as described later. Here we see the importance of having the *large* scale separation: without it all the infinite number of terms will be important, and thus will make the theory non-predictive. On the other hand if there is a large scale separation we can limit ourselves to consider just a finite number of operators to get results precise up to $O((\frac{E}{\Lambda})^J)$, where J is the order at which we decided to truncate the expansion[7]. The $\mathcal{L}_{EFT}$ is strictly nonrenormalizable (while the $\mathcal{L}_{full}$ could be), however, it is still possible to renormalise the operators at a given order j.

Looking at the effective Lagrangian in Eq. (2.20) we can conclude that it can actually be written down without any knowledge about the $\boldsymbol{\phi}$ fields. This is the basis of the *bottom-up* EFT approach in which we start from a well established low energy theory working at the energy scale we can probe at present experiments and augment it with the operators build up from the available fields, obeying the gauge and Lorentz symmetries. Again, the suppression of operators with higher and higher mass dimension by some high mass scale results in a hierarchy of importance of operators, and thus we can truncate them at a desired order. This approach is *effective* in the sense that it can be used to describe phenomena about which we have no intrinsic knowledge, but we want to parametrise this ignorance systematically. A priori we do not know what are the values of the Wilson coefficients, but they can be determined from experimental measurements. This approach adds some flexibility to the model, and thus is a framework to parametrise the deviations from the low energy model encoded in $\mathcal{L}_{low}(\varphi)$.

A very successful application of the EFT in particle physics is Fermi theory, and it is a good example to show the complementarity of top-down and bottom-up approaches. The Fermi theory was proposed as an effective theory allowing to describe the radioactive β decay: $n \to p + e + \bar{\nu}_e$ and its general Lagrangian is given by:

$$\mathcal{L}_{Fermi} = 4\frac{G_F}{\sqrt{2}} \mathcal{J}^\mu \mathcal{J}_\mu^\dagger \tag{2.21}$$

where $\mathcal{J}^\mu$ are fermion currents which can be separated into leptonic and hadronic parts $\mathcal{J}^\mu = l^\mu + h^\mu$. The currents can be generically expressed as

$$\mathcal{J}_{jk}^\mu = \bar{\psi}_j \gamma^\mu P_L \psi_k \tag{2.22}$$

[5]Note that if $\mathcal{L}_{int}(\varphi, \boldsymbol{\phi}) = 0$, one can just drop the heavy fields.

[6]All the terms in the Lagrangian need to have overall mass dimension four due to the action construction.

[7]This is analogous to e.g. the perturbative QCD calculations in orders of α_s.

in terms of fermion fields, with $P_L = \frac{1-\gamma_5}{2}$. Since the mass dimension of the fermion fields is equal to 3/2 it follows that in order to keep the Lagrangian's dimension 4, the coupling constant G_F needs to have dimension -2. This can be reinterpreted in the language of EFTs as the high energy scale[8]:

$$G_F^{-1/2} \approx \Lambda_F \approx 300 \text{ GeV} \tag{2.23}$$

As discussed earlier, using the EFT above this scale would require considering an infinite number of operators, not only the four fermion interactions of dimension six above. Alternatively, we can consider the unitarity bounds of the Fermi theory. The cross section grows linearly with the interaction energy ($\sigma \sim s$), and breaks unitarity at the scale around 600 GeV. This *bottom-up* effective description hinted towards New Physics at the $O(100 \text{ GeV})$ scale, which would be able to cure this behaviour, and that was confirmed decades later with the discovery of electroweak vector bosons with masses around 80-90 GeV.

With the knowledge of the underlying mechanism of the exchange of the massive vector bosons between the fermion currents, it is still possible to use the effective description at energies below the masses of the new particles. However, using the *top-down* EFT approach we can now link the dimensional effective coupling G_F with the fundamental constants of the full theory. For that we write the expression in the full theory:

$$(\bar{\psi}_j \frac{ig}{\sqrt{2}} \gamma^\mu P_L \psi_k) \frac{-ig_{\mu\nu}}{p^2 - m_W^2} (\bar{\psi}_l \frac{ig}{\sqrt{2}} \gamma^\nu P_L \psi_m) = \frac{g^2}{8} \frac{ig_{\mu\nu}}{p^2 - m_W^2} (\bar{\psi}_j \gamma^\mu (1-\gamma_5) \psi_k)(\bar{\psi}_l \gamma_\mu (1-\gamma_5) \psi_m) \tag{2.24}$$

and then we expand the denominator with the $W^\pm$ boson mass in a Taylor series in the limit when the exchanged momentum is much smaller than the mass:

$$\frac{-g^{\mu\nu}}{p^2 - m_W^2} = \frac{g^{\mu\nu}}{m_W^2} \frac{1}{1 - \frac{p^2}{m_W^2}} \overset{p^2 \ll m_W^2}{=} \frac{g^{\mu\nu}}{m_W^2} \left(1 + \frac{p^2}{m_W^2} + O((\frac{p^2}{m_W^2})^2)\right). \tag{2.25}$$

Keeping the first term we obtain the dimension 6 four-fermion term described above. The next terms in the expansion will contribute to terms of dimension 8 and higher, that will also involve the derivatives of the fermion fields. From this we can derive the expression of the G_F constant in terms of the fundamental model's parameters:

$$\frac{G_F}{\sqrt{2}} = \frac{g^2}{8M_W^2}. \tag{2.26}$$

A very similar approach as applied to the β decay can be followed nowadays, with using the effective description build up on the SM Lagrangian, as described in Section 2.5. Note that this complementarity between the bottom-up and top-down EFT is welcome since we have a huge number of New Physics models, and it would not be possible to test them all in independent experimental analyses. A more desirable approach would be to set experimental bounds on the Wilson coefficients, and then the BSM phenomenologists can use the top-down EFT approach—shortly reviewed in Section 2.4—to obtain the expressions of the measured Wilson coefficients in terms of the model parameters, and thus conclude on bounds and properties of the model.

[8] Assuming that the Wilson coefficients are of order 1.

2.4 The Top-Down approach

The observation that the particles heavier than the energy available in the experiment will not be produced, may lead to a false intuition, that the heavy fields can simply be removed to facilitate the calculations. However, as the Fermi theory example shows, this is not the case: the heavy states need to be consistently integrated out, since they contribute also as virtual particles, and in this way they contribute to the new interactions in the *low-energy* theory. This process of finding the higher dimension interactions appearing in the effective theory as a consequence of integrating out the heavy degrees of freedom, together with finding expressions for their Wilson coefficients in terms of the fundamental UV constants is called *matching*. The Wilson coefficients—as most of the couplings—are a function of the scale, and thus one needs to include *running* from the scale of matching (Λ) to the scale of the observables. The one loop RGE running of dimension 6 SMEFT Wilson coefficients was presented in Refs. [50–52] for the Warsaw basis[9] and in [54] partially for the SILH basis[10]. Note that the anomalous dimension matrices mix the Wilson coefficients, and thus some new operators can contribute at the energy scale lower than the matching scale.

The integration of the heavy states proceeds through taking the limit of their infinite masses and/or zero couplings, as sketched in Equation (2.25). However the situation is not always that simple, since the fields to be integrated out may also occur in the loops. This also indicates, that it is actually important for the matching how many loops are included in the *"starting"* theory. The method of integrating out the heavy fields—diagram by diagram—to all possible interactions of the SM fields of dimension 6 was applied to a set of simple SM extensions, such as an additional scalar or fermion [55–61]. There is also an ongoing Matchmaker project aiming at the inclusion of the matching at the tree and one-loop level in the diagrammatic approach [62].

An alternative method of integrating out the heavy degrees of freedom, called the *Covariant Derivative Expansion*, based on the path integral formulation rather than the Feynman diagrams, was developed in the 80's [63] and recently revisited [64], and gained popularity (see applications in [65, 66]). It provides a promising way to automate the matching of an arbitrary UV model to SMEFT, e.g. the MatchingTool for tree-level matching [67]. Shortly after its reintroduction, a problem with the correct accounting for the mixed loops—containing the heavy and light fields—was pointed out [68, 69], and few alternative ways of fixing it were proposed [70–73].

2.5 The Bottom-Up approach

The bottom up EFT—as mentioned previously—can be used in the cases in which we want to use the experimental input to parametrise our ignorance about the high-scale physics. Having a theory that describes quite well the physics at the scale we explore, we can use the EFT framework to consistently build up the new interactions which would account for the small deviations. This description is model independent—we do not make any assumptions about the type of the underlying UV theory. The approach which is heavily discussed in context of usage at the LHC [1, 6], takes the so far very successful SM as the basis, and extends it with dimension 6 operators. In this section

[9] There is also its Mathematica implementation in DsixTools [53].

[10] The different bases of SMEFT will be discussed in Sec. 2.5.1.1.

we will take a closer look at this extension. For further reading we refer to a recently published review of *'The Standard Model as an Effective Field Theory'* [74].

We emphasise that throughout this section we discuss the SMEFT: the EFT of the SM in which the Higgs field is considered as a complex doublet of $SU(2)_L$. An alternative approach, called *the Higgs Effective Field Theory* (HEFT) is relaxing this assumption, and introduces the three would-be Goldstone bosons (becoming the longitudinal polarisations of the EW bosons) together with a singlet Higgs field, without imposing the doublet structure. We can say, that the HEFT is a generalisation of the SMEFT, however, due to the more complicated structure of the Higgs field, SMEFT contains also operators that are not present in the HEFT.

2.5.1 The SMEFT in the Warsaw Basis

The general form of the SMEFT Lagrangian reads, following Eq. (2.20) :

$$\mathcal{L} = \mathcal{L}_{SM} + \frac{c^{(5)}}{\Lambda}\mathcal{O}^{(5)} + \sum_j \frac{c_j^{(6)}}{\Lambda^2}\mathcal{O}_j^{(6)} + O(\Lambda^{-3}) \tag{2.27}$$

where $\mathcal{L}_{SM}$ corresponds to the usual SM Lagrangian of Eq. (2.1), the dimensionless coefficients c_j are the Wilson coefficients suppressed by the powers of Λ. The scale Λ plays an analogous role as the $W^{\pm}$ boson mass in Fermi theory. Since we do not make any assumptions about the NP—just that it is well separable from the SM, and obeys the Lorentz and gauge symmetries—we do not automatically identify the scale Λ with the onset of new resonances.

All the operators of the SM Lagrangian have mass dimension four[11]. To consistently build the SMEFT operators, let us start with recalling the gauge representations and mass-dimensionalities of the SM fields in Tables 2.2 and 2.1. Using the Tables as a guidance, one can combine the fields in a way to obtain the gauge and Lorentz invariant operators of dimension higher than four[12] .

	φ	ψ	$X_{\mu\nu}$	D_μ
$[M]$	1	3/2	2	1

Table 2.2: The mass dimensions of the ingredients of the SM Lagrangian.

Trying to build the operators of dimension 5, one realises that there is just one combination, leading to the neutrino Majorana mass term:

$$(\tilde{\varphi}^\dagger l_i)^T C(\tilde{\varphi}^\dagger l_j) \tag{2.28}$$

[11]Note that the Higgs mass term is the only field combination of dimension 2 and it is topped up with μ_H^2, which in consequence leads to *the hierarchy problem.*

[12]Note, that in the SM Lagrangian all possible gauge and Lorentz invariant dimension 4 terms built of the SM fields are present except for the $G_{\mu\nu}\tilde{G}^{\mu\nu}$ term, which leads to the *strong CP problem.*

which was first discussed by Weinberg [75]. This operator is mainly explored in neutrino experiments, and is of minor phenomenological relevance for LHC physics.

If we combine the fields further we will find out that there are many more operators arising at dimension six. As a first example we have the operators which were present in the Fermi theory: the four fermion interactions (see Tab. 2.4). We now have a complete picture of the weak interactions, with the exchange of the massive vector bosons, but these four fermion interactions are nowadays used e.g. in the analysis of flavour physics experiments in which the decays of heavy-quark mesons are studied and their deviation from the SM predictions is parametrised.

With the whole particle content of the SM we can build many additional operators. Let us first note that the square of the Higgs doublet (not to be confused with the physical Higgs field), $\varphi^\dagger\varphi$, is Lorentz and gauge invariant. From Table 2.2 we easily conclude that $\varphi^\dagger\varphi$ has mass dimension 2, and thus multiplying the SM terms by it, we will obtain terms of dimension 6. In this way we find the following terms (see Tab. 2.3):

- terms like $(\varphi^\dagger\varphi)^3$ (class φ^6 of Tab. 2.3),
- gauge boson kinetic terms multiplied by $\varphi^\dagger\varphi$ (class $X^2\varphi^2$)
- modified Yukawa couplings (class $\psi^2\varphi^3$)

Note, that since the φ field can be expanded around the vacuum expectation value (v), which is a constant, we can use the presented operators as a modification of the SM values. For example, in the SM the cubic Higgs coupling is fully determined by the quartic coupling constant λ and v, while the $(\varphi^\dagger\varphi)^3$ operator gives more flexibility to this relation. An analogous consideration applies to the Yukawa couplings, which in the SM are just dependent on the particle mass and the *vev*, while using the operators of the form $v^2\bar{l}_L\varphi e_R$ this dependence is modified.

Other classes of operators are not simple multiplications of those present in the SM:

- the cubic field strength operators (class X^3), that for the gauge independence need to be multiplied by the appropriate structure constant ($SU(3)$ or $SU(2)$)
- the magnetic dipole operators, that combine the Higgs doublet, fermions and gauge field in a way not present in the SM (class $\psi^2X\varphi$)
- the operators coupling the fermions of the same helicity with the Higgs field derivative (class $\psi^2\varphi^2D$)

Looking at the Tables 2.2 and 2.1 one can think of other classes of dimension 6 operators which we can write down, e.g. $D^4\varphi^2$ or $XD^2\varphi^2$. However, these can be reduced into the other classes of operators mentioned above with the use of the *equations of motion* (EoM) and the *Fierz identities*. We consider here explicitly an example reducing the class of the operators X^2D^2, with $X = W$ for simplicity. We start with recalling the EoMs for the W gauge bosons:

$$(D^\mu W_{\mu\nu})^I = \frac{g}{2}(\varphi^\dagger i\overleftrightarrow{D}^I_\nu\varphi + \bar{l}\gamma_\nu\sigma^I l + \bar{q}\gamma_\nu\sigma^I q), \tag{2.29}$$

X^3		φ^6 and $\varphi^4 D^2$		$\psi^2\varphi^3$	
Q_G	$f^{ABC}G_\mu^{A\nu}G_\nu^{B\rho}G_\rho^{C\mu}$	Q_φ	$(\varphi^\dagger\varphi)^3$	$Q_{e\varphi}$	$(\varphi^\dagger\varphi)(\bar{l}_p e_r \varphi)$
$Q_{\widetilde{G}}$	$f^{ABC}\widetilde{G}_\mu^{A\nu}G_\nu^{B\rho}G_\rho^{C\mu}$	$Q_{\varphi\Box}$	$(\varphi^\dagger\varphi)\Box(\varphi^\dagger\varphi)$	$Q_{u\varphi}$	$(\varphi^\dagger\varphi)(\bar{q}_p u_r \widetilde{\varphi})$
Q_W	$\varepsilon^{IJK}W_\mu^{I\nu}W_\nu^{J\rho}W_\rho^{K\mu}$	$Q_{\varphi D}$	$\left(\varphi^\dagger D^\mu\varphi\right)^\star\left(\varphi^\dagger D_\mu\varphi\right)$	$Q_{d\varphi}$	$(\varphi^\dagger\varphi)(\bar{q}_p d_r \varphi)$
$Q_{\widetilde{W}}$	$\varepsilon^{IJK}\widetilde{W}_\mu^{I\nu}W_\nu^{J\rho}W_\rho^{K\mu}$				
$X^2\varphi^2$		$\psi^2 X\varphi$		$\psi^2\varphi^2 D$	
$Q_{\varphi G}$	$\varphi^\dagger\varphi\, G_{\mu\nu}^A G^{A\mu\nu}$	Q_{eW}	$(\bar{l}_p\sigma^{\mu\nu}e_r)\tau^I\varphi W_{\mu\nu}^I$	$Q_{\varphi l}^{(1)}$	$(\varphi^\dagger i\overleftrightarrow{D}_\mu\varphi)(\bar{l}_p\gamma^\mu l_r)$
$Q_{\varphi\widetilde{G}}$	$\varphi^\dagger\varphi\,\widetilde{G}_{\mu\nu}^A G^{A\mu\nu}$	Q_{eB}	$(\bar{l}_p\sigma^{\mu\nu}e_r)\varphi B_{\mu\nu}$	$Q_{\varphi l}^{(3)}$	$(\varphi^\dagger i\overleftrightarrow{D}_\mu^I\varphi)(\bar{l}_p\tau^I\gamma^\mu l_r)$
$Q_{\varphi W}$	$\varphi^\dagger\varphi\, W_{\mu\nu}^I W^{I\mu\nu}$	Q_{uG}	$(\bar{q}_p\sigma^{\mu\nu}T^A u_r)\widetilde{\varphi}\, G_{\mu\nu}^A$	$Q_{\varphi e}$	$(\varphi^\dagger i\overleftrightarrow{D}_\mu\varphi)(\bar{e}_p\gamma^\mu e_r)$
$Q_{\varphi\widetilde{W}}$	$\varphi^\dagger\varphi\,\widetilde{W}_{\mu\nu}^I W^{I\mu\nu}$	Q_{uW}	$(\bar{q}_p\sigma^{\mu\nu}u_r)\tau^I\widetilde{\varphi}\, W_{\mu\nu}^I$	$Q_{\varphi q}^{(1)}$	$(\varphi^\dagger i\overleftrightarrow{D}_\mu\varphi)(\bar{q}_p\gamma^\mu q_r)$
$Q_{\varphi B}$	$\varphi^\dagger\varphi\, B_{\mu\nu}B^{\mu\nu}$	Q_{uB}	$(\bar{q}_p\sigma^{\mu\nu}u_r)\widetilde{\varphi}\, B_{\mu\nu}$	$Q_{\varphi q}^{(3)}$	$(\varphi^\dagger i\overleftrightarrow{D}_\mu^I\varphi)(\bar{q}_p\tau^I\gamma^\mu q_r)$
$Q_{\varphi\widetilde{B}}$	$\varphi^\dagger\varphi\,\widetilde{B}_{\mu\nu}B^{\mu\nu}$	Q_{dG}	$(\bar{q}_p\sigma^{\mu\nu}T^A d_r)\varphi\, G_{\mu\nu}^A$	$Q_{\varphi u}$	$(\varphi^\dagger i\overleftrightarrow{D}_\mu\varphi)(\bar{u}_p\gamma^\mu u_r)$
$Q_{\varphi WB}$	$\varphi^\dagger\tau^I\varphi\, W_{\mu\nu}^I B^{\mu\nu}$	Q_{dW}	$(\bar{q}_p\sigma^{\mu\nu}d_r)\tau^I\varphi\, W_{\mu\nu}^I$	$Q_{\varphi d}$	$(\varphi^\dagger i\overleftrightarrow{D}_\mu\varphi)(\bar{d}_p\gamma^\mu d_r)$
$Q_{\varphi\widetilde{W}B}$	$\varphi^\dagger\tau^I\varphi\,\widetilde{W}_{\mu\nu}^I B^{\mu\nu}$	Q_{dB}	$(\bar{q}_p\sigma^{\mu\nu}d_r)\varphi\, B_{\mu\nu}$	$Q_{\varphi ud}$	$i(\widetilde{\varphi}^\dagger D_\mu\varphi)(\bar{u}_p\gamma^\mu d_r)$

Table 2.3: Bosonic operators of the Warsaw basis. The Table is taken from Ref. [37].

where σ^I are the generators of $SU(2)_L$ (Pauli matrices). Now let us consider the contraction of the Lorentz indices in the operator of type X^2D^2. If both are contracted with the same tensor X, we obtain the term $[D_\mu, D_\nu] \sim X_{\mu\nu}$, and thus the class X^3. In the case that derivatives are contracted with different tensors, we find terms of the type $D^\mu X_{\mu\nu}$, which we can replace by the EoM from Eq. (2.29):

$$D_\rho W^{\rho\nu} D^\mu W_{\mu\nu} = \frac{g}{2} D_\rho W^{I\rho\nu}(\varphi^\dagger i\overleftrightarrow{D}^I_\nu\varphi + \bar{l}\gamma_\nu\sigma^I l + \bar{q}\gamma_\nu\sigma^I q) \tag{2.30}$$

and as we see in the result, this substitution leads to classes $\varphi^2 X D^2$ and $\psi^2 X D$, which can again be reduced to classes $\varphi^2 X^2$, $\varphi^4 D^2$, $\psi^2\varphi^2 D$ and $\psi^2\varphi X$, $\psi^2\varphi^2 D$, ψ^4, respectively. How these and other classes of operators can be reduced to the presented minimal basis can be inferred from Ref. [37].

Recently, also a basis of dimension 7 operators for the SM was proposed, however since these operators are subleading, at the present state we do not consider them for the LHC phenomenology [76].

2.5.1.1 Different operator basis

As in many other physical problems, there is a freedom in choosing the parametrisation, i.e. the *basis* of the operators. The two concepts that the basis needs to fulfil are:

$(\bar{L}L)(\bar{L}L)$		$(\bar{R}R)(\bar{R}R)$		$(\bar{L}L)(\bar{R}R)$	
Q_{ll}	$(\bar{l}_p\gamma_\mu l_r)(\bar{l}_s\gamma^\mu l_t)$	Q_{ee}	$(\bar{e}_p\gamma_\mu e_r)(\bar{e}_s\gamma^\mu e_t)$	Q_{le}	$(\bar{l}_p\gamma_\mu l_r)(\bar{e}_s\gamma^\mu e_t)$
$Q_{qq}^{(1)}$	$(\bar{q}_p\gamma_\mu q_r)(\bar{q}_s\gamma^\mu q_t)$	Q_{uu}	$(\bar{u}_p\gamma_\mu u_r)(\bar{u}_s\gamma^\mu u_t)$	Q_{lu}	$(\bar{l}_p\gamma_\mu l_r)(\bar{u}_s\gamma^\mu u_t)$
$Q_{qq}^{(3)}$	$(\bar{q}_p\gamma_\mu\tau^I q_r)(\bar{q}_s\gamma^\mu\tau^I q_t)$	Q_{dd}	$(\bar{d}_p\gamma_\mu d_r)(\bar{d}_s\gamma^\mu d_t)$	Q_{ld}	$(\bar{l}_p\gamma_\mu l_r)(\bar{d}_s\gamma^\mu d_t)$
$Q_{lq}^{(1)}$	$(\bar{l}_p\gamma_\mu l_r)(\bar{q}_s\gamma^\mu q_t)$	Q_{eu}	$(\bar{e}_p\gamma_\mu e_r)(\bar{u}_s\gamma^\mu u_t)$	Q_{qe}	$(\bar{q}_p\gamma_\mu q_r)(\bar{e}_s\gamma^\mu e_t)$
$Q_{lq}^{(3)}$	$(\bar{l}_p\gamma_\mu\tau^I l_r)(\bar{q}_s\gamma^\mu\tau^I q_t)$	Q_{ed}	$(\bar{e}_p\gamma_\mu e_r)(\bar{d}_s\gamma^\mu d_t)$	$Q_{qu}^{(1)}$	$(\bar{q}_p\gamma_\mu q_r)(\bar{u}_s\gamma^\mu u_t)$
		$Q_{ud}^{(1)}$	$(\bar{u}_p\gamma_\mu u_r)(\bar{d}_s\gamma^\mu d_t)$	$Q_{qu}^{(8)}$	$(\bar{q}_p\gamma_\mu T^A q_r)(\bar{u}_s\gamma^\mu T^A u_t)$
		$Q_{ud}^{(8)}$	$(\bar{u}_p\gamma_\mu T^A u_r)(\bar{d}_s\gamma^\mu T^A d_t)$	$Q_{qd}^{(1)}$	$(\bar{q}_p\gamma_\mu q_r)(\bar{d}_s\gamma^\mu d_t)$
				$Q_{qd}^{(8)}$	$(\bar{q}_p\gamma_\mu T^A q_r)(\bar{d}_s\gamma^\mu T^A d_t)$

$(\bar{L}R)(\bar{R}L)$ and $(\bar{L}R)(\bar{L}R)$		B-violating	
Q_{ledq}	$(\bar{l}_p^j e_r)(\bar{d}_s q_t^j)$	Q_{duq}	$\varepsilon^{\alpha\beta\gamma}\varepsilon_{jk}\left[(d_p^\alpha)^T C u_r^\beta\right]\left[(q_s^{\gamma j})^T C l_t^k\right]$
$Q_{quqd}^{(1)}$	$(\bar{q}_p^j u_r)\varepsilon_{jk}(\bar{q}_s^k d_t)$	Q_{qqu}	$\varepsilon^{\alpha\beta\gamma}\varepsilon_{jk}\left[(q_p^{\alpha j})^T C q_r^{\beta k}\right]\left[(u_s^\gamma)^T C e_t\right]$
$Q_{quqd}^{(8)}$	$(\bar{q}_p^j T^A u_r)\varepsilon_{jk}(\bar{q}_s^k T^A d_t)$	Q_{qqq}	$\varepsilon^{\alpha\beta\gamma}\varepsilon_{jn}\varepsilon_{km}\left[(q_p^{\alpha j})^T C q_r^{\beta k}\right]\left[(q_s^{\gamma m})^T C l_t^n\right]$
$Q_{lequ}^{(1)}$	$(\bar{l}_p^j e_r)\varepsilon_{jk}(\bar{q}_s^k u_t)$	Q_{duu}	$\varepsilon^{\alpha\beta\gamma}\left[(d_p^\alpha)^T C u_r^\beta\right]\left[(u_s^\gamma)^T C e_t\right]$
$Q_{lequ}^{(3)}$	$(\bar{l}_p^j\sigma_{\mu\nu} e_r)\varepsilon_{jk}(\bar{q}_s^k\sigma^{\mu\nu} u_t)$		

Table 2.4: Fermionic operators of the Warsaw basis. The Table is taken from Ref. [37].

- completeness: contain all the operators at the given order
- non-redundancy: do not contain any operators which can be reduced to the others.

The basis presented in Tables 2.3 and 2.4, commonly known as the *Warsaw basis* [37] is the first to fulfil those two requirements. It is heavily based on the work preceeding it for over 20 years [36], but the latter included redundant operators. The Warsaw basis is very commonly used, however it is not the only one proposed. Another (partial) basis, called *the Strongly Interacting Light Higgs* (SILH) basis, was presented in Ref. [77], but it contained just the subset of operators modifying the Higgs properties. Further developments were needed [54, 78] in order to complete it into an actual basis. This basis can be divided in subparts, as:

$$\mathcal{L}_{SMEFT} = \mathcal{L}_{SM} + \Delta\mathcal{L}_{SILH} + \Delta\mathcal{L}_{F1} + \Delta\mathcal{L}_{F2} + \Delta\mathcal{L}_{4f} + \Delta\mathcal{L}_{Gauge}(+\Delta\mathcal{L}_{CP}), \tag{2.31}$$

where

- $\Delta\mathcal{L}_{SILH}$ is the original SILH Lagrangian [77]
- $\Delta\mathcal{L}_{F1}$ contains the 2-fermion operators
- $\Delta\mathcal{L}_{F2}$ contains the 2-fermion dipole-type operators
- $\Delta\mathcal{L}_{4f}$ contains the 4-fermion interactions

- $\Delta\mathcal{L}_{Gauge}$ contains the self interactions of the gauge bosons
- $\Delta\mathcal{L}_{CP}$ is a possible extension in case of CP violation

The first three subsets of the Lagrangian, containing the Higgs field, are presented in Figure 2.1. Note, that in this basis the operators, unlike in the Warsaw basis, have fixed normalisation in terms of the SM parameters following the canonical normalisation of the kinetic terms. Also, some classes of Higgs related operators are expressed in a different way compared to the Warsaw basis, eg. there is the class $D^2\varphi^2X$ not present in the former basis and there are no operators of class φ^2X^2 mixing the $W_{\mu\nu}$ and $B_{\mu\nu}$ fields in the latter. The authors of the SILH basis argue that this formulation is better suited for the Higgs phenomenology application since it allows for an easier expression of the experimentally measured Higgs observables in terms of the dimension 6 operators.

$$
\begin{aligned}
\Delta\mathcal{L}_{SILH} = {} & \frac{\bar{c}_H}{2v^2}\partial^\mu(H^\dagger H)\partial_\mu(H^\dagger H) + \frac{\bar{c}_T}{2v^2}\left(H^\dagger\overleftrightarrow{D^\mu}H\right)\left(H^\dagger\overleftrightarrow{D_\mu}H\right) - \frac{\bar{c}_6\,\lambda}{v^2}(H^\dagger H)^3 \\
& + \frac{H^\dagger H}{v^2}\left(\bar{c}_u y_u \overline{q_L} H^c u_R + \bar{c}_d y_d \overline{q_L} H d_R + \bar{c}_l y_l \overline{L_L} H l_R + \text{h.c.}\right) \\
& + \frac{i\,\bar{c}_W\,g}{2m_W^2}\left(H^\dagger\sigma^i\overleftrightarrow{D^\mu}H\right)(D^\nu W_{\mu\nu})^i + \frac{i\,\bar{c}_B\,g'}{2m_W^2}\left(H^\dagger\overleftrightarrow{D^\mu}H\right)(\partial^\nu B_{\mu\nu}) \\
& + \frac{i\,\bar{c}_{HW}\,g}{m_W^2}(D^\mu H)^\dagger\sigma^i(D^\nu H)W^i_{\mu\nu} + \frac{i\,\bar{c}_{HB}\,g'}{m_W^2}(D^\mu H)^\dagger(D^\nu H)B_{\mu\nu} \\
& + \frac{\bar{c}_\gamma\,g'^2}{m_W^2}(H^\dagger H)B_{\mu\nu}B^{\mu\nu} + \frac{\bar{c}_g\,g_S^2}{m_W^2}(H^\dagger H)G^a_{\mu\nu}G^{a\mu\nu}\,,
\end{aligned}
$$

$$
\begin{aligned}
\Delta\mathcal{L}_{F_1} = {} & \frac{i\,\bar{c}_{Hq}}{v^2}(\overline{q_L}\gamma^\mu q_L)\left(H^\dagger\overleftrightarrow{D_\mu}H\right) + \frac{i\,\bar{c}'_{Hq}}{v^2}(\overline{q_L}\gamma^\mu\sigma^i q_L)\left(H^\dagger\sigma^i\overleftrightarrow{D_\mu}H\right) \\
& + \frac{i\,\bar{c}_{Hu}}{v^2}(\overline{u_R}\gamma^\mu u_R)\left(H^\dagger\overleftrightarrow{D_\mu}H\right) + \frac{i\,\bar{c}_{Hd}}{v^2}(\overline{d_R}\gamma^\mu d_R)\left(H^\dagger\overleftrightarrow{D_\mu}H\right) \\
& + \left[\frac{i\,\bar{c}_{Hud}}{v^2}(\overline{u_R}\gamma^\mu d_R)\left(H^{c\dagger}\overleftrightarrow{D_\mu}H\right) + \text{h.c.}\right] \\
& + \frac{i\,\bar{c}_{HL}}{v^2}(\overline{L_L}\gamma^\mu L_L)\left(H^\dagger\overleftrightarrow{D_\mu}H\right) + \frac{i\,\bar{c}'_{HL}}{v^2}(\overline{L_L}\gamma^\mu\sigma^i L_L)\left(H^\dagger\sigma^i\overleftrightarrow{D_\mu}H\right) \\
& + \frac{i\,\bar{c}_{Hl}}{v^2}(\overline{l_R}\gamma^\mu l_R)\left(H^\dagger\overleftrightarrow{D_\mu}H\right)\,,
\end{aligned}
$$

$$
\begin{aligned}
\Delta\mathcal{L}_{F_2} = {} & \frac{\bar{c}_{uB}\,g'}{m_W^2}y_u(\overline{q_L}H^c\sigma^{\mu\nu}u_R)B_{\mu\nu} + \frac{\bar{c}_{dB}\,g'}{m_W^2}y_d(\overline{q_L}H\sigma^{\mu\nu}d_R)B_{\mu\nu} \\
& + \frac{\bar{c}_{uW}\,g}{m_W^2}y_u(\overline{q_L}\sigma^i H^c\sigma^{\mu\nu}u_R)W^i_{\mu\nu} + \frac{\bar{c}_{dW}\,g}{m_W^2}y_d(\overline{q_L}\sigma^i H\sigma^{\mu\nu}d_R)W^i_{\mu\nu} \\
& + \frac{\bar{c}_{uG}\,g_S}{m_W^2}y_u(\overline{q_L}H^c\sigma^{\mu\nu}\lambda^a u_R)G^a_{\mu\nu} + \frac{\bar{c}_{dG}\,g_S}{m_W^2}y_d(\overline{q_L}H\sigma^{\mu\nu}\lambda^a d_R)G^a_{\mu\nu} \\
& + \frac{\bar{c}_{lB}\,g'}{m_W^2}y_l(\overline{L_L}H\sigma^{\mu\nu}l_R)B_{\mu\nu} + \frac{\bar{c}_{lW}\,g}{m_W^2}y_l(\overline{L_L}\sigma^i H\sigma^{\mu\nu}l_R)W^i_{\mu\nu} + \text{h.c.}\,,
\end{aligned}
$$

Figure 2.1: The operators of the SILH basis containing the Higgs field [78].

Another basis, called *the BSM primaries* [79], comes even closer to the experiment, since it is expressed in terms of mass- rather than gauge-eigenstates. In the same spirit *the BSM characterisation* basis [80][13] was proposed, mainly as a framework for the Monte Carlo (MC)

[13]This is an extension of the Higgs characterisation framework [81].

generators. It goes even further since it is based on the $SU(3)_C \times U(1)_Q$ gauge symmetry rather than the $SU(3)_C \times SU(2)_L \times U(1)_Y$.

The general spirit is that the theoretical advances such as renormalisation were performed in the Warsaw or the SILH bases, while the other two are mainly used in tools[14]. Since the bases are equivalent, it would be useful to translate between them, and this was a motivation for the Rosetta program [80], which not only translates between the different bases, but also provides a link to MC generators via the BSM Characterisation basis expressed in the FeynRules framework.

2.5.1.2 The operators' origin and importance

Although all the operators presented in the Tables 2.3 and 2.4 are of the same order in the EFT expansion (in $1/\Lambda$), one can discuss their importance based on their origin from the UV model [85]. Some of the operators can be generated by integrating out heavy states at tree level as was shown in the case of the Fermi theory (*potentially tree generated* (PTG)), however others can be generated only through integrating out particles in the loops (*loop generated* LG). The classification of the operators of the Warsaw basis reads:

- PTG: φ^6, $\varphi^4 D^2$, $\varphi^3\psi^2$, $\varphi^2\psi^2 D$, ψ^4 classes
- LG: X^3, $X^2\varphi^2$, $\psi^2 X\varphi$ classes.

One could argue that the loop processes are suppressed by roughly a factor $1/16\pi^2$ and the coefficients of the LG operators will be suppressed with respect to the PTG ones. Although a consistent approach would require including all (both LG and PTG) operators which can contribute to the considered observable, this classification may be used as a guiding principle in order to simplify[15] both the calculation and the experimental analysis in the case when many operators contribute.

2.5.2 SMEFT in use

After discussing the properties of SMEFT on the Lagrangian level, let us move to more practical applications. As far as the LHC phenomenology is concerned, we need the theoretical predictions for cross sections and kinematic distributions. Therefore in this section the steps required on the way are discussed: operators (Lagrangian) → diagrams → amplitudes → cross sections.

[14]Note however an implementation of SILH basis operators into the HDECAY program: eHDECAY [82] or a recent implementation of the Warsaw basis into the FeynRules framework: SMEFTsim in unitary gauge [83] and SMEFT in R_ξ gauge [84].

[15]The simplification is made by assuming an importance hierarchy, which allows to neglect some of the operators, which should be suppressed.

2.5.2.1 Operators vs Observables

In the SMEFT, there is no one-to-one correspondence between the Wilson coefficients and the observables, as it was somehow implied in the κ-framework. One operator can contribute to many observables and one observable may depend on more than one operator. This suggests that the most consistent strategy would be to perform a global fit to the Wilson coefficients based on as many of both the observables and the operators as possible. This would be, however, extremely challenging[16].

Let us show this on the example of the gluon fusion Higgs production at the LHC, which is the main topic of this thesis. Note that the gluonic Higgs production is a loop induced process at LO in the SM[17] and there is just one diagram that contributes[18,19]:

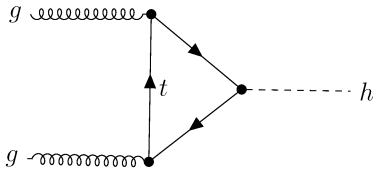

If we consider the SMEFT then we have one diagram[20] that contributes at the tree level (LO SMEFT):

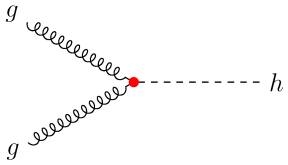

However we may want to add a diagram that resembles the structure of the SM LO—just modifying the top quark Yukawa—this diagram corresponds to the NLO SMEFT[21]:

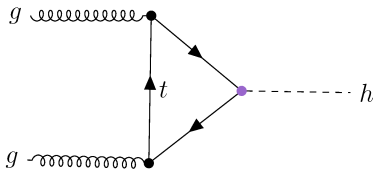

To complete the NLO SMEFT we need to add two more diagrams arising from the insertion of the chromomagnetic operator[22]:

[16] See the discussion in Sec. I.6.4 of Ref. [1]

[17] A more detailed discussion of the SM Higgs production at the LHC is the topic of Chapter 3.

[18] For simplicity we consider here only the generic loop diagram, in general there can be different quarks running in the loop (t, b, c).

[19] The Feynman diagrams in this thesis were drawn with the use of the TikZ-Feynman package [86].

[20] In the diagrams the SMEFT vertices are marked in colour, and the colour coding will remain unchanged throughout this thesis.

[21] The subtleties about the NLO SMEFT will be discussed in the next section.

[22] Note that the chromomagnetic operator should have subleading importance compared to the Yukawa modifyer when we consider the PTG-LG classification.

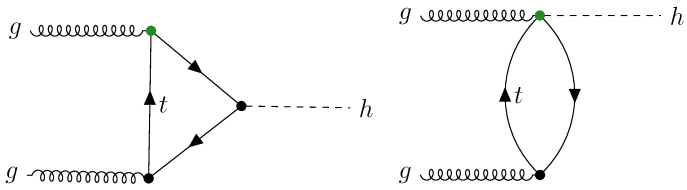

When one considers Higgs production with associated tops, the two last operators contribute, together with another, four fermion, operator, already at LO SMEFT:

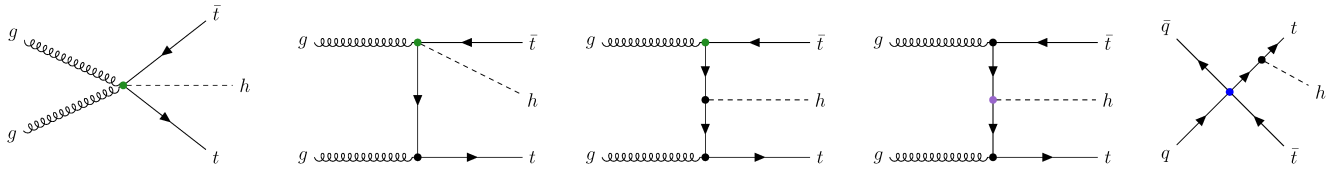

and a similar situation arise in $t\bar{t}$ production:

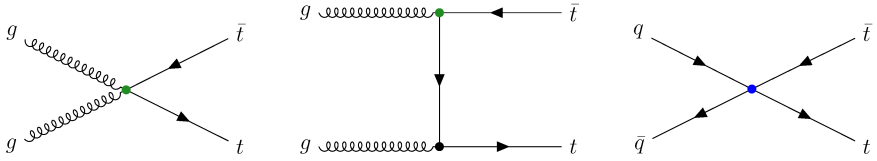

Observe that there is just one insertion of the SMEFT operator per diagram.

2.5.2.2 Amplitudes in the SMEFT

Any amplitude for a process in the SMEFT can be written in the following way [87]:

$$\mathcal{A} = \sum_{n=0}^{\infty} g^n \mathcal{A}_n^{(4)} + \sum_{n=0}^{\infty} \sum_{l=1}^{n} \sum_{k=l}^{\infty} \sum_{j=1}^{N_{4+2k}} g^n \frac{c_1 \cdot \ldots \cdot c_k}{\Lambda^{2kl}} \mathcal{A}_{nlkj}^{(4+2k)} \tag{2.32}$$

where g is the generic gauge coupling[23] constant, Λ is the scale of New Physics, c_is are the Wilson coefficients and the sums count the n - insertion of the vertices dependent on the g coupling, k - the dimension of SMEFT operators, l - insertion of the SMEFT operators and j - the different types of SMEFT operators (N_{4+2k} of them in total). Note that the sum over n does not run from zero for all the processes, i.e. in the case of the gluon fusion Higgs production we start with one loop contributing at g_S^2.

As we can see from Eq. (2.32), there is more than one expansion parameter for the amplitude, and this is a key fact to consider for the EFT predictions. Namely, the power counting for the perturbative expansion grows simultaneously in two directions: we can go to higher loops, like in SM perturbation theory[24], or we can go higher in the $1/\Lambda$ expansion. Because these corrections depend on the relative sizes of the coupling constants and Λ, and the latter is unknown, it is a

[23]Note that in the SM we have 2 of the gauge coupling constants: the QCD and the EW.

[24]Note, that in the SM we consider usually QCD and EW correction independently since they contribute with different coupling constants, so this can be viewed as a triple expansion even.

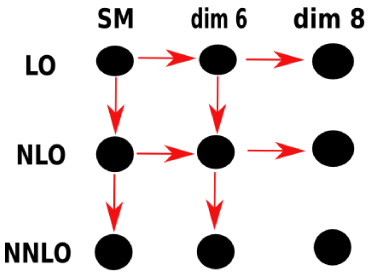

Figure 2.2: The power counting in perturbative SMEFT grows in two directions: higher loops, and higher dimensional operators. Figure taken from Ref. [1].

priori not possible to determine which are more relevant (see Fig. 2.2). Even when we consider going to higher orders in perturbation theory, but restricting ourselves to dimension 6, there is the question of how many operator insertions should we include at each level what was already mentioned in the previous section. For example: if a tree level diagram with one dimension 6 operator is *LO EFT* and a one-loop diagram with one dimension 6 operator is *NLO EFT*, where do we put a diagram with tree topology but two dimension 6 operators?

It is commonly assumed in the community that only one dimension 6 operator is inserted per diagram, both at tree and loop levels, since each of these vertices is suppressed by two powers of the cut-off scale ($1/\Lambda^2$), which we consider to be *big enough*. The double insertions of the dimension 6 operators should be considered on the same footing as the single insertion of a dimension 8 one.

2.5.2.3 To square or not to square?

Even knowing how to build the SMEFT amplitudes there remains the question: which terms shall be kept while squaring? Shall only the interference term be kept, since it is the only one truly at the level of $1/\Lambda^2$? Or shall also the squared term be kept, since it is already available? Despite this term is formally of the order of $1/\Lambda^4$, and contributes at the same order as the dimension 8 insertion or two dimension 6 insertions. However, dimension 8 insertions are usually not available. To simplify the discussion let us define the *linear* and *quadratic EFT* as:

$$\begin{aligned} |\mathcal{A}|^2 =& |\mathcal{A}_{\rm SM} + \mathcal{A}^{(6)} + \mathcal{A}^{(8)} + ...|^2 = \\ =& |\mathcal{A}_{\rm SM}|^2 + \underbrace{|\mathcal{A}_{\rm SM} \times \mathcal{A}^{(6)}|}_{\text{linear EFT}} + \underbrace{|\mathcal{A}^{(6)}|^2}_{\text{quadratic EFT}} + \underbrace{|\mathcal{A}_{\rm SM} \times \mathcal{A}^{(8)}|}_{\text{usually not available}} + \dots \end{aligned} \tag{2.33}$$

We can now discuss the effects of using the linear and the quadratic EFT in real examples. In Fig. 2.3a, the transverse momentum spectra of the Z boson from the Zh production is shown, in scenarios with two scales $\Lambda = 1$, 2 TeV (solid and dashed lines respectively) and in linear and quadratic SMEFT (blue and red lines respectively). The linear SMEFT for $\Lambda = 1$ TeV starts to have a negative cross section above $p_t \approx 200$ GeV, which is cured by the inclusion of squared terms, which make the distribution positive by definition. It is also clearly visible that the two approaches significantly deviate at higher p_t. This behaviour signals the breakdown of the EFT approximation.

In Fig. 2.3b, where again the p_t spectra of the associated vector boson are presented, four cases are plotted: the SM, the full theory of triplet vector boson of mass 591 GeV and the SMEFT

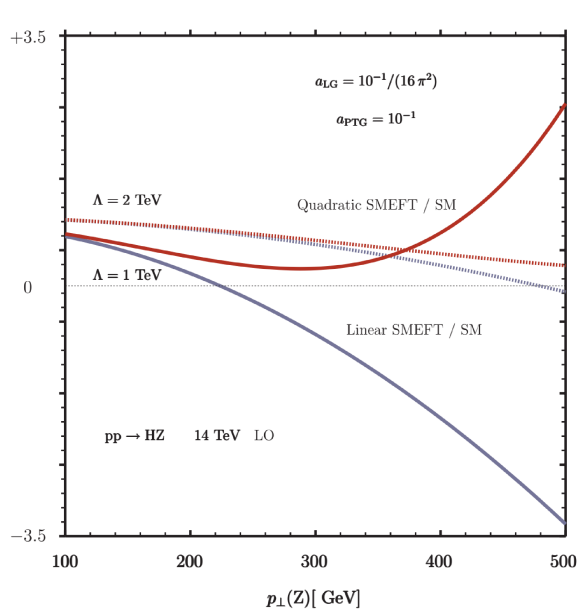

(a)

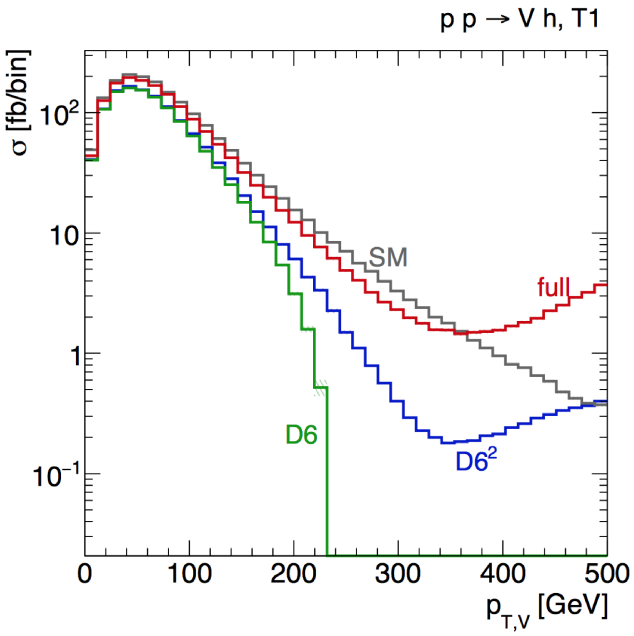

(b)

Figure 2.3: The transverse momentum distribution of the vector boson in Vh production. In Fig. 2.3a, different ratios of SMEFT and SM cross sections are depicted, the blue lines represent the cross sections where only the linear EFT terms are considered, while the red lines include also quadratic contributions. Solid and dashed lines represent two different choices for the Λ scale. In Fig. 2.3b, we see a similar prediction, obtained by means of the top-down approach, where the effective Lagrangian for a UV vector triplet model is studied. These Figures are taken from Ref. [1] and [88], respectively.

both linear and quadratic. The linear and quadratic realisations have very similar behaviour at low p_t, but then the linear approximation breaks down, with an abrupt drop at around 220 GeV, below the mass of the new particle of the full theory. The squared SMEFT also falls significantly below the full theory predictions, but reproduces the behaviour better.

Since the effective operators should be used to describe small deviations from the SM, the situation in which the inclusion of $|\mathcal{A}^{(6)}|^2$ (which should be additionally suppressed) becomes necessary, calls for caution. When the SMEFT amplitudes are known, both the linear and the quadratic SMEFT observables can be generated, the comparison of their behaviour is a good check for the validity of the EFT approximation and the difference between them should definitely be included into the theoretical uncertainty. When this missing higher order uncertainty is large, the SMEFT should be used with great care.

2.5.2.4 The SMEFT validity and unitarity

The example of how the inclusion of the $|\mathcal{A}^{(6)}|^2$ term can change the behaviour of the SMEFT prediction, calls for a more detailed analysis of the validity of the approach. Although we roughly describe Λ as the *scale of New Physics*, it is evident from the previous example that it does not

correspond to the breakdown of the approach, since in Fig. 2.3a the problems start to appear at $p_t \approx 200$ GeV, well below 1 TeV. One of the usual checks for the validity of the perturbative expansion is (perturbative) unitarity. Perturbative unitarity is in general violated in the EFT, however it can be used to investigate energies lower than Λ, since above Λ the EFT should definitely be replaced by the full theory.

Calculationally this is similar to the way renormalisable theories satisfy unitarity in perturbation theory; a perturbative expansion in E/Λ always becomes difficult at high enough energies, since one will need an infinite number of parameters. Stated differently, unfortunately the SMEFT will break down in the tails of distributions (or new physics will be seen before the breakdown); projecting data into the SMEFT will have a large intrinsic uncertainty.

To give a short example, we consider the scattering of longitudinal $W^{\pm}$. We start by recalling the SM case:

$$T_{\rm SM}(W_L^+W_L^- \to W_L^+W_L^-) \sim -\frac{G_F m_h^2}{4\sqrt{2}\pi} \text{ for } \ s \to \infty \tag{2.34}$$

Unitarity is not violated in this case, since the amplitude is constant in the limit of large s. Let us report here the result for the SMEFT:

$$T_{\rm SMEFT}(W_L^+W_L^- \to W_L^+W_L^-) \sim -\frac{1}{32\pi}(c_{\varphi D} + 2c_{\varphi\Box})\frac{s}{\Lambda^2} + \mathcal{O}(1) \tag{2.35}$$

where c_X are specific Wilson coefficients. The SM part is contributing to the constant part, while the contribution growing with s is driven by the new dimension 6 interactions. From this equation, we can, by imposing $|T_{\rm SMEFT}| < 1/2$, estimate the scale at which perturbative unitarity is broken (named here s_C):

$$\begin{aligned} |T_{\rm SMEFT}| &\sim \frac{1}{32\pi\Lambda^2}(c_{\varphi D} + 2c_{\varphi\Box})\frac{s}{\Lambda^2} < \frac{1}{2} \\ s_C &< \frac{16\pi}{(c_{\varphi D} + 2c_{\varphi\Box})}\Lambda^2 \end{aligned} \tag{2.36}$$

Note, that from this equation it is not straightforward that the scale s_C is smaller than Λ^2, however there is no sense to talk about the EFT above Λ. Thus, in general, we can define various scales in the EFT, at which we may anticipate the breakdown of the EFT approximation, and we should consider case by case which gives the strongest constraint. Calculations performed above these scales, although still technically possible, should be treated with caution.

Yet another situation which would break a specific EFT description will be when new resonances will be found in the LHC. This would require to add them to the effective formalism. First attempts in building such an extended EFT were made, and the basis of operators of dimension up to 6 for the two Higgs doublet model was proposed [89, 90].

3

Higgs boson production at the LHC

Precise theoretical predictions for Higgs boson production and decay, play a crucial role in testing the Standard Model. They are not only used in the experimental analysis, but also provide benchmarks to check if the scalar resonance found at the LHC is indeed the Higgs boson of the Standard Model, or rather something different. In this chapter the methodology of calculations at hadron colliders is shortly recalled and the advances in the calculation of Higgs production cross sections for the SM and the SMEFT in the four dominant production channels at the LHC are reviewed.

3.1 Generalities on the calculations for hadron colliders

Contrary to what happens at lepton colliders, the entities colliding at hadron colliders are composite objects rather than fundamental particles. Due to this key difference, the theoretical predictions for hadron colliders are more complex, and require a multi-layer approach which allows us to separate effects of different scales. At the heart of precise predictions for hadron collider processes lies the factorisation theorem, which for Higgs boson production reads:

$$\sigma_{had}(s, m_h) = \sum_{i,j} \int_0^1 dx_1 \int_0^1 dx_2 f_{i/h_1}(x_1; \mu_F) f_{j/h_2}(x_2; \mu_F) \hat{\sigma}(x_1 x_2 s, m_h; Q^2, \mu_R, \mu_F) \tag{3.1}$$

where f_{i/h_i} are parton distribution functions (PDFs) (and i and j are initial partons of the process), while σ_{had} is the hadronic cross-section and $\hat{\sigma}$ is the partonic cross-section. The scales on which the partonic cross-section depends are μ_R and μ_F - the renormalisation and factorisation scales, respectively, and Q^2 is the momentum transfer. This general formula corresponds to a process $pp \to ij \to h + X$, where X denotes the inclusive QCD final state. Thus this type of calculation is separated into the partonic cross section part, which is process dependent, and the process-independent PDFs. Note that this formula holds only when the momentum transfer of the colliding partons (Q^2) is large, and thus the strong coupling constant α_s is small. This condition is naturally fulfilled when heavy particles, such as the EW or Higgs boson, are produced. The PDF fits are driven by the experimental data, mostly from the deep-inelastic scattering experiments,

but also from the collider data on jets, Drell-Yan process, top-pair production and others [91]. The partonic cross-sections are calculated process by process, and follow a perturbative expansion in α_s, i.e. the corrections can be calculated order-by-order.

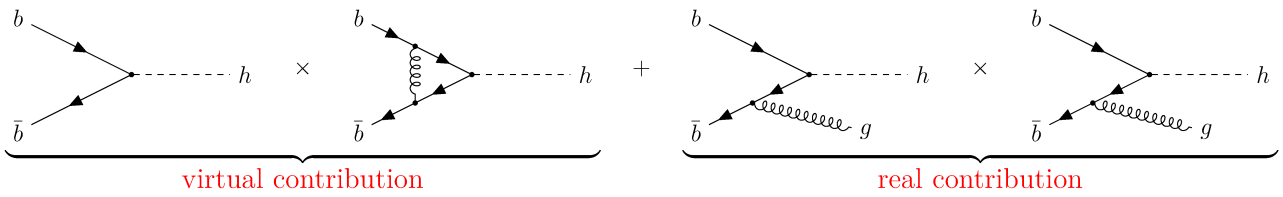

Figure 3.1: The schematic picture of the next to leading order corrections: the virtual correction as an interference of the LO and loop amplitudes and the real correction in the extended space. We show here the simplest example of Higgs production in the bottom-quark fusion in the 5 flavour scheme.

Having separated the hard process from the non-perturbative part it is possible to systematically calculate partonic cross-sections with higher and higher precision within the well established framework of perturbation theory. Let us consider a process which is tree-level at the leading order (LO). Then, at the next to leading order (NLO) we need to consider two contributions with different partonic multiplicity, as depicted in Figure 3.1. One part, called *virtual* contribution, is the interference between the tree-level diagram and a loop diagram [1]. Additionally one needs to consider also the diagrams with an additional parton in the final state, contributing to the inclusive final state X. This part, called *real* contribution, enters at the same order of α_s as the virtual one, what can be easily inferred from Fig. 3.1, however, with the phase space enlarged by the additional particle.

The NLO cross sections develop infinities which need to be taken care of. The first class of infinities are the *UV divergences*, coming from the loop integration up to arbitrary large virtual momenta. They are removed by the renormalisation of the theory: the addition of divergent counterterms allows us to absorb the singularities in the renormalised parameters. Note, that the renormalisation procedure is model dependent and needs to be repeated, for any change of the model. Additionally the renormalisation procedure leads to arbitrariness in choosing the value of the renormalisation scale, which needs to be accounted for in estimating the uncertainties. A different type of infinities are the *IR divergences*, which appear due to the vanishing of scalar products of the particles' momenta, and are a consequence of the presence of massless particles. This can be caused by two situations: low momentum values, leading to *soft* singularities, and parallel momenta leading to *collinear* singularities in the massless limit. Note that IR singularities appear both in the real and virtual parts of the calculation, however they cancel exactly, as proven by the Kinoshita-Lee-Nauenberg theorem [92, 93]. This bears however some subtlety since the integration of the virtual and real contribution is independent, proceeding in phase spaces of different multiplicities, and thus some approach to extract the infinities from real and virtual contributions need to be applied: this is called *subtraction scheme*. On the other hand, the hadron collider specific collinear divergences from the incoming partons are absorbed into the renormalised parton densities. This arbitrariness of splitting the calculation into a hard subprocess and the PDFs goes with the cost of introducing yet another scale, the so called *factorisation scale*, and the

[1] Note that all one-loop integrals (in 4 dimensions) can be expressed in 4 basic scalar integrals (tadpoles, bubbles, triangles and boxes). This is not the case for two- or more-loop integrals.

dependence of the calculation on this scale also needs to be taken into account while assessing the uncertainty. The variation of the renormalisation and the factorisation scales suggests the order of magnitude of the missing higher order contributions.

The NNLO and even higher-order calculations follow a similar scheme, but are more complicated, due to the presence of more contributions, i.e. double virtual (two loops, same phase space as the tree level (i.e. N particles)), real-virtual (one loop, $N+1$ particle phase space) and double real ($N+2$ particle phase space) contributions with a much more complicated singularity structure.

Finally, one should keep in mind that actually in the SM we have two sources of radiative corrections: QCD and EW. Since the strong coupling constant g_s is considerably larger than the electroweak coupling g, roughly $g \approx g_s^2$, it is customary to consider the NLO EW corrections to enter with a similar impact as the NNLO QCD corrections[2]. NLO EW corrections, however, become increasingly important at high energies and transverse momenta.

3.2 Higgs boson production in the SM

Higgs physics in the era of the LHC undergoes a rapid development both on the theoretical and the experimental side. In this section, the current status of the phenomenological advances in the calculation of Higgs production cross section is reviewed. As a starting point in Figure 3.2a and 3.2b the cross sections of the different Higgs production channels in the energy range of the LHC and the leading order diagrams corresponding to these channels are presented, respectively. The Higgs production channels allow to explore different sectors of the SM: the Vector Boson Fusion (VBS) and Higgsstrahlung (VH) explore the EW sector, while the gluon fusion (GGF) and Higgs production associated with top quarks ($\bar{\text{t}}$tH) the Yukawa sector. It is immediately visible that GGF is by far the dominant production channel, even though it is loop suppressed already at LO. As shown in Eq. (3.1), the hadronic cross section does not depend only on the partonic process, but also on the parton content of the proton, and thus the vast dominance of the gluonic PDFs at small x yields the GGF to be the leading channel [94].

Although in Fig. 3.2(b) it seems to be easy to differentiate between the production channels, this is not the case when we consider higher order corrections. For example, VBF, which is characterised by two jets with large rapidity interval, can actually interfer with the gluonic production of Higgs associated with 2 jets. Also the radiative corrections open new partonic channels, e.g. going from LO to NLO in GGF in the real contribution not only the gg initial state contributes, but also gq and $\bar{q}q$.

Another important item is that actually all the particles we see in Fig. 3.2(b) as the final states, are not the *real* final states: what is seen in the detectors are electrons, muons, photons and jets. And thus the Higgs particle will never be seen *per se* in the detectors, its existence is manifested as a bump above all the other processes which yield the same final state (or a state which can be misidentified). Thus, despite we report here only on advances in the Higgs boson production calculations, modelling the background is just as important, especially in the processes in which the Higgs is not manifested as a narrow peak.

[2]This of course is a rough statement, and depends on the process.

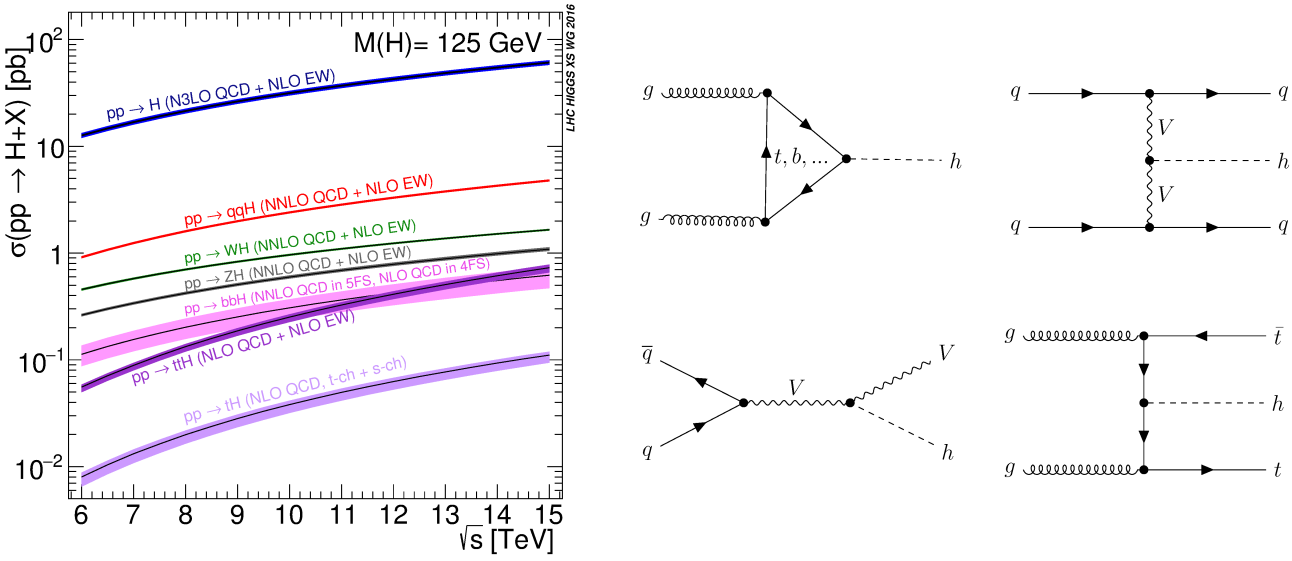

(a) (b)

Figure 3.2: Higgs production at the LHC. (a) On the left the rates of the individual channels depending on the collider energy are shown; taken from the Ref. [6]. (b) On the right the LO Feynman diagrams for the most abundant channels are presented.

In the following we briefly review the current status in the calculations of Higgs production in the four main production channels at the LHC in the SM and SMEFT, with the emphasis on gluon fusion as it is of main interest in this work. In this context also the Higgs transverse momentum spectrum will be discussed together with the resummation formalism, needed to correctly predict the low p_T range. Note that we will limit ourselves to cite just the calculations, omitting the references for the programs and frameworks which include those calculations. Further details and references can be found in Ref. [95].

3.2.1 The inclusive cross sections

3.2.1.1 Gluon Fusion

Gluon fusion, despite being a loop induced process, profits from the dominance of the gluon PDFs [94] and is the most abundant channel at the LHC. The loop-induced nature of the process makes it challenging to calculate higher order corrections and they are known exactly only up to NLO both in QCD [96–99] and EW [100, 101]. Although the EW corrections are small, the QCD corrections were found to be huge, accounting for over 50% of the cross section, and called for yet higher order calculations. Fortunately, since the Higgs mass is smaller than the top quark mass, it is possible to use the heavy top limit (HTL) approximation. In this approximation we work in an EFT in which the top quark field is integrated out, and the triangle loop at LO is shrunk to a point, thus gaining direct Higgs couplings to gluons. This approximation allowed to calculate the NNLO corrections [102–107] which accounted for a $\sim 20\%$ increase of the cross section. The recently completed N^{3}LO calculation in the HTL [38–40, 108–113] yields a correction at the percent

level, thus suggesting that the theoretical uncertainty is now under control.

To account at least partially for the finite top mass, at NNLO subleading terms in the heavy top expansion [114–117] were included. Additionally the HTL was used in the threshold-resummed calculations at the NNLL [118–126] and the N^{3}LL [127–129], which provide a good estimate of the remaining perturbative uncertainties. Recently, also the finite quark-mass effects in the resummation at the NLL has been included [130–132].

3.2.1.2 Vector Boson Fusion

Vector boson fusion is the second most abundant channel at the LHC (accounting for $\sim 10\%$ of the Higgs production rate). However, the possibility of tagging the jets (via suitable jets cuts) and the direct Higgs-vector boson interaction make it a suitable laboratory to study the electroweak symmetry breaking. Looking at the Feynman diagram in Figure 3.2(b) we see that the process resembles two *deep inelastic scatterings* (DIS) connected by the Higgs-vector boson coupling. This DIS approximation of treating independently the two quark lines, neglecting the cross talk between them, is commonly used to simplify the higher order calculations. It was used to calculate the process at the LO [133–136], as well to include the QCD corrections at NLO [137] of $\sim 10\%$ size, NNLO [138–141] with a 1% effect and recently at N^{3}LO [41]. The validity of the DIS approximation was confirmed by performing the full calculations at LO and NLO QCD [142–144]. The NLO EW corrections [145, 146] turned out to be of the same size as the NLO QCD corrections.

3.2.1.3 Higgsstrahlung off W$^\pm$ or Z

Although the Higgsstrahlung process accounts for just $\sim 1\%$ of the produced Higgs bosons it is important due to the possibility to tag the coproduced vector boson. This channel was the main search mode of the Higgs boson at the Tevatron. However, its utility at the LHC was questioned until the study of Ref. [147] in which it was shown that the sensitivity can be significantly improved by considering large transverse momenta and using jet substructure techniques. The LO calculation [148, 149] was extended by including the NLO QCD corrections [150] yielding a $\sim 30\%$ increase, and also the NNLO QCD corrections [151]. At the NNLO QCD level, the channel $gg \to ZH$ opens up where the Higgs and the Z bosons are produced through a heavy-quark loop to which the dominant contribution is given by the top quark. Although formally NNLO these corrections are enhanced by the large gluon luminosity and they are rather important (accounting for a $\sim 25\%$ change), especially in the region of large transverse momenta.The NLO EW corrections, causing a $\sim 10\%$ decrease of the cross section, are also available [152, 153].

3.2.1.4 Higgs boson production associated with top quarks

The $\bar{\text{t}}$tH is a challenging process both theoretically and experimentally, mainly because of its high multiplicity including top quarks in the final state. Due to the complicated final state (note, that t quarks decay into b-quarks and $W^\pm$ bosons which decay further) as well as the low rate, just recently the LHC has become sensitive to this channel [154–157]. This channel profits the most

from the increase of energy, and hopefully more precise measurements will become available soon, since it is crucial due to its direct connection to the top Yukawa coupling. The LO calculation was presented in Refs. [158–162], while the NLO QCD corrections were derived in Refs. [163–167]. The corrections account for about a 20% increase of the cross section. Recently also the EW corrections were included [168–170] yielding percent effects. Although we limit ourselves to discuss only the signal calculations, we emphasise here the importance of background estimates for this production channel. The high multiplicity, non resonant production and problems with the treatment of b quarks[3] make these estimates very model dependent and challenging (see e.g. the discussion in Section I.1.6 of Ref. [6].)

Double Higgs production The cross section for double Higgs production (HH) is unfortunately extremely small. However, the production rates in the different channels roughly follow the hierarchy of single Higgs production [171]. Due to this suppression, we will mostly review here the GGF channel. Double Higgs production is foreseen to be observed by the end of the LHC run, and it has a very important impact on the understanding of the Higgs potential, since it allows to set bounds on the Higgs trilinear coupling. Its value is fixed in the SM by the Higgs mass and the *vev*, but this needs to be confirmed experimentally. In the context of the GGF channel, the situation is even more critical, since the SM value of the trilinear coupling leads to a destructive interference between two LO contributions [172, 173]: the top loop box with two Yukawa radiations of Higgs bosons and the triangle top loop with the subsequent split of the Higgs into two. This means that a variation of the trilinear coupling from the SM value, would lead to a strong enhancement of the cross section [171]. As in the single Higgs production case, the existence of the loop already at leading order made the calculation of higher order corrections challenging and for a long time only NLO QCD corrections in the HTL were known [174], and they accounted for nearly doubling the LO cross section. Just recently the NLO QCD calculation including the top loops was presented [175–177] accounting for a $\sim 15\%$ decrease of the NLO cross section. A quite similar result was earlier obtained in the mixed approach in which the real part of the NLO corrections was included exactly and the virtual part was kept in the HTL [178, 179]. Also recently, the HTL was used again for the NNLO QCD corrections [180–182], which increases the cross section by $\sim 20\%$. The radiative corrections for the subleading channels are known at: NLO [171, 178] and NNLO QCD [183] in the DIS approximation for VBF, NLO [178] and NNLO QCD [171, 184] for VH and NLO QCD [178] for $\bar{\text{t}}\text{tH}$.

As a short summary of the current theoretical status in the inclusive calculations Table 3.1 shows the known perturbative corrections for the individual processes.

3.2.2 Transverse momentum spectrum of the Higgs boson

So far we have discussed inclusive cross sections, however differential cross sections and kinematic distributions, although more complicated to compute than the total rates, are just as important. This has a threefold motivation: the experiments have a limited acceptance and some cuts need to be applied in order to define a fiducial region. Additionally, applying kinematic cuts to a

[3]There exist two approaches to the treatment of the b quarks: when they are treated as massless and thus can originate directly from the proton PDFs (five flavour scheme (5FS)) or when they are massive and need to be produced explicitly in the hard process (four flavour scheme (4FS)).

Table 3.1: The summary of the current theoretical status of the Higgs production

Process	State-of-the-art	Remarks
GGF	N^3LO QCD + NLO EW	QCD corr. obtained in the HTL, exact known at NLO
HH in GGF	NNLO QCD	QCD corr. obtained in the HTL, exact known at NLO
VBF	N^3LO QCD + NLO EW	QCD corr. obtained in the DIS approximation, exact known at NLO
HV	NNLO QCD + NLO EW	
ttH	NLO QCD + NLO EW	

given final state can significantly increase the signal over background ratio. Finally, the kinematic distributions may reveal some effects which are hidden while just looking at the total rates. One of the most important kinematic distributions is the transverse momentum (p_T) spectrum of the Higgs boson, and we concentrate on it in this section.

As we already reviewed in Chapter 1, the first results on the Higgs p_T spectrum were obtained with the Run 1 [23–29] and first Run 2 data [30, 31]. The best resolution is obtained in the channels in which Higgs boson decay is fully reconstructed: di-photon and four-lepton. Although the uncertainties so far are large, exceeding the deviations of the measurements from the SM predictions, with the perspective of 3000 fb^{-1} of integrated luminosity [21], the experimental precision is expected to improve significantly. This calls for an effort not only on the experimental side but also from the theoretical side: new calculations and tools to predict the Higgs p_T spectrum are needed.

One of the important features of the Higgs p_T spectrum is that the scale explored in it is not only the Higgs mass m_h, but rather $\sqrt{m_h^2 + p_T^2}$ and thus the high p_T tail of the distribution allows to explore high energies, where there is hope to find New Physics effects. The significant drop of the cross section in the high-p_T region allows for still huge deviations from the SM predictions, even when the total rate will be measured to be very close to the SM one. Some of the effects hidden within the total rate, may become disentangled while the whole spectrum will be measured, since the latter provides more information than the total rate: the changes in the shape of the spectra may point towards deviations from the SM. As an example, the nature of the gluon-Higgs coupling may be elucidated from the Higgs transverse momentum spectrum.

The transverse momentum spectrum, as modelled directly from the fixed order (FO) calculations (i.e. Higgs + any fixed number of partons) suffers from a divergent behaviour at the low p_T region. Physically it is due to the fact, that the initial state partons radiate soft and colinear partons, which are neglected in the FO approach. There are several ways to improve the description in the low p_T region, such as parton showers (PS) usually used in the Monte Carlo generators, but in this work the analytic resummation is used.

In the past years a significant amount of work has been done to improve the theoretical predictions for the Higgs p_T spectrum. Let us address first the fixed order Higgs+jet calculations and then the problem of low p_T divergence and briefly outline the analytic resummation formalism.

3.2.2.1 Fixed-order resuls

The first results at the lowest order ($\mathcal{O}(\alpha_S^3)$) were known since a long time [185, 186] including the full quark-mass dependence. It took nearly ten years until the $\mathcal{O}(\alpha_S^4)$ corrections were computed [187–190], although in the HTL. Finite top-mass effects on the Higgs p_T distribution at NLO were estimated in Refs. [191–196]. The first partial results were also presented for the process including the full top mass dependence [197] in the analytic approach, and very recently the complete calculation was presented in the approach in which the two-loop virtual amplitude is calculated numerically [198]. In last years, also results on Higgs+jet production at $\mathcal{O}(\alpha_S^5)$ (NNLO) have been obtained in the HTL [199–201].

3.2.2.2 Low p_T resummation

In the low-p_T region ($p_T \ll m_h$), the convergence of the perturbative expansion is spoiled by the presence of large logarithmic terms of the form $\alpha_S^n \ln^m(m_h^2/p_T^2)$. In order to obtain reliable predictions also in this region, the large logarithmic terms must be resummed to all orders [202–206]. It is then essential to consistently match the resummed and fixed-order calculations in the intermediate p_T region, so as to obtain accurate predictions in the entire region of transverse momenta. In the case of the Higgs p_T spectrum the resummation has been performed up to next-to-next-to-leading logarithmic accuracy (NNLL) and matched to the fixed-order NNLO result up to $\mathcal{O}(\alpha_S^4)$ in the HTL [205]. Finite quark-mass effects have been included in the resummed spectrum up to NLL+NLO [207,208]. The recent computation of the $\mathcal{O}(\alpha_S^5)$ corrections at high-p_T, together with new available information on the logarithmic structure at the same order [209] would in principle allow to extend the accuracy of this calculation.[4]

We consider the inclusive hard-scattering process

$$h_1(p_1) + h_2(p_2) \to h(p_T) + X \tag{3.2}$$

where the colliding hadrons h_1 and h_2 with momenta p_1 and p_2 produce the Higgs boson h with transverse momentum p_T accompanied by an arbitrary and undetected final state X. Analogously to Eq. (3.1) the QCD factorisation theorem allows us to write

$$\frac{d\sigma}{dp_T^2}(p_T, s) = \sum_{i,j} \int_0^1 dx_1 dx_2 f_{i/h_1}(x_1, \mu_F^2) f_{j/h_2}(x_2, \mu_F^2) \frac{d\hat{\sigma}_{h,ij}}{dp_T^2}(p_T, \hat{s}, \alpha_S(\mu_R^2), \mu_R^2, \mu_F^2)\,, \tag{3.3}$$

where $f_{i/h}(x, \mu_F^2)$ are the parton densities of the colliding hadrons at the factorization scale μ_F^2, $d\hat{\sigma}_{h,ij}/dp_T^2$ is the partonic cross section, $\hat{s} = x_1 x_2 s$ is the squared partonic centre-of-mass energy, and μ_R is the renormalization scale[5]. In the low-p_T region ($p_T \ll m_h$), the perturbative expansion is affected by large logarithmic terms of the form $\alpha_S^n \ln^m(m_h^2/p_T^2)$, with $1 \le m \le 2n$. This results in a singular behaviour of the cross section as $p_T \to 0$. To cure this problem we need to resum these terms to all orders in α_S. To properly account for transverse-momentum conservation, the

[4] Work in this direction has been recently presented in Ref. [210].

[5] Throughout this work we use parton densities as defined in the $\overline{\text{MS}}$ factorization scheme and $\alpha_S(q^2)$ is the QCD running coupling in the $\overline{\text{MS}}$ renormalization scheme, with top quarks decoupled.

resummation is carried out in impact parameter (b) space [203, 204, 211]. In the following we use the formalism of Ref. [205]. The partonic transverse-momentum cross section is decomposed as

$$\frac{d\hat{\sigma}_{h,ij}}{dp_T^2} = \frac{d\hat{\sigma}^{(\mathrm{res.})}_{h,ij}}{dp_T^2} + \left(\frac{d\hat{\sigma}_{h,ij}}{dp_T^2} - \frac{d\hat{\sigma}^{(\mathrm{res.})}_{h,ij}}{dp_T^2}\right)_{\mathrm{f.o.}} . \tag{3.4}$$

The first term, $d\hat{\sigma}^{(\mathrm{res.})}_{h,ij}$, on the right-hand side of Eq. (3.4) contains all the logarithmically enhanced terms, and is evaluated by resumming them to all orders. The second term is finite, and can be computed by a fixed-order truncation of the perturbative series: It is obtained by computing the standard fixed-order result valid at large p_T and subtracting the expansion of the resummed term up to the same fixed order. This matching procedure ensures that the resummed and fixed-order components are combined to achieve uniform formal accuracy from the small- to the large-p_T region.

The explicit expression of the resummed component is

$$\frac{d\hat{\sigma}^{(\mathrm{res.})}_{h,ij}}{dp_T^2} = \frac{m_h^2}{\hat{s}} \int_0^\infty db\, \frac{b}{2} J_0(bp_T) \mathcal{W}_{ij}(b, m_h, \hat{s}; \alpha_{\mathrm{S}}) \,, \tag{3.5}$$

where $J_0(x)$ is the 0th-order Bessel function and the factor $\mathcal{W}$ embodies the all-order resummation of the large logarithmic terms. Let us recall here the N-th Mellin moment g_N of a function $g(x)$:

$$g_N = \int_0^1 dx x^{N-1} g(x), \tag{3.6}$$

since the all-order structure of $\mathcal{W}_{ij}$ is better expressed by considering the N-moments with respect to $z = m_h^2/\hat{s}$ at fixed m_h given by

$$\mathcal{W}_N(b, m_h, \alpha_{\mathrm{S}}) = \mathcal{H}_N(m_h, \alpha_{\mathrm{S}}, m_h^2/Q^2) \exp\{\mathcal{G}_N(\alpha_{\mathrm{S}}, \tilde{L}, m_h^2/Q^2)\} \tag{3.7}$$

where

$$\tilde{L} = \ln\left(Q^2 b^2/b_0^2 + 1\right) \tag{3.8}$$

and $b_0 = 2e^{-\gamma_E}$ ($\gamma_E = 0.5772...$ is the Euler number). The function $\mathcal{H}_N$ in Eq. (3.7) does not depend on the impact parameter b and can thus be expanded in powers of α_{S} as

$$\mathcal{H}_N(m_h, \alpha_{\mathrm{S}}, m_h^2/Q^2) = \sigma_0(\alpha_{\mathrm{S}}, m_h)\left[1 + \left(\frac{\alpha_{\mathrm{S}}}{\pi}\right)\mathcal{H}_N^{(1)} + \left(\frac{\alpha_{\mathrm{S}}}{\pi}\right)^2 \mathcal{H}_N^{(2)} + \dots\right] \tag{3.9}$$

where $\sigma_0(\alpha_{\mathrm{S}}, m_h)$ is the lowest order partonic cross section. The dependence on b is fully contained in the exponent $\mathcal{G}_N(\alpha_{\mathrm{S}}, \tilde{L}, m_h^2/Q^2)$ whose expansion reads

$$\mathcal{G}_N(\alpha_{\mathrm{S}}, \tilde{L}, m_h^2/Q^2) = \tilde{L} g^{(1)}(\alpha_{\mathrm{S}}, \tilde{L}) + g_N^{(2)}(\alpha_{\mathrm{S}}, \tilde{L}) + \frac{\alpha_{\mathrm{S}}}{\pi} g_N^{(3)}(\alpha_{\mathrm{S}}, \tilde{L}) + \dots \tag{3.10}$$

where $g^{(1)}$ controls the leading logarithmic (LL) terms, $g_N^{(2)}$ the NLL terms, and so forth. The formalism we have briefly recalled defines a systematic expansion of Eq. (3.4), whose terms are denoted by NLL+NLO, NNLL+NNLO and so forth. The first label in this notation denotes the logarithmic accuracy, while the second one is referred to the accuracy of the matched fixed-order

calculation. In particular, the NLL+NLO accuracy is obtained by computing the resummed component including the coefficient $\mathcal{H}^{(1)}$ together with the functions $g^{(1)}$ and $g^{(2)}$, and by matching it to the $\mathcal{O}(\alpha_{\rm S}^3)$ fixed-order result valid at high p_T. The NNLL+NNLO accuracy is obtained by including also the coefficient $\mathcal{H}^{(2)}$ and the function $g_N^{(3)}$, and the finite component up to $\mathcal{O}(\alpha_{\rm S}^4)$.

The scale Q appearing in Eq. (3.7), called resummation scale, parametrizes the arbitrariness in the resummation procedure. Its role is analogous to the role played by the renormalization (factorization) scale in the renormalization (factorization) procedure. Although $\mathcal{W}_N$ does not depend on Q when evaluated at all perturbative orders, an explicit dependence on Q appears when the logarithmic expansion is truncated at a given order. In particular, since the scale Q appears in the definition of the large logarithmic term $\tilde{L}$, the resummation scale sets the scale up to which the resummation is effective.

As is well known (see Sect. 3 of Ref. [205]), the extrapolation of the resummed result to large transverse momenta, where the resummation cannot improve the accuracy of the fixed-order expansion, may lead to unjustified large uncertainties and ensuing lack of predictivity. In the numerical implementation of Eq. (3.4) we thus apply a smooth switching procedure as described in Ref. [212], where we combine the resummed and fixed order calculations

$$\frac{d\hat{\sigma}_{h,ij}}{dp_T^2} \to w(p_T)\left(\frac{d\hat{\sigma}_{h,ij}^{(\rm res.)}}{dp_T^2} + \left(\frac{d\hat{\sigma}_{h,ij}}{dp_T^2} - \frac{d\hat{\sigma}_{h,ij}^{(\rm res.)}}{dp_T^2}\right)_{\rm f.o.}\right) + (1-w(p_T))\left(\frac{d\hat{\sigma}_{h,ij}}{dp_T^2}\right)_{\rm f.o.}, \tag{3.11}$$

where the $w(p_T)$ function is defined as:

$$w(p_T) = \begin{cases} 1 & \text{for } p_T \le p_T^{sw} - \Delta p_T \\ f(p_T) & \text{for } p_T^{sw} - \Delta p_T \le p_T \le p_T^{sw} + \Delta p_T \\ 0 & \text{for } p_T \ge p_T^{sw} + \Delta p_T, \end{cases} \tag{3.12}$$

and $f(p_T)$ is a function which ensures that $w(p_T)$ is of class $\mathbf{C^1}$, i.e.:

$$f(p_T) = \frac{1}{2}\left(\cos\left(\pi\frac{p_T - (p_T^{sw} - \Delta p_T)}{2\Delta p_T}\right) + 1\right), \tag{3.13}$$

with p_T^{sw} and Δp_T being the parameters which need to be sensibly chosen. We also point out that, due to the definition of the logarithmic parameter in Eq. (3.8), the formalism of Ref. [205] fulfils a *unitarity constraint* such that, upon integration over p_T, the customary fixed-order prediction for the inclusive cross section is recovered. More precisely, by performing the resummation at NLL accuracy and including the fixed-order result up to $O(\alpha_{\rm S}^3)$ we obtain NLL+NLO accuracy, and the integral of the spectrum is fixed to the NLO total cross section. Despite the switching procedure discussed above the p_T spectra we are going to present fulfil such unitarity constraint to better than 1%.

Top- and bottom-mass effects can be included in the resummed spectrum along the lines of Refs. [207, 208][6]. The inclusion of the top mass does not lead to complications: since $m_t \sim m_h$ the computation of the p_T spectrum is still a *two scale* problem. The inclusion of the bottom-mass instead is more difficult. Since $m_b \ll m_h$, the computation of the p_T spectrum becomes a *three*

[6]For studies of the resummed p_T spectrum in explicit BSM models see for example Refs. [213–216].

scale problem, whose all-order solution is far from being trivial[7]. In Ref. [208] a simple solution to this problem was proposed, which implies a choice of different resummation scales for the top and bottom contributions. In particular, since, as discussed above, the resummation scale is the scale up to which the resummation is effective, it was suggested to choose for the bottom contribution a *lower* scale as compared to the top contribution. In Ref. [214] this approach has been extended to consider three different resummation scales for the top contribution, the bottom contribution, and the top-bottom interference.

3.3 Higgs boson production in the SMEFT

Moving from the SM predictions towards SMEFT, one may question if the basis of the hadronic calculations—outlined in Section 3.1—is not affected by the new interactions. But the idea of the effective field theory description is that it changes the UV behaviour while keeping the low energy behaviour intact. Thus the SMEFT effects will enter the hard process of the partonic cross-section, but should not affect the general framework of the factorisation theorem. The SMEFT impact on the UV behaviour implies that the renormalisation of the SMEFT[8] is different than that of the pure SM.

The utility of the SMEFT is dictated by available calculations and their implementations in the tools that enable the analysis of the LHC data. The usual case is that only a subset of all the relevant operators is included in the predictions, based e.g. on the primary SILH "basis" [77] or on the assumption that some of the contributing operators can be bounded by another measurement. This approach, although not fully consistent from the EFT viewpoint, is actually very useful in practice, and it goes sometimes under the name of the *Phenomenological Lagrangians*. One of the earliest Phenomenological Lagrangians for Higgs physics is the κ framework [22] (see Sec. 2.2.1) extensively used by the LHC experiments [17], interpreted in terms of the Lagrangian in which the usual SM couplings are rescaled and two effective couplings $(\kappa_g, \kappa_\gamma)$ are added for the loop induced processes.

In the early days of the Higgs discovery, the Higgs Characterisation (HC) model [81] gained popularity. The HC Langrangian includes the effective terms, but is not a SMEFT as we defined it in the previous section. In this framework, for generality, the 125 GeV resonance discovered in the LHC could be identified as a spin 0, 1, or 2 boson with allowed CP violating interactions. The effective Lagrangian contains the rescaled SM-like terms, as well as the effective terms coupling the resonance with the gauge bosons. This Lagrangian is compact, as it omits many operators which appear in the SMEFT, e.g. all non-Higgs interactions, the chromomagnetic operators involving the "Higgs" field or operators involving more than one physical "Higgs" boson. This limits the generality of the HC framework, however the gained simplicity makes it very useful when it comes to the phenomenological and experimental analysis, especially in the context of determining the spin and CP properties of the new resonance. The model was used in many phenomenological applications, in particular for Higgs production: in the electroweak channels [221], the top induced channels [222, 223] or the multiple Higgs production including the top mass effects [179]. The use

[7] For recent work on this subject see Ref. [217–220].

[8] The SMEFT is not renormalisable in general, but can be renormalised order by order in the $1/\Lambda$ expansion.

of the framework was extended to NLO matched to the parton shower (PS) [224]. Experimental studies exploiting the HC model allowed the determination of the resonance's spin and parity in many production and decay channels, summarised in [225].

As already mentioned, there exist FeynRules [226] implementations of the genuine EFT basis: the BSM Characterisation [80] or the Warsaw basis [83, 84], which can be linked to various Monte Carlo generators. Despite that, there were so far very few reported applications and e.g. use of the SMEFTsim [83] was reported only in non-Higgs applications. Also the partial, only Higgs-involving, SILH-like basis—called *Higgs Effective Lagrangian* was implemented [227], and the applications for the single and double Higgs production in the electroweak channels were presented.

In recent years a number of independent calculations for Higgs production at the LHC—also at NLO—were presented, independent of the automated MC frameworks. The HV channel was studied including the SMEFT effects at NLO with PS [228]. This work was extended by adding the study of VBF at the same accuracy [229][9]. The vector boson fusion production mode was also studied at LO in [231].

The approximate results for the total gluon fusion Higgs production cross section including modified top and bottom Yukawa couplings and an additional direct Hgg interaction have been obtained at NNLO in Ref. [232] and at N^{3}LO in Refs. [233, 234]. In the context of the gluon fusion the inclusion of dimension 6 and 8 operators in the Higgs p_T-spectrum has been considered in Refs. [235–237] and [238, 239], respectively. Strategies for extracting information on the Higgs-gluon couplings from the measurements were studied in Ref. [237], and only there the inclusion of PS allowed to study the low-p_T range. Also in Ref. [240] the prospects of the determination of the Wilson coefficients in the HL-LHC and future colliders were considered. The mentioned studies usually omitted the effects of the chromomagnetic operator, but a dedicated paper analysing its effect on the LO Higgs production appeared [241]. It was followed by a LO study [242] on the interplay of the SMEFT operators entering top-induced Higgs production channels—with the chromomagnetic operator treated in the HTL. Recently, the program of the SMEFT at NLO QCD was started by the `MadGraph5_aMC@NLO` group [243] and in the context of Higgs physics led to the calculation of the $\bar{\text{t}}$tH, tH [244] and also recently the GGF [245] Higgs production[10]. Note that, due to the automated character of the calculations in the `MadGraph5_aMC@NLO` framework, they are complementary to the analytic calculations presented in this thesis. Also the double Higgs production in the GGF channel was studied, due to its crucial role in determining the Higgs potential and the sensitivity to the Higgs trilinear coupling leading to a possible enhancement of the production rate [171]. The LO results including the full top mass dependence were presented [247]. The HTL was used to obtain the NLO corrections [248], and recently also the NNLO corrections [249].

[9] This paper including the genuine SMEFT study was an extension of the anomalous coupling study of Ref. [230].
[10] Another strong interest of this program is top physics, see Ref. [246].

4

Higgs boson production via gluon fusion in the SMEFT – analytical results

In this Chapter we outline the details of the analytical calculations of Higgs boson production through gluon fusion, as well as of Higgs plus jet[1] production in the SMEFT. The chapter begins with defining our conventions: the operators considered in the calculation and the Feynman rules associated with them are presented. Next we present the analytical results of the LO calculation of the Higgs gluon fusion production, and afterwards the real part of the NLO corrections.

4.1 The Lagrangian and Feynman rules

We consider the effective Lagrangian, in the form of Eq. (2.27):

$$\mathcal{L} = \mathcal{L}_{SM} + \sum_i \frac{c_i^{(6)}}{\Lambda^2} \mathcal{O}_i^{(6)} + ... \tag{4.1}$$

where the SM is supplemented by a set of dimension-6 operators describing New Physics effects at a scale Λ well above the electroweak scale. In our study we consider the following four operators which enter gluon fusion Higgs production:

$$\begin{aligned} \mathcal{O}_1 &= |H|^2 G^a_{\mu\nu} G^{a,\mu\nu} \,, & \mathcal{O}_2 &= |H|^2 \bar{q}_L H^c t_R + h.c. \,, \\ \mathcal{O}_3 &= |H|^2 \bar{q}_L H b_R + h.c. \,, & \mathcal{O}_4 &= \bar{Q}_L H \sigma^{\mu\nu} T^a t_R G^a_{\mu\nu} + h.c. \,. \end{aligned} \tag{4.2}$$

[1] This accounts also for the real part of the NLO QCD corrections to inclusive gluon fusion Higgs production.

These operators, in the case of single Higgs production, may be rewritten as:

$$\frac{c_1}{\Lambda^2}\,\mathcal{O}_1 \to \frac{\alpha_S}{\pi v} c_g h G^a_{\mu\nu} G^{a,\mu\nu}\,, \tag{4.3}$$

$$\frac{c_2}{\Lambda^2}\,\mathcal{O}_2 \to \frac{m_t}{v} c_t h \bar{t}t\,, \tag{4.4}$$

$$\frac{c_3}{\Lambda^2}\,\mathcal{O}_3 \to \frac{m_b}{v} c_b h \bar{b}b\,, \tag{4.5}$$

$$\frac{c_4}{\Lambda^2}\,\mathcal{O}_4 \to c_{tg}\frac{g_S m_t}{2v^3}(v+h) G^a_{\mu\nu}(\bar{t}_L \sigma^{\mu\nu} T^a t_R + h.c), \tag{4.6}$$

where c_t and c_b contain the SM parts, too.

The Feynman rules for the new vertices arising from those operators are[2]:

- $\mathcal{O}_1$ - the gluon-Higgs point like coupling:

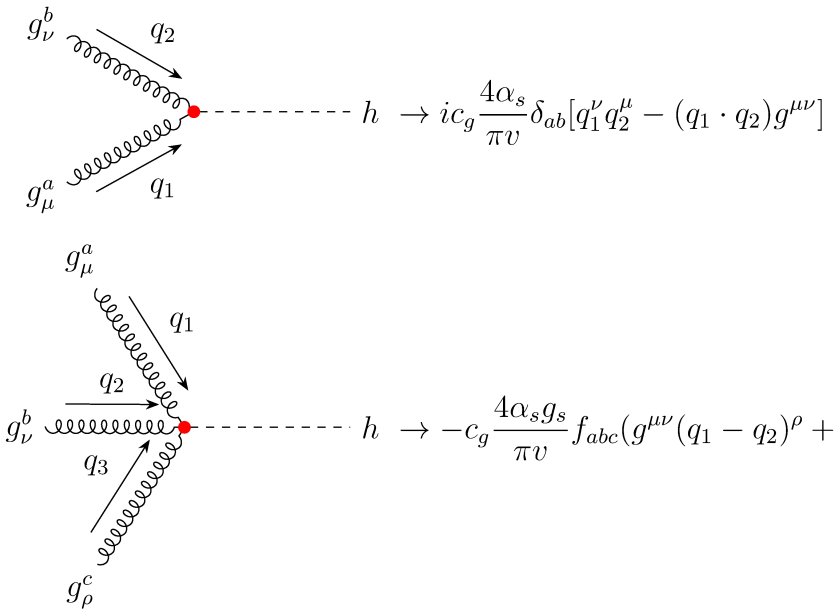

(4.7)

- $\mathcal{O}_2$ (and $\mathcal{O}_3$) - the modifications of the Yukawa couplings

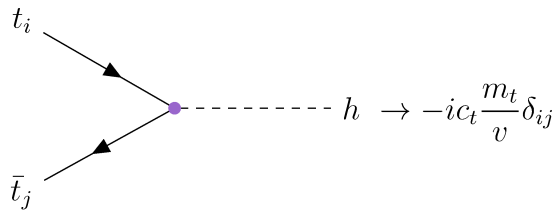

(4.8)

- $\mathcal{O}_4$ - the chromomagnetic operator yields a number of vertices which need to be considered in the calculations:

[2]We present only the Feynman rules relevant for single Higgs and Higgs plus jet production. Other Feynamn rules arising from these operators may be needed when considering e.g. the multiple Higgs production.

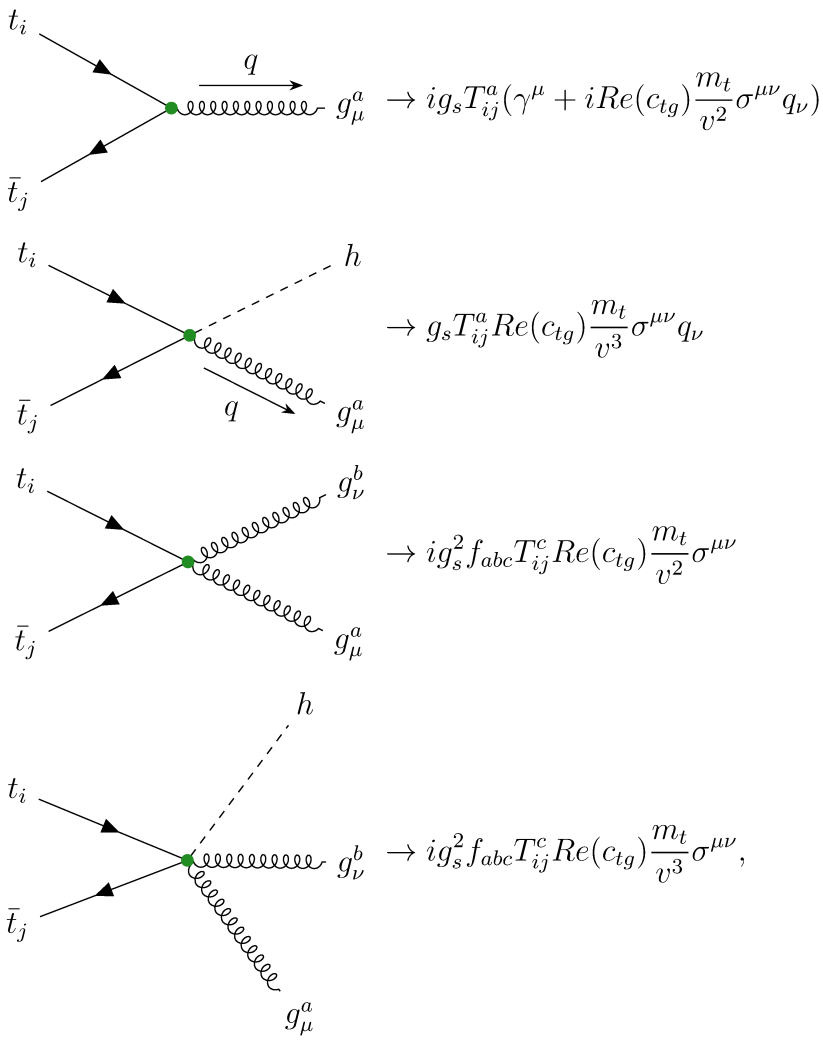

(4.9)

where $\sigma^{\mu\nu} = \frac{i}{2}[\gamma^\mu, \gamma^\nu]$ and in the first Feynman rule of Eq. (4.9) also the SM part is included.

When considering the Higgs production cross section, we will consider only diagrams which are of leading order in the effective couplings (i.e. only one insertion of c_g, c_t or c_{tg}), following the convention outlined in Section 2.5.2.2.

Let us extend here the discussion from Section 2.5.2.1, for simplification we keep only a top quark running in the loop. In the SM, the gluon fusion is a loop-induced process, due to the lack of direct couplings between the Higgs and gluons. In the SMEFT this situation changes, and this process is available already at the tree level. In the language of Section 2.5.2.2 this would be the LO SMEFT contribution. However, the loop-induced process including the modified Yukawa coupling seems to be a natural extension that should also be added to the effective description. This is additionally justified because the point like Higgs-gluon coupling is a loop-generated operator, while the modification of the Yukawa coupling is potentially a tree-level generated operator, and thus the loop suppression of order $1/16\pi^2$ should be compensated between these operators. The chromomagnetic operator, which also contributes to the full NLO SMEFT amplitude at one loop, is however a loop-generated operator, and thus its contribution should be doubly suppressed.

4.2 Higgs production via gluon fusion

We now consider the contribution of the effective operators from Eqs. (4.3)–(4.6) on the production cross section, by limiting ourselves to consider only the top quark contribution for simplicity. The relevant Feynman diagrams are displayed with the gluon-Higgs point-like coupling, Yukawa coupling modification and chromomagnetic operator marked in red, violet and green respectively:

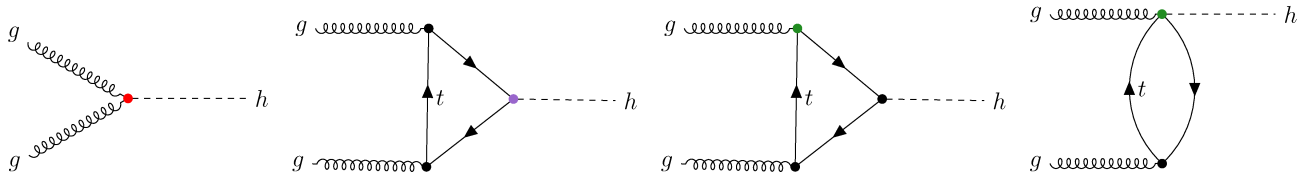

There is one more diagram which can be built with the contribution of the chromomagnetic operator:

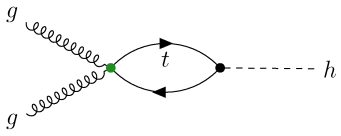

however it is identically equal zero due to colour conservation.

As outlined in Section 3.1, the cross section of the $pp \to (gg) \to h$ process factorises into the process independent parton density functions and a process dependent part. The leading order hadronic cross section can be written as:

$$\sigma_{LO}(pp \to h) = \sigma_0 \tau_H \frac{d\mathcal{L}_{gg}}{d\tau_H}, \tag{4.10}$$

with $\tau_H = {}^{m_h^2}/_{S_{pp}}$, where S_{pp} is the squared collider energy and

$$\frac{d\mathcal{L}_{gg}}{d\tau_H} = \int_{\tau_H}^{1} \frac{dx}{x} f_g(x;\mu_F) f_g(\tau_H/x;\mu_F) \tag{4.11}$$

denotes the gluonic luminosity depending on the gluon PDFs f_g. The σ_0 contribution is the partonic cross section factor which is defined as:

$$\sigma_0 = \frac{\pi}{64 m_h^4} |\mathcal{M}|^2 \tag{4.12}$$

with the corresponding amplitude, which can be cast into the form

$$\mathcal{M}(g(p_1) + g(p_2) \to h) = i \frac{\alpha_S}{3\pi v} \epsilon_{1\mu} \epsilon_{2\nu} [p_1^\nu p_2^\mu - (p_1 p_2) g^{\mu\nu}] F(\tau) \tag{4.13}$$

where $\tau = 4m_t^2/m_h^2$ and ϵ_1 and ϵ_2 are the polarization vectors of the incoming gluons. The computation of the function $F(\tau)$ has been addressed in the literature with contradicting results for the contribution of the chromomagnetic dipole operator [241, 242] (see also Ref. [250]). In Ref. [241] it has been found that the UV divergences in the bubble and triangle contributions

cancel out. In the revised version of Ref. [242] it is instead stated that the UV divergence is present and it has to be reabsorbed into the renormalised coefficient c_g.

Our results are consistent with the latter statement. We find

$$F(\tau) = \Gamma(1+\varepsilon)(\frac{4\pi\mu^2}{m_t^2})^{\varepsilon}(c_t F^{c_t}(\tau) + c_{g0} F^{c_g}(\tau) + Re(c_{tg})\frac{m_t^2}{v^2} F_0^{c_{tg}}(\tau)) \tag{4.14}$$

where

$$F^{c_t}(\tau) = \frac{3}{2}\tau[1 + (1-\tau)f(\tau)] \tag{4.15}$$

$$F^{c_g}(\tau) = 12 \tag{4.16}$$

$$F_0^{c_{tg}}(\tau) = -\frac{6}{\varepsilon} - 3[1 - \tau f(\tau) - 2g(\tau)] \tag{4.17}$$

with the functions

$$f(\tau) = \begin{cases} \arcsin^2 \dfrac{1}{\sqrt{\tau}} & \tau \geq 1 \\ -\dfrac{1}{4}\left[\ln \dfrac{1+\sqrt{1-\tau}}{1-\sqrt{1-\tau}} - i\pi\right]^2 & \tau < 1 \end{cases} \tag{4.18}$$

$$g(\tau) = \begin{cases} \sqrt{\tau-1}\arcsin \dfrac{1}{\sqrt{\tau}} & \tau \geq 1 \\ \sqrt{1-\tau}\left[\ln \dfrac{1+\sqrt{1-\tau}}{1-\sqrt{1-\tau}} - i\pi\right] & \tau < 1 \end{cases} . \tag{4.19}$$

The $1/\varepsilon$ divergence can be absorbed in the $\overline{\text{MS}}$ renormalisation of the coefficient c_g:

$$c_{g0} = c_g(\mu_R) + \delta c_g \tag{4.20}$$

with

$$\delta c_g = \frac{m_t^2}{2v^2} Re(c_{tg})\Gamma(1+\varepsilon)(4\pi)^{\varepsilon}(\frac{1}{\varepsilon} + \ln\frac{\mu^2}{\mu_R^2}), \tag{4.21}$$

where μ_R denotes the renormalization scale of c_g. The final result reads

$$F(\tau) = c_t F^{c_t}(\tau) + c_g(\mu_R) F^{c_g}(\tau) + Re(c_{tg})\frac{m_t^2}{v^2} F^{c_{tg}}(\tau) \tag{4.22}$$

where

$$F^{c_{tg}}(\tau) = -3(1 - \tau f(\tau) - 2g(\tau) + 2\ln\frac{\mu_R^2}{m_t^2}). \tag{4.23}$$

In the HTL $m_t^2 \gg m_h^2$ we arrive at:

$$F^{c_t}(\tau) \to 1 \qquad F^{c_g}(\tau) \to 12 \qquad F^{c_{tg}}(\tau) \to 6(1 - \ln\frac{\mu_R^2}{m_t^2}) \tag{4.24}$$

In the SM we have $c_t = 1$ and $c_g = c_{tg} = 0$, so that $F(\tau) \to F^{c_t}(\tau)$.

In Ref. [251] data on top production are used to extract constraints on c_{tg}. The resulting region of allowed values of c_{tg} has been found to be

$$-0.04 \lesssim c_{tg} \lesssim 0.04. \tag{4.25}$$

This bound implies that the impact of the chromomagnetic operator contribution on the total cross section should be less than 20%. We conclude that although smaller than the impact of c_g the effect of c_{tg} can still be relevant. We note, however, that the chromomagnetic operator provides a contribution which is formally $\mathcal{O}(y_t^2)$ with respect to the others[3]. In a strict expansion in α_S it can be neglected, thus providing the second formal reason to treat this operator as subleading.

Focusing on the impact of c_t and c_g, we note that the total cross section alone does not allow us to disentangle the coefficients c_g and c_t, since:

$$\sigma \approx |12c_g + c_t|^2 \sigma_{SM} \quad (HTL)\,. \tag{4.26}$$

As already noted in the literature [236], the transverse momentum spectrum allows us to lift this degeneracy.

4.3 Higgs plus jet production

The amplitude for Higgs plus jet production is essential to model the p_T spectra of the Higgs boson. Additionally, this contribution enters as a real part of the NLO QCD corrections. In case of the gluon fusion Higgs production, the NLO QCD cross section can be written as:

$$\sigma_{NLO}(pp \to H + X) = (1 + C_{virt})\sigma_{LO} + \Delta\sigma_{gg} + \Delta\sigma_{gq} + \Delta\sigma_{q\bar{q}} \tag{4.27}$$

where C_{virt} corresponds to the finite part of the virtual correction obtained from the two loop calculation, σ_{LO} is the LO hadronic cross section of Eq. (4.10), while $\Delta\sigma_{ij}$ are the finite parts of the real corrections with ij denoting the incoming partons. The $\Delta\sigma_{ij}$s receive contributions from the four leg amplitudes with one Higgs and three partons on the external lines. Here the calculation of these amplitudes is outlined for the relevant SMEFT operators. The calculation of the two-loop virtual corrections is beyond the scope of this thesis. The results has been recently obtained in Ref. [245].

The contributions to $\Delta\sigma_{ij}$ are build up from several pieces [97]:

$$\begin{aligned}
\Delta\sigma_{gg} &= \int_{\tau_H}^1 d\tau \frac{d\mathcal{L}^{gg}}{d\tau} \frac{\alpha_s(\mu_R^2)}{\pi}\sigma_0 \\
&\quad \times \left(-\hat{\tau} P_{gg}(\hat{\tau}) \log(\frac{\mu_F^2}{\hat{s}}) + 12 \left(\left(\frac{\log(1-\hat{\tau})}{1-\hat{\tau}} \right)_+ - \hat{\tau}(2 - \hat{\tau}(1-\hat{\tau})) \log(1-\hat{\tau}) \right) + d_{gg}(\hat{\tau}, \tau_h) \right) \\
\Delta\sigma_{gq} &= \int_{\tau_H}^1 d\tau \sum_{q,\bar{q}} \frac{d\mathcal{L}^{gq}}{d\tau} \frac{\alpha_s(\mu_R^2)}{\pi}\sigma_0 \left(\hat{\tau} P_{gq}(\hat{\tau}) \left(-\frac{1}{2} \log(\frac{\mu_F^2}{\hat{s}}) + \log(1-\hat{\tau}) \right) + d_{gq}(\hat{\tau}, \tau_h) \right) \\
\Delta\sigma_{q\bar{q}} &= \int_{\tau_H}^1 d\tau \sum_{q} \frac{d\mathcal{L}^{q\bar{q}}}{d\tau} \frac{\alpha_s(\mu_R^2)}{\pi}\sigma_0 d_{q\bar{q}}(\hat{\tau}, \tau_h).
\end{aligned} \tag{4.28}$$

[3]One order of y_t comes indeed from the Lagrangian coefficient, but the second is related to the helicity flip in the loop.

In these equations $\hat{\tau} = {}^{\tau_H}/_{\tau}$. The process dependent parts are: d_{ij} - presented in the next sections - and σ_0 - the LO partonic cross section presented in Eq. (4.12). The other contributions are universal quantities: $\mathcal{L}^{ij}$ - the parton luminosities - and P_{ij} - the Altarelli-Parisi splitting functions [252]. We see the direct impact of the factorisation scale μ_F, while the renormalisation scale dependence enters through the QCD coupling $\alpha_s(\mu_R^2)$, which also contribute to the LO cross section σ_0.

In our calculations of the amplitudes we used: QGRAPH [253] for the generation of diagram topologies, FORM [254] for the algebraic manipulation on the amplitudes, the Clifford algebra and the tensor reduction, and MATHEMATICA [255] for the simplification of the results. For the tensor integral reduction we used the Passarino-Veltman approach [256], reducing them to the scalar integrals, with the help of MATHEMATICA and MAPLE [257] for the solving linear equation systems. These were also cross-checked against the FEYNCALC package [258, 259], and especially the PaVeReduce routine.

4.3.1 The gg channel

In this section we concentrate on the calculation of the amplitude $\mathcal{A}_{ggg}$ of the process dependent $d_{gg}(\hat{\tau}, \tau_h)$ part of the Eq. (4.28), which contributes to the real correction coming from the radiation of the extra gluon in the final state $gg \to hg$. It can be expressed as a one dimensional integral [97]:

$$d_{gg}(\hat{\tau}, \tau_h) = \frac{2}{1-\hat{\tau}} \int_0^1 \frac{dz}{z} \left(\hat{\tau}^4 \frac{|\sum_Q \mathcal{A}_{ggg}(s,t,u;m_Q)|^2}{|\sum_Q F(\tau_h; m_Q)|^2} - 1 - \hat{\tau}^4 - (1-\hat{\tau})^4 \right), \tag{4.29}$$

where $\tau_h = {}^{4m_Q^2}/_{m_h^2}$, $F(\tau_h; m_Q)$ is defined in Eq. (4.14). This is a subtracted formula which is needed as a real part of the inclusive NLO QCD calculation. In the case of the Higgs p_T spectrum only the $\mathcal{A}_{ggg}$ amplitude is needed.

When considering the $gg \to Hg$ process, the generic SM diagrams corresponding also to the Yukawa modifying operator are:

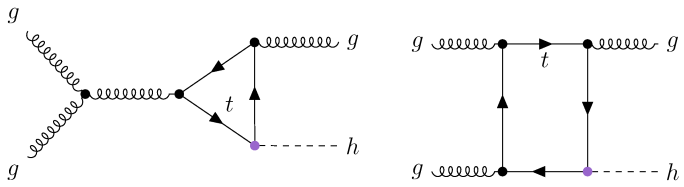

When considering the insertion of the chromomagnetic operator we obtain 54 additional diagrams, out of which just 2 types are the topological equivalents of the SM ones:

- Bubble-type diagrams:

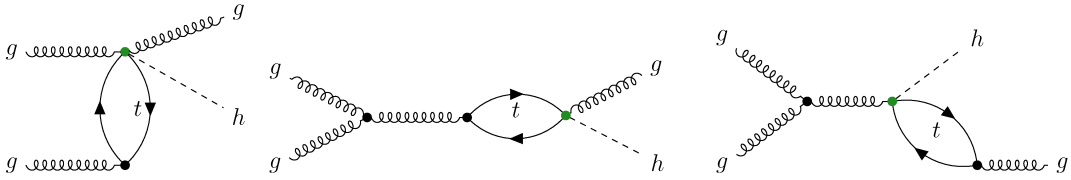

Analogously as in the LO case there is one additional type of bubble diagrams which is however identically equal to zero due to the vanishing trace of the Gell-Mann matrix:

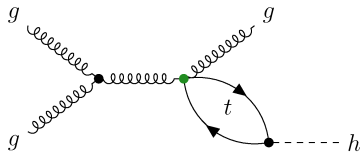

- Triangle-type diagrams:

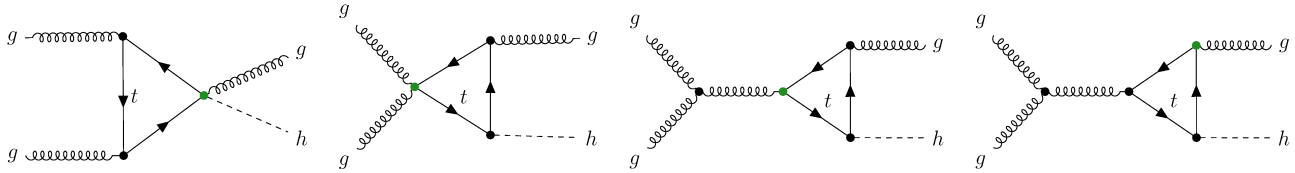

- Box-type diagrams:

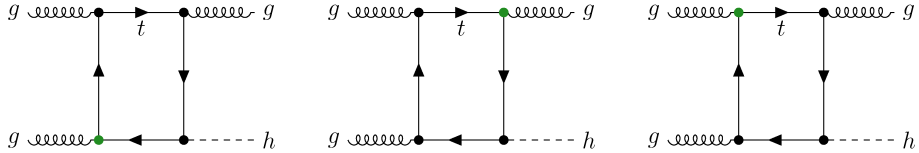

The presented diagrams are only the representatives of different types of diagrams, and each of them corresponds to a full set which is obtained by permutations of the gluons, i.e. every bubble-type diagram presented here correspond to a set of 3 diagrams, and the triangle- and box-type diagrams correspond to a set of 6 diagrams each, respectively. Finally, there are two types of diagrams arising from the point-like Higgs coupling to gluons:

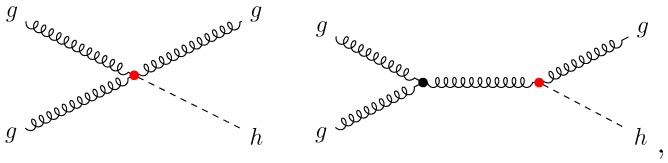

where again the 3 permutations of the gluons should be considered.

As an initial step towards the tensor integral reduction we projected the amplitudes onto four form factors (we follow the procedure of Ref. [260]), which correspond to all possible tensor structures of the three gluons system:

$$\mathcal{A}_{ggg}(p_1,p_2,p_3) = \frac{g_S^3}{12\pi^2 v} f_{abc} \mathcal{A}^{\mu\nu\rho}_{ggg} \epsilon_\mu(p_1)\epsilon_\nu(p_2)\epsilon_\rho(p_3) \tag{4.30}$$

$$\begin{aligned}\mathcal{A}^{\mu\nu\rho}_{ggg}(p_1,p_2,p_3) = {} & F_1(p_1,p_2,p_3)\mathcal{Q}_1^{\mu\nu\rho} + F_2(p_1,p_2,p_3)\mathcal{Q}_2^{\mu\nu\rho} \\ & + F_3(p_1,p_2,p_3)\mathcal{Q}_3^{\mu\nu\rho} + F_4(p_1,p_2,p_3)\mathcal{Q}_4^{\mu\nu\rho}\end{aligned} \tag{4.31}$$

The projectors needed to obtain the F_i form factors in D=4-2ε dimensions read:

$$\begin{aligned}
\mathcal{P}_1^{\mu\nu\rho} &= \mathcal{N}[-(2-\varepsilon)\mathcal{Q}_1^{\mu\nu\rho} + (1-\varepsilon)\mathcal{Q}_2^{\mu\nu\rho} - (1-\varepsilon)\mathcal{Q}_3^{\mu\nu\rho} + (1-\varepsilon)\mathcal{Q}_4^{\mu\nu\rho}] \\
\mathcal{P}_2^{\mu\nu\rho} &= \mathcal{N}[(1-\varepsilon)\mathcal{Q}_1^{\mu\nu\rho} - (2-\varepsilon)\mathcal{Q}_2^{\mu\nu\rho} - \varepsilon\mathcal{Q}_3^{\mu\nu\rho} + \varepsilon\mathcal{Q}_4^{\mu\nu\rho}] \\
\mathcal{P}_3^{\mu\nu\rho} &= \mathcal{N}[-(1-\varepsilon)\mathcal{Q}_1^{\mu\nu\rho} - (2-\varepsilon)\mathcal{Q}_3^{\mu\nu\rho} - \varepsilon\mathcal{Q}_2^{\mu\nu\rho} - \varepsilon)\mathcal{Q}_4^{\mu\nu\rho}] \\
\mathcal{P}_4^{\mu\nu\rho} &= \mathcal{N}[(1-\varepsilon)\mathcal{Q}_1^{\mu\nu\rho} - (2-\varepsilon)\mathcal{Q}_4^{\mu\nu\rho} - \varepsilon\mathcal{Q}_3^{\mu\nu\rho} + \varepsilon\mathcal{Q}_2^{\mu\nu\rho}]
\end{aligned} \tag{4.32}$$

where

$$\mathcal{N} = \frac{1}{4(1-2\varepsilon)(p_1\cdot p_2)(p_1\cdot p_3)(p_2\cdot p_3)} \tag{4.33}$$

and $\mathcal{Q}_i^{\mu\nu\rho}$ are the four possible tensor structures:

$$\begin{aligned}
\mathcal{Q}_1^{\mu\nu\rho} &= p_1^\rho p_2^\mu p_3^\nu - p_1^\nu p_2^\rho p_3^\mu + g^{\mu\nu}[(p_1\cdot p_3)p_2^\rho - (p_2\cdot p_3)p_1^\rho] \\
&\quad + g^{\mu\rho}[(p_2\cdot p_3)p_1^\nu - (p_1\cdot p_2)p_3^\nu] + g^{\nu\rho}[(p_1\cdot p_2)p_3^\mu - (p_1\cdot p_3)p_2^\mu] \\
\mathcal{Q}_2^{\mu\nu\rho} &= [(p_2\cdot p_3)p_1^\rho - (p_1\cdot p_3)p_2^\rho]\frac{p_1^\nu p_2^\mu - (p_1\cdot p_2)g^{\mu\nu}}{(p_1\cdot p_2)} \\
\mathcal{Q}_3^{\mu\nu\rho} &= [(p_2\cdot p_3)p_1^\nu - (p_1\cdot p_2)p_3^\nu]\frac{p_1^\rho p_3^\mu - (p_1\cdot p_3)g^{\mu\rho}}{(p_1\cdot p_3)} \\
\mathcal{Q}_4^{\mu\nu\rho} &= [(p_1\cdot p_3)p_2^\mu - (p_1\cdot p_2)p_3^\mu]\frac{p_2^\rho p_3^\nu - (p_2\cdot p_3)g^{\nu\rho}}{(p_2\cdot p_3)}
\end{aligned} \tag{4.34}$$

The derivation of the form factors follows from:

$$F_i(p_1,p_2,p_3) = \mathcal{P}_i^{\mu\nu\rho}\mathcal{A}_{ggg\,\mu\nu\rho}. \tag{4.35}$$

It is useful to note that due to the definitions of the tensor structures the form factors have the following property originating from the Bose symmetry between the external gluons:

$$F_2(p_1,p_2,p_3) = F_2(p_2,p_1,p_3) = -F_3(p_1,p_3,p_2) = F_4(p_3,p_2,p_1) \tag{4.36}$$

and F_1 is totally symmetric. Note that those relations hold only for the full set of gauge invariant diagrams, not for every single diagram separately.

While presenting the results of the calculation we use the Mandelstam variables, defined as:

$$s = 2p_1\cdot p_2 \qquad t = -2p_1\cdot p_3 \qquad u = -2p_2\cdot p_3. \tag{4.37}$$

The relative signs arise from momentum conservation:

$$p_1 + p_2 = p_3 + q \tag{4.38}$$

where q is the Higgs momentum. If we square the Higgs momentum taking into the account the above relation we get:

$$s + t + u = m_h^2. \tag{4.39}$$

The relations of the Mandelstam variables to the variables used in Eq. (4.28) read:

$$s = \frac{m_h^2}{\hat{\tau}} \qquad t = -s(1-\hat{\tau})z \qquad u = -s(1-\hat{\tau})(1-z) \tag{4.40}$$

Thus the form factors will be presented as functions of $s, t, u, m_h^2 (= s + t + u)$ and m_Q^2 - mass of the quark running in the loop.

To avoid problems arising from QCD ghosts coming from the three-gluon vertices we used the axial gauge to square the amplitudes for the $gg \to gh$ process. This corresponds to polarisation sums of the form:

$$\sum_{pol} (\epsilon_i(p_i)^\mu)^* \epsilon_i(p_i)^{\mu'} = -g^{\mu\mu'} + \frac{p_i^\mu n_i^{\mu'} + p_i^{\mu'} n_i^\mu}{p_i \cdot n_i} := P^{\mu\mu'} \tag{4.41}$$

where $i = 1, 2, 3$, for all three gluon momenta p_i, and the auxiliary vector n_i we choose to be one of the other gluon momenta ($\neq p_i$) what allowed to omit the terms proportional to n_i^2. For the squared amplitudes we obtain:

$$|\mathcal{A}_{ggg}|^2 = \frac{4\alpha_S^3}{9\pi v^2} \mathcal{A}^*_{ggg_{\mu\nu\rho}} P^{\mu\mu'} P^{\nu\nu'} P^{\rho\rho'} \mathcal{A}_{ggg_{\mu'\nu'\rho'}} = \frac{4\alpha_S^3}{9\pi v^2} \sum_{i,j=1}^{4} (F_i \mathcal{Q}_{i\mu\nu\rho})^* P^{\mu\mu'} P^{\nu\nu'} P^{\rho\rho'} F_j \mathcal{Q}_{j\mu'\nu'\rho'}. \tag{4.42}$$

The obtained expression for the squared amplitude is a function of s, t and u and includes also the mixed terms between form factors $F_i^* F_j$. We redefined the form factors in such a way,

$$\{F_1, F_2, F_3, F_4\} \to \{C_1, C_2, C_3, C_4\} \tag{4.43}$$

that we yield a simple expression for the squared amplitude:

$$|\mathcal{A}_{ggg}|^2 = \frac{4\alpha_S^3}{9\pi v^2} \frac{1}{stu} (|C_1|^2 + |C_2|^2 + |C_3|^2 + |C_4|^2). \tag{4.44}$$

The new form factors C_i are expressed by the form factors F_i:

$$\begin{aligned}
C_1(s,t,u;m_Q) &= \frac{1}{2} stu(2F_1(s,t,u;m_Q) + F_2(s,t,u;m_Q) - F_3(s,t,u;m_Q) + F_4(s,t,u;m_Q)) \\
C_2(s,t,u;m_Q) &= \frac{1}{2} stu F_2(s,t,u;m_Q) \\
C_3(s,t,u;m_Q) &= \frac{1}{2} stu F_3(s,t,u;m_Q) \\
C_4(s,t,u;m_Q) &= \frac{1}{2} stu F_4(s,t,u;m_Q)
\end{aligned} \tag{4.45}$$

Note that the C_i have the analogous s, t, u symmetry properties as the previous form factors, namely:

$$\begin{aligned}
C_3(s,t,u;m_Q) &= -C_2(t,s,u;m_Q) \\
C_4(s,t,u;m_Q) &= C_2(u,t,s;m_Q).
\end{aligned} \tag{4.46}$$

Here we present the results of $C_1(s,t,u;m_t)$ and $C_2(s,t,u;m_t)$ (C_3 and C_4 can be obtained from C_2 following Eq. (4.46)) in terms of the scalar integrals[4]:

$$C_i^{c_k} = \frac{1}{2\rho^2} \sum_{j=1}^{12} P_{i,j}^{c_k} T_j, \tag{4.47}$$

[4]Here we present the results for the top quark running in the loop, however the generalisation for the arbitrary quark Q is straightforward: $m_t \to m_Q$, $c_t \to c_Q$ and $c_{tg} \to c_{Qg}$.

where $\rho = {}^{m_h^2}/_{m_t^2}$, c_k is a coupling from which the form factor originates and the basis of the scalar integrals is defined as:

$$\begin{aligned}
T_1 &= 1 & T_2 &= 2(1 - g({}^4/_{\tilde{s}})) \\
T_3 &= 2(1 - g({}^4/_{\tilde{t}})) & T_4 &= 2(1 - g({}^4/_{\tilde{u}})) \\
T_5 &= 2(1 - g({}^4/_{\rho})) & T_6 &= 2f({}^4/_{\tilde{s}}) \\
T_7 &= 2f({}^4/_{\tilde{t}}) & T_8 &= 2f({}^4/_{\tilde{u}}) \\
T_9 &= 2f({}^4/_{\rho}) & T_{10} &= J(\tilde{s}, \tilde{t}, \tilde{u}) \\
T_{11} &= J(\tilde{s}, \tilde{u}, \tilde{t}) & T_{12} &= J(\tilde{u}, \tilde{s}, \tilde{t})
\end{aligned} \tag{4.48}$$

where $\tilde{x} = {}^{x}/_{m_t^2}$ for $x = s, t, u$. The $f(\tau)$ and $g(\tau)$ functions were given in Eq. (4.18) and (4.19) respectively. The $J(\tilde{s}, \tilde{t}, \tilde{u})$ function, coming from the box scalar diagram can be expressed as:

$$\begin{aligned}
J(\tilde{s}, \tilde{t}, \tilde{u}) &= I_3(\tilde{s}, \tilde{t}, \tilde{u}, \tilde{s}) + I_3(\tilde{s}, \tilde{t}, \tilde{u}, \tilde{u}) - I_3(\tilde{s}, \tilde{t}, \tilde{u}, \tilde{s} + \tilde{t} + \tilde{u}) \\
I_3(\tilde{s}, \tilde{t}, \tilde{u}, \tilde{x}) &= \frac{1}{\tilde{s}\tilde{u}} \frac{2}{\beta_+ - \beta_-} \left(\mathrm{Li}_2\left(\frac{\beta_-}{\beta_- - \alpha_-}\right) - \mathrm{Li}_2\left(\frac{\beta_+}{\beta_+ - \alpha_+}\right) + \mathrm{Li}_2\left(\frac{\beta_-}{\beta_- - \alpha_+}\right) \right. \\
&\quad \left. - \mathrm{Li}_2\left(\frac{\beta_+}{\beta_+ - \alpha_-}\right) + \log\left(-\frac{\beta_+}{\beta_-}\right) \log\left(1 + \frac{\tilde{x}\tilde{t}}{\tilde{s}\tilde{u}}\right) \right),
\end{aligned} \tag{4.49}$$

with $\alpha_\pm = \frac{1}{2}(1 \pm \sqrt{1 - \frac{4}{\tilde{x}}})$ and $\beta_\pm = \frac{1}{2}(1 \pm \sqrt{1 - \frac{4\tilde{t}}{\tilde{s}\tilde{u}}})$.

We begin by presenting the coefficients of the form factors arising from the SM-like diagrams, which also correspond to the contribution of the operator modifying the Yukawa coupling in the SMEFT:

$$\begin{aligned}
P^{c_t}_{1,1} &= 12\rho & P^{c_t}_{1,2} &= 0 \\
P^{c_t}_{1,3} &= 0 & P^{c_t}_{1,4} &= 0 \\
P^{c_t}_{1,5} &= 0 & P^{c_t}_{1,6} &= 3(4 - \rho) \\
P^{c_t}_{1,7} &= 3(4 - \rho) & P^{c_t}_{1,8} &= 3(4 - \rho) \\
P^{c_t}_{1,9} &= -9(4 - \rho) & P^{c_t}_{1,10} &= -\tfrac{3}{2}\tilde{s}\tilde{u}(4 - \rho) \\
P^{c_t}_{1,11} &= -\tfrac{3}{2}\tilde{s}\tilde{t}(4 - \rho) & P^{c_t}_{1,12} &= -\tfrac{3}{2}\tilde{t}\tilde{u}(4 - \rho)
\end{aligned} \tag{4.50}$$

$$\begin{aligned}
P^{c_t}_{2,1} &= -12\tilde{s}\frac{\tilde{u}\tilde{t} - \tilde{s}^2}{(\tilde{s} + \tilde{u})(\tilde{s} + \tilde{t})} \\
P^{c_t}_{2,2} &= 0 \\
P^{c_t}_{2,3} &= \frac{12\tilde{t}\tilde{u}\,(\tilde{u} + 2\tilde{s})}{(\tilde{s} + \tilde{u})^2} \\
P^{c_t}_{2,4} &= \frac{12\tilde{t}\tilde{u}\,\left(\tilde{t} + 2\tilde{s}\right)}{(\tilde{s} + \tilde{t})^2}
\end{aligned} \tag{4.51}$$

$$
\begin{aligned}
P_{2,5}^{c_t} &= -\frac{12\tilde{t}\tilde{u}}{(\tilde{s}+\tilde{t})^2(\tilde{s}+\tilde{u})^2}(\tilde{u}^2\tilde{t}+2\tilde{u}^2\tilde{s}+\tilde{u}\tilde{t}^2+4\tilde{u}\tilde{t}\tilde{s}+5\tilde{u}\tilde{s}^2+2\tilde{t}^2\tilde{s}+5\tilde{t}\tilde{s}^2+4\tilde{s}^3)\\
P_{2,6}^{c_t} &= -3(\tilde{s}-4)\\
P_{2,7}^{c_t} &= -\frac{3\left(4\tilde{u}^3\tilde{t}+8\tilde{u}^2\tilde{t}\tilde{s}-\tilde{u}^2\tilde{s}^2+4\tilde{u}^2\tilde{s}+4\tilde{u}\tilde{t}\tilde{s}^2+8\tilde{u}\tilde{s}^2+\tilde{s}^4-4\tilde{s}^3\right)}{\tilde{s}(\tilde{s}+\tilde{u})^2}\\
P_{2,8}^{c_t} &= -\frac{3\left(4\tilde{t}^3\tilde{u}+8\tilde{t}^2\tilde{u}\tilde{s}-\tilde{t}^2\tilde{s}^2+4\tilde{t}^2\tilde{s}+4\tilde{u}\tilde{t}\tilde{s}^2+8\tilde{t}\tilde{s}^2+\tilde{s}^4-4\tilde{s}^3\right)}{\tilde{s}(\tilde{s}+\tilde{t})^2}\\
P_{2,9}^{c_t} &= \frac{3}{\tilde{s}(\tilde{s}+\tilde{t})^2(\tilde{s}+\tilde{u})^2}(4\tilde{u}^3\tilde{t}^3+8\tilde{u}^3\tilde{t}^2\tilde{s}+4\tilde{u}^3\tilde{t}\tilde{s}^2+8\tilde{u}^2\tilde{t}^3\tilde{s}+15\tilde{u}^2\tilde{t}^2\tilde{s}^2\\
&\quad+4\tilde{u}^2\tilde{t}^2\tilde{s}+8\tilde{u}^2\tilde{t}\tilde{s}^3+8\tilde{u}^2\tilde{t}\tilde{s}^2+\tilde{u}^2\tilde{s}^4-4\tilde{u}^2\tilde{s}^3+4\tilde{u}\tilde{t}^3\tilde{s}^2+8\tilde{u}\tilde{t}^2\tilde{s}^3+8\tilde{u}\tilde{t}^2\tilde{s}^2\\
&\quad+8\tilde{u}\tilde{t}\tilde{s}^4+16\tilde{u}\tilde{t}\tilde{s}^3+4\tilde{u}\tilde{s}^5-8\tilde{u}\tilde{s}^4+\tilde{t}^2\tilde{s}^4-4\tilde{t}^2\tilde{s}^3+4\tilde{t}\tilde{s}^5-8\tilde{t}\tilde{s}^4+3\tilde{s}^6-12\tilde{s}^5)\\
P_{2,10}^{c_t} &= \frac{3\tilde{s}\tilde{u}(4-\tilde{s})}{2}\\
P_{2,11}^{c_t} &= \frac{3\tilde{s}\tilde{t}(4-\tilde{s})}{2}\\
P_{2,12}^{c_t} &= -\frac{3\tilde{t}\tilde{u}\left(4\tilde{u}\tilde{t}-\tilde{s}^2+12\tilde{s}\right)}{2\tilde{s}}
\end{aligned}
\tag{4.51}
$$

This result agrees with the one presented in Refs. [97, 185, 260].

The coefficients for the contribution arising from the chromomagnetic operator read:

$$
\begin{aligned}
P_{1,1}^{c_{tg}} &= 6\rho^2\left(1-2\log\tfrac{\mu_R^2}{m_t^2}\right) & P_{1,2}^{c_{tg}} &= -6\tilde{t}\tilde{u}\\
P_{1,3}^{c_{tg}} &= -6\tilde{s}\tilde{u} & P_{1,4}^{c_{tg}} &= -6\tilde{s}\tilde{t}\\
P_{1,5}^{c_{tg}} &= -6\rho^2 & P_{1,6}^{c_{tg}} &= -3\left(2\rho-\tilde{t}\tilde{u}\right)\\
P_{1,7}^{c_{tg}} &= -3\left(2\rho-\tilde{s}\tilde{u}\right) & P_{1,8}^{c_{tg}} &= -3\left(2\rho-\tilde{s}\tilde{t}\right)\\
P_{1,9}^{c_{tg}} &= 18\rho & P_{1,10}^{c_{tg}} &= -3\tilde{s}\tilde{u}(\rho+\tilde{t})\\
P_{1,11}^{c_{tg}} &= -3\tilde{s}\tilde{t}(\rho+\tilde{u}) & P_{1,12}^{c_{tg}} &= -3\tilde{t}\tilde{u}(\rho+\tilde{s})
\end{aligned}
\tag{4.52}
$$

$$
\begin{aligned}
P_{2,1}^{c_{tg}} &= \frac{6\tilde{s}\left(\tilde{s}^3+\tilde{s}^2(\tilde{t}+\tilde{u})-\tilde{s}\tilde{t}\tilde{u}-\tilde{t}\tilde{u}(\tilde{t}+\tilde{u})\right)}{(\tilde{s}+\tilde{t})(\tilde{s}+\tilde{u})}-12\tilde{s}^2\log\frac{\mu_R^2}{m_t^2}\\
P_{2,2}^{c_{tg}} &= 0\\
P_{2,3}^{c_{tg}} &= \frac{6\tilde{t}\tilde{u}\left(\tilde{s}^2+2\tilde{s}(\tilde{t}+\tilde{u})+\tilde{u}(\tilde{t}+\tilde{u})\right)}{(\tilde{s}+\tilde{u})^2}\\
P_{2,4}^{c_{tg}} &= \frac{6\tilde{t}\tilde{u}\left(\tilde{s}^2+2\tilde{s}(\tilde{t}+\tilde{u})+\tilde{t}(\tilde{t}+\tilde{u})\right)}{(\tilde{s}+\tilde{t})^2}
\end{aligned}
\tag{4.53}
$$

$$
\begin{aligned}
P_{2,5}^{c_{tg}} &= -\frac{6}{(\tilde{s}+\tilde{t})^2(\tilde{s}+\tilde{u})^2}(\tilde{s}^6+2\tilde{s}^5(\tilde{t}+\tilde{u})+\tilde{s}^4\left(\tilde{t}^2+6\tilde{t}\tilde{u}+\tilde{u}^2\right)+8\tilde{s}^3\tilde{t}\tilde{u}(\tilde{t}+\tilde{u})\\
&\quad+\tilde{s}^2\tilde{t}\tilde{u}\left(6\tilde{t}^2+11\tilde{t}\tilde{u}+6\tilde{u}^2\right)+2\tilde{s}\tilde{t}\tilde{u}(\tilde{t}+\tilde{u})^3+\tilde{t}^2\tilde{u}^2(\tilde{t}+\tilde{u})^2)\\
P_{2,6}^{c_{tg}} &= -6(\tilde{s}-\tilde{t}-\tilde{u})\\
P_{2,7}^{c_{tg}} &= -\frac{3\left(2\tilde{s}\left(\tilde{s}^3+\tilde{s}^2(\tilde{u}-\tilde{t})+\tilde{s}\tilde{u}(2\tilde{t}+\tilde{u})+\tilde{u}^2(\tilde{t}+\tilde{u})\right)+\tilde{t}\tilde{u}(\tilde{s}+\tilde{u})^2(\tilde{s}+2(\tilde{t}+\tilde{u}))\right)}{\tilde{s}(\tilde{s}+\tilde{u})^2}\\
P_{2,8}^{c_{tg}} &= -\frac{3\left(2\tilde{s}\left(\tilde{s}^3+\tilde{s}^2(\tilde{t}-\tilde{u})+\tilde{s}\tilde{t}(\tilde{t}+2\tilde{u})+\tilde{t}^2(\tilde{t}+\tilde{u})\right)+\tilde{t}\tilde{u}(\tilde{s}+\tilde{t})^2(\tilde{s}+2(\tilde{t}+\tilde{u}))\right)}{\tilde{s}(\tilde{s}+\tilde{t})^2}\\
P_{2,9}^{c_{tg}} &= \frac{3}{\tilde{s}(\tilde{s}+\tilde{t})^2(\tilde{s}+\tilde{u})^2}(2\tilde{s}(3\tilde{s}^5+3\tilde{s}^4(\tilde{t}+\tilde{u})-\tilde{s}^3\left(\tilde{t}^2-8\tilde{t}\tilde{u}+\tilde{u}^2\right)\\
&\quad-\tilde{s}^2\left(\tilde{t}^3-5\tilde{t}^2\tilde{u}-5\tilde{t}\tilde{u}^2+\tilde{u}^3\right)+\tilde{s}\tilde{t}\tilde{u}\left(2\tilde{t}^2+3\tilde{t}\tilde{u}+2\tilde{u}^2\right)+\tilde{t}^2\tilde{u}^2(\tilde{t}+\tilde{u}))\\
&\quad+\tilde{t}\tilde{u}(\tilde{s}+\tilde{t})^2(\tilde{s}+\tilde{u})^2(\tilde{s}+2(\tilde{t}+\tilde{u})))\\
P_{2,10}^{c_{tg}} &= -3\tilde{s}\tilde{u}(\tilde{s}-\tilde{u})\\
P_{2,11}^{c_{tg}} &= -3\tilde{s}\tilde{t}(\tilde{s}-\tilde{t})\\
P_{2,12}^{c_{tg}} &= -\frac{3\tilde{t}\tilde{u}\left(6\tilde{s}(\tilde{t}+\tilde{u})+\tilde{t}\tilde{u}(\tilde{s}+2(\tilde{t}+\tilde{u}))\right)}{2\tilde{s}}
\end{aligned}
\tag{4.53}
$$

The $\log\frac{\mu_R^2}{m_t^2}$ terms arise from the absorption of the $1/\varepsilon$ divergence in the renormalisation of the c_g coupling, as it was also done in the LO case, see Eqs. (4.17)–(4.23).

Finally we display also the results for the form factors arising from the point-like Higgs coupling to gluons:

$$
\begin{aligned}
C_1^{c_g}(s,t,u) &= 12\\
C_2^{c_g}(s,t,u) &= \frac{12s^2}{m_h^4},
\end{aligned}
\tag{4.54}
$$

which correspond also to the HTL of the SM multiplied by 12. Thus for completeness we cite the HTL for all the relevant operators, which is analogous to Eq. (4.24):

$$
C_i^{c_t}(s,t,u;m_t)\to\frac{1}{12}C_i^{c_g}(s,t,u)\qquad C_i^{c_{tg}}(s,t,u;m_t)\to\frac{1}{2}(1-\ln\frac{\mu_R^2}{m_t^2})C_i^{c_g}(s,t,u)\,.
$$

The final results for the form factors C_i can then be obtained analogously to Eq. (4.22) and for simplicity we again consider only the top loop contributions:

$$
C_i(s,t,u;m_t)=c_tC_i^{c_t}(s,t,u;m_t)+c_g(\mu_R)C_i^{c_g}(s,t,u)+Re(c_{tg})\frac{m_t^2}{v^2}C_i^{c_{tg}}(s,t,u;m_t).
\tag{4.55}
$$

4.3.2 The qg and $q\bar{q}$ channels

Unlike Higgs production at LO, in the case of an additional jet in the final state we need to also consider two other channels originating from the quark-gluon and the quark-antiquark initial states.

Their contributions to the NLO cross section read:

$$d_{q\bar{q}}(\hat{\tau},\tau_h) = \frac{2(1-\hat{\tau})^3}{3}\left|\frac{3\sum_Q \mathcal{A}_{qqg}(s;m_Q)}{4\sum_Q F(\tau_h;m_Q)}\right|^2$$
$$d_{gq}(\hat{\tau},\tau_h) = \frac{2}{3}\hat{\tau}^2\left[1+\int_0^1 \frac{dz}{z}\left(-1-2\frac{1-\hat{\tau}}{\hat{\tau}^2}+\frac{1+(1-\hat{\tau})^2(1-z)^2}{\hat{\tau}^2}\left|\frac{3\sum_Q \mathcal{A}_{qqg}(t;m_Q)}{4\sum_Q F(\tau_h;m_Q)}\right|^2\right)\right]. \tag{4.56}$$

It is visible that the contributions depend on the same function $\mathcal{A}_{qqg}(s;m_Q)$, which is needed for the p_T spectra calculation. This becomes clear looking at the contributing diagrams. The topologies of diagrams present in the SM and the HTL (corresponding to the c_t and c_g contributions) are:

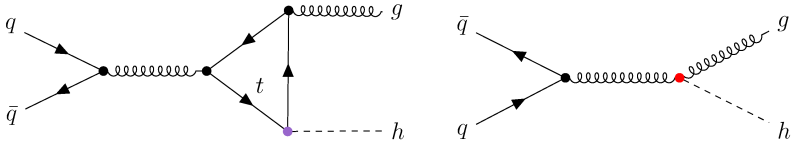

and for the inclusion of the chromomagnetic operator there are two bubble-type diagrams:

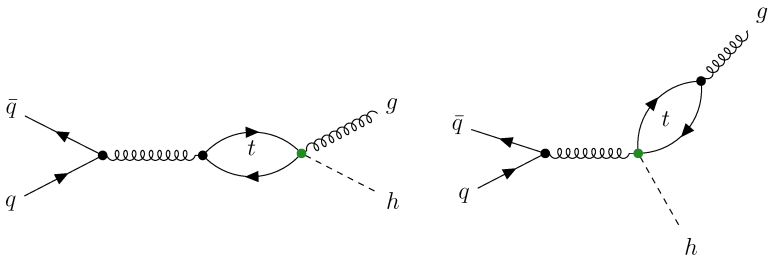

and two triangle-type diagrams:

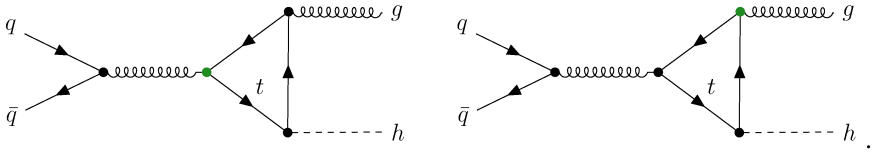

We present here only the $q\bar{q}$ contribution but it is clear that the qg diagrams can be obtained by crossing.

The amplitude of the $q\bar{q} \to gh$ process can be written in a form:

$$\mathcal{A}_{qqg}(p_1,p_2,p_3) = \frac{g_S^3}{12\pi^2 v}\bar{u}(p_2)\gamma^\mu T^a u(p_1)\left(g_{\mu\nu}-\frac{p_{3\mu}(p_1+p_2)_\nu}{(p_1+p_2)\cdot p_3}\right)\epsilon^\nu(p_3)\,A_{qqg}(s,t,u), \tag{4.57}$$

with the scalar part:

$$A_{qqg}^{c_k}(s;m_t) = \sum_{j=1}^{5} P_j^{c_k} T_j, \tag{4.58}$$

with the basis of the scalar integrals:

$$\begin{aligned} T_1 &= 1 \\ T_2 &= 2(1 - g(4/\tilde{s})) \quad T_3 = 2(1 - g(4/\rho)) \\ T_4 &= 2f(4/\tilde{s}) \qquad\quad T_5 = 2f(4/\rho) \end{aligned} \tag{4.59}$$

The coefficients corresponding to the SM and the Yukawa modifying operator in the SMEFT case read:

$$\begin{aligned} P_1^{c_t} &= \frac{8}{(\tilde{s} - \rho)} \\ P_2^{c_t} &= \frac{8}{(\tilde{s} - \rho)^2} \\ P_3^{c_t} &= -\frac{8}{(\tilde{s} - \rho)^2} \\ P_4^{c_t} &= \frac{4\,(4 - (\rho - \tilde{s}))}{(\tilde{s} - \rho)^2} \\ P_5^{c_t} &= \frac{4\,(-4 + (\rho - \tilde{s}))}{(\tilde{s} - \rho)^2}. \end{aligned} \tag{4.60}$$

While the chromomagnetic operator contribution reads:

$$\begin{aligned} P_1^{c_{tg}} &= -\frac{8(\rho - 2(\rho - \tilde{s}) \ln \frac{\mu_R^2}{m_t^2})}{(\rho - \tilde{s})} \\ P_2^{c_{tg}} &= -\frac{4\,((\rho - \tilde{s})^2 + 2\tilde{s}^2)}{(\rho - \tilde{s})^2} \\ P_3^{c_{tg}} &= -\frac{8\,((\rho - \tilde{s})^2 - \tilde{s}^2)}{(\rho - \tilde{s})^2} \\ P_4^{c_{tg}} &= -\frac{8(\rho - 2\tilde{s})}{(\rho - \tilde{s})^2} \\ P_5^{c_{tg}} &= \frac{8(\rho - 2\tilde{s})}{(\rho - \tilde{s})^2}. \end{aligned} \tag{4.61}$$

Again, we finalise the results by presenting the amplitude for the point-like Higgs gluon coupling which corresponds to the HTL of the SM:

$$A_{qqg}^{c_g} = -16 \tag{4.62}$$

The HTL of the relevant operators reads:

$$A_{qqg}^{c_t}(s; m_t) \to \frac{1}{12} A_{qqg}^{c_g} = -\frac{4}{3} \qquad A_{qqg}^{c_{tg}}(s; m_t) \to \frac{1}{2}(1 - \ln \frac{\mu_R^2}{m_t^2}) A_{qqg}^{c_g} = -8(1 - \ln \frac{\mu_R^2}{m_t^2})\,.$$

Again to obtain the full expression the individual terms need to be combined:

$$A_{qqg}(s; m_t) = c_t A_{qqg}^{c_t}(s; m_t) + c_g(\mu_R) A_{qqg}^{c_g}(s) + Re(c_{tg}) \frac{m_t^2}{v^2} A_{qqg}^{c_{tg}}(s; m_t), \tag{4.63}$$

considering only the top loop contributions for simplicity.

The analytical results presented in here were implemented in a modified, private version of HQT program [261, 262]. Whenever it was possible (i.e. in the SM and HTL case) the implementation was crosschecked numerically agains other programs. The definitions of the functions $g(\tau)$, $f(\tau)$ and $J(\tilde{s}, \tilde{t}, \tilde{u})$ were based on the HIGLU program [263]. The modified HQT program allowed us to perform the detailed phenomenological study of the Higgs transverse momentum spectra that is presented in the next Chapter.

5

Higgs boson transverse momentum spectra in the SMEFT – numerical results

5.1 Higgs Transverse-Momentum Spectra at NLL+NLO[1]

In this Section we discuss the inclusion of BSM effects in the computation. We first consider the effect of the operators in Eqs. (4.3)–(4.5) at NLL+NLO level, and then in Section 5.2 their approximate extension to NNLL+NNLO level, finally in Section 5.3 we study the impact of the chromomagnetic operator (Eq. (4.6)) at high-p_T. Our implementation is based on a modification of the program HqT [261,262]: a public tool for the analytic computation of the transverse-momentum spectrum of the Higgs boson. The contributions from finite top and bottom masses as well as the dimension-six operators are consistently included up to NLL+NLO accuracy. The fixed-order cross section is then cross checked with HIGLU [263] and HNNLO [208, 264, 265].

The operators in Eqs. (4.3)–(4.5) modify the computation of both the resummed and the fixed-order component in Eq. (3.4). However, by limiting ourselves to NLL+NLO, the computation can be greatly simplified. Indeed, the fixed-order result valid at high p_T can be obtained by introducing the c_t and c_b coefficients in the SM amplitude, and supplementing it with an additional contribution, proportional to c_g, which corresponds to the QCD amplitude computed in the HTL. As for the resummed component, due to the universality of our formalism [266], its only process-dependent contribution is encoded in the coefficients σ_0 and $\mathcal{H}^{(1)}$ of [266], which are determined by the Born- and one-loop-level, respectively. These amplitudes can also be easily obtained from the SM result by introducing the factors c_t and c_b where appropriate, and adding the point-like HTL amplitude in the SM with a coefficient c_g. We emphasise that the first EFT correction to the SM is obtained by interfering the EFT amplitudes with the corresponding SM contributions. With this strategy, we can obtain NLL+NLO predictions for the p_T spectrum consistently including the effects of the dimension-six operators. Thanks to the unitarity constraint according to the method of [205],

[1] Most of the Figures presented here come from Ref. [2].

the integral of the p_T spectrum exactly reproduces the fixed-order NLO result obtained with the inclusion of the same operators.

We consider pp collisions at $\sqrt{s} = 13$ TeV. Our computation is performed in the five-flavor scheme with the corresponding NLO set of the PDF4LHC2015 [267–272] parton distribution functions and the respective value of the strong coupling constant. For the top and bottom quarks running in the loop and for their Yukawa couplings on-shell masses $m_b = 4.92\,\text{GeV}$ and $m_t = 172.5\,\text{GeV}$ are used. As discussed in the previous paragraph, our computation of the NLL+NLO p_T spectrum fulfils a unitarity constraint, such that by integrating over p_T we recover the fixed-order NLO cross section. The appropriate scale choice for such a resummed computation is of the order of the Higgs boson mass m_h. In our study, however, we are also interested in the high-p_T region, where a dynamical scale choice has to be preferred. We thus proceed as follows: in the fixed-order computation, which is valid at high p_T, our central renormalization and factorization scales are set to $\mu_R = \mu_F = \mu_0 = \sqrt{p_T^2 + m_h^2}/2$. In the resummed computation (and its fixed-order expansion) we fix the central scales to $\mu_R = \mu_F = m_h/2$. To ensure a proper assignment of the resummation scales for the individual contributions to the cross section we follow the splitting of the SM cross section into a top, a bottom and an interference contribution as suggested in Ref. [214] and assign different scales to each of these contributions. In particular we choose:

$$Q_t = m_h/2 = 62.5\,\text{GeV}\,, \quad Q_b = 4\,m_b = 19.68\,\text{GeV}\,, \quad Q_{\text{int}} = \sqrt{Q_t\,Q_b} = 35.07\,\text{GeV}\,. \tag{5.1}$$

These values are motivated by the findings of Refs. [208,214,273,274]. As the top contribution is essentially insensitive to the top-quark mass in the small-p_T region, where resummation is relevant, we assign Q_t also to the contribution with the point-like ggh coupling, when choosing $c_g \neq 0$. In fact, regarding the splitting of the cross section into the three contributions outlined above we consider the c_g amplitude as part of the top amplitude. To ensure the smooth transition between the resummed and fixed-order calculations we used the switching parameters $p_T^{sw} = 125$ GeV and $\Delta p_T = 75$ GeV in the procedure described in Eqs. (3.11)–(3.13).

In summary, our results for the p_T spectrum depend on five scales: the renormalization and factorization scales and the three resummation scales discussed above. In order to estimate the perturbative uncertainty we study the corresponding scale variations. As far as renormalization and factorization scales are concerned, the uncertainties are estimated by performing the customary seven-point μ_R, μ_F variation, i. e. we consider independent variations within the range $\mu_0/2 \leq \mu_F, \mu_R \leq 2\mu_0$ with $1/2 < \mu_R/\mu_F < 2$. We then vary each of the three resummation scales (Q_t, Q_b, Q_{int}) by a factor of two around their central values (by keeping all the other scales at their central values). We finally combine the ensuing four uncertainty bands by taking the envelope, i.e. the minimum and maximum of the values obtained with the different scale choices for a given p_T. Figure 5.1 shows the reference SM prediction together with its perturbative uncertainty. We see that the uncertainty ranges from about ±20% at the peak, to about +50%, −30% at $p_T = 400$ GeV.

We start our analysis by considering the individual contribution of exactly one operator. The values of the coefficients c_t, c_g and c_b are varied as much as possible, while requiring the total cross section (integrating over p_T) to not deviate by more than 20% from the SM prediction, which is roughly the current experimental uncertainty on the measured Higgs cross section[2]. Fig. 5.2

[2]Note that variations of the p_T distributions can be much larger due to the large experimental uncertainties.

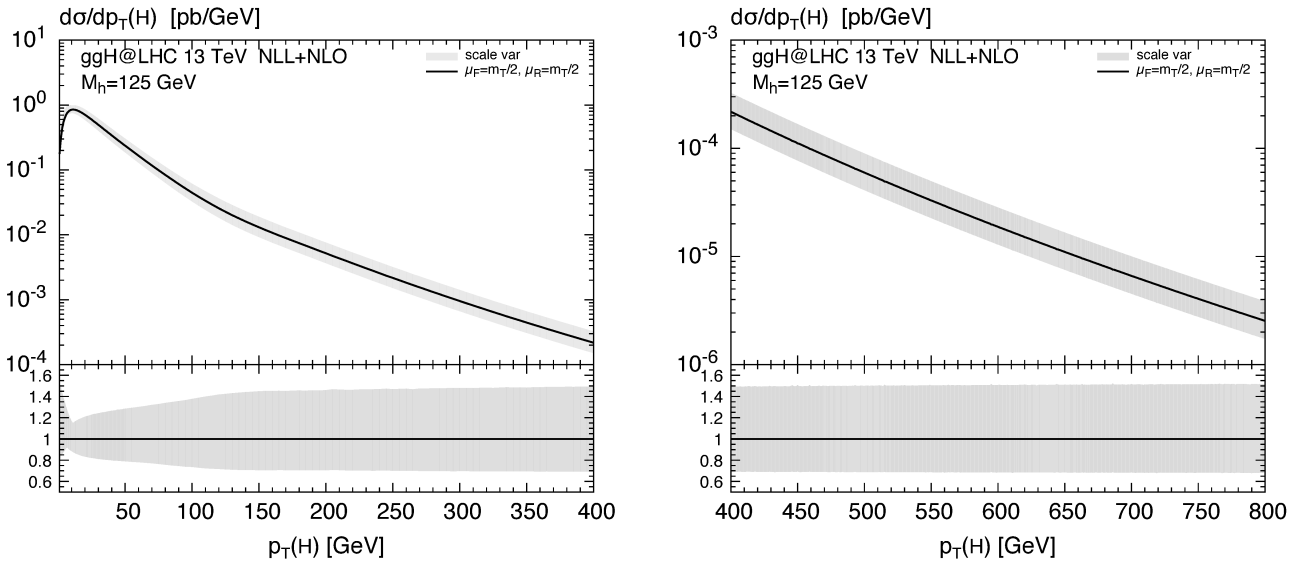

(a) (b)

Figure 5.1: SM prediction of the Higgs transverse momentum distribution at NLL+NLO for (a) $p_T \leq 400\,\text{GeV}$ and (b) $400\,\text{GeV} \leq p_T \leq 800\,\text{GeV}$, with the uncertainty bands due to scale variations as outlined in the text.

shows various predictions of the Higgs transverse-momentum spectrum: SM (black, solid), $c_t = 1.1$ (red, dotted), $c_t = 0.9$ (blue, dashed), $c_b = 4$ (green, dash-dotted), $c_b = -2$ (yellow, short-dashed), $c_g = 0.008$ (magenta, long-dashed) and $c_g = -0.008$ (light-blue, short-dotted). The lower frame illustrates the deviation from the SM prediction by taking the ratio of the curves in the main frame to the black, solid one. The grey-shaded band indicates the uncertainty of the SM result due to scale variations as defined above.

Looking at the low-p_T interval ($0 \leq p_T \leq 400\,\text{GeV}$) in Fig. 5.2 (a) we can directly deduce from the green, dash-dotted and yellow, short-dashed curves that modifications of the bottom Yukawa coupling through c_b dominantly affect the low-p_T shape of the distribution. In fact, at very low p_T we find effects that can even exceed the uncertainty of the SM prediction. As expected, $c_b < 1$ ($c_b > 1$) softens (hardens) the spectrum in that region.[3] The point-like Higgs-gluon coupling c_g, on the other hand, modifies the p_T-shape most notably at large transverse momenta ($400\,\text{GeV} \leq p_T \leq 800\,\text{GeV}$), see Fig. 5.2 (b), where a positive (negative) c_g value hardens (softens) the spectrum. As expected, modifications of solely the top Yukawa through c_t have almost exclusively the effect of a rescaling of the total cross section and the corresponding p_T distribution.

By and large all the deviations from the SM prediction through the separate inclusion of the dimension-six operators are within the scale uncertainty, although the differences in shape give some additional sensitivity to distinguish such effects. It is clear that in order to disentangle effects of this order it is necessary to start from a more accurate SM prediction.

[3]We point out, however, that this is true only when small deviations of c_b from its SM value $c_b = 1$ are considered. In this case the dominant effect of c_b is on the top-bottom interference. When c_b is significantly different from unity the squared bottom-loop contribution can change the picture.

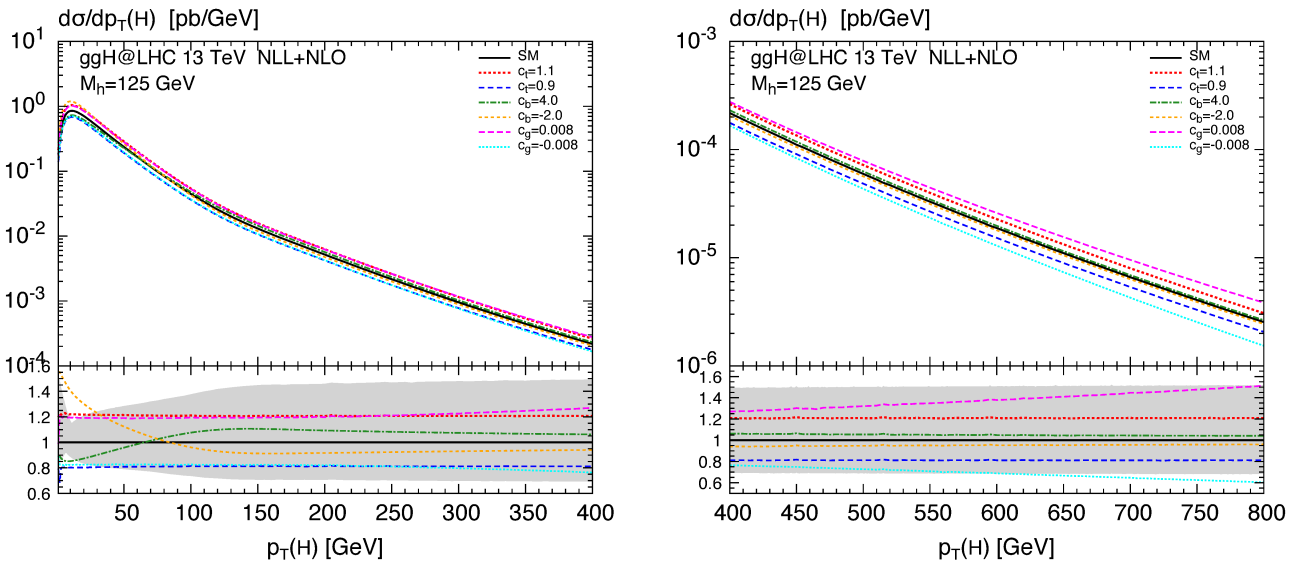

(a) (b)

Figure 5.2: Higgs transverse-momentum spectrum in the SM (black, solid) compared to separate variations of the dimension-six operators for (a) $p_T \leq 400\,\text{GeV}$ and (b) $400\,\text{GeV} \leq p_T \leq 800\,\text{GeV}$. The lower frame shows the ratio with respect to the SM prediction. The shaded band in the ratio indicates the uncertainty due to scale variations. See the text for more details.

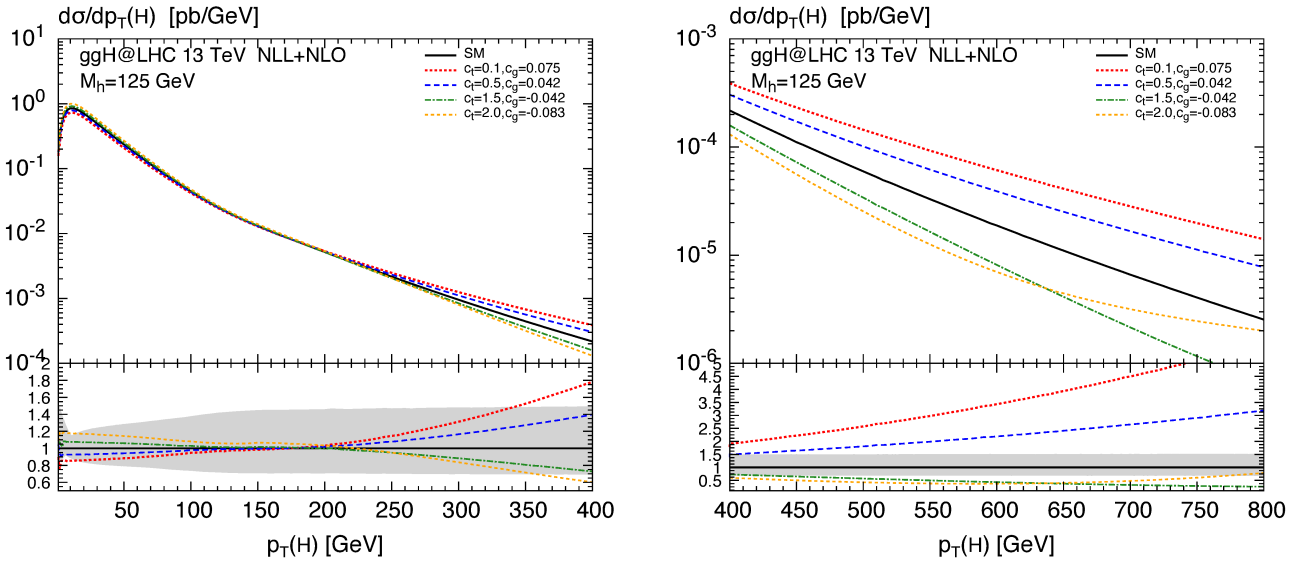

(a) (b)

Figure 5.3: Higgs transverse-momentum spectrum in the SM (black, solid) compared to simultaneous variations of c_t and c_g for (a) $p_T \leq 400\,\text{GeV}$ and (b) $400\,\text{GeV} \leq p_T \leq 800\,\text{GeV}$. The lower frame shows the ratio with respect to the SM prediction. The shaded band in the ratio indicates the uncertainty due to scale variations. See the text for more details.

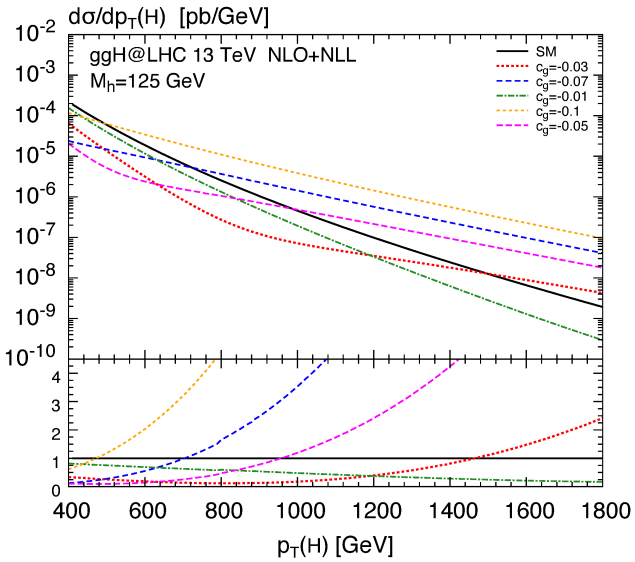

Figure 5.4: Higgs transverse-momentum spectrum in the SM (black, solid) compared to variations of the c_g dimension-six operator for high p_T. The lower frame shows the ratio with respect to the SM prediction. See the text for more details.

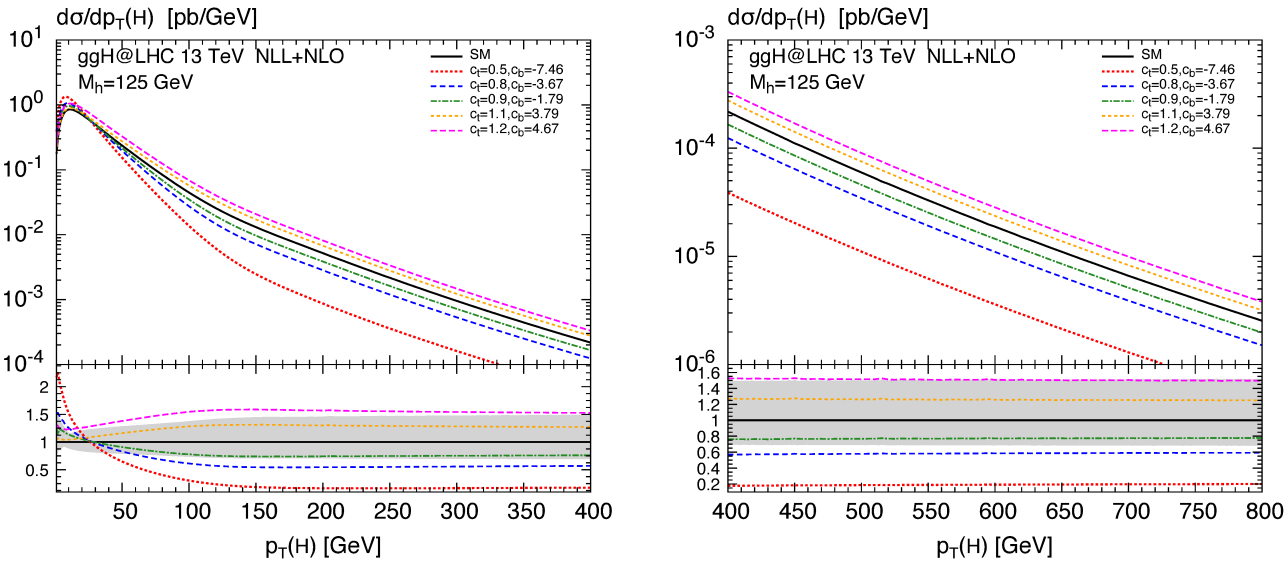

(a) (b)

Figure 5.5: Higgs transverse-momentum spectrum in the SM (black, solid) compared to simultaneous variations of c_t and c_b for (a) $p_T \leq 400\,\text{GeV}$ and (b) $400\,\text{GeV} \leq p_T \leq 800\,\text{GeV}$. The lower frame shows the ratio with respect to the SM prediction. The shaded band in the ratio indicates the uncertainty due to scale variations. See the text for more details.

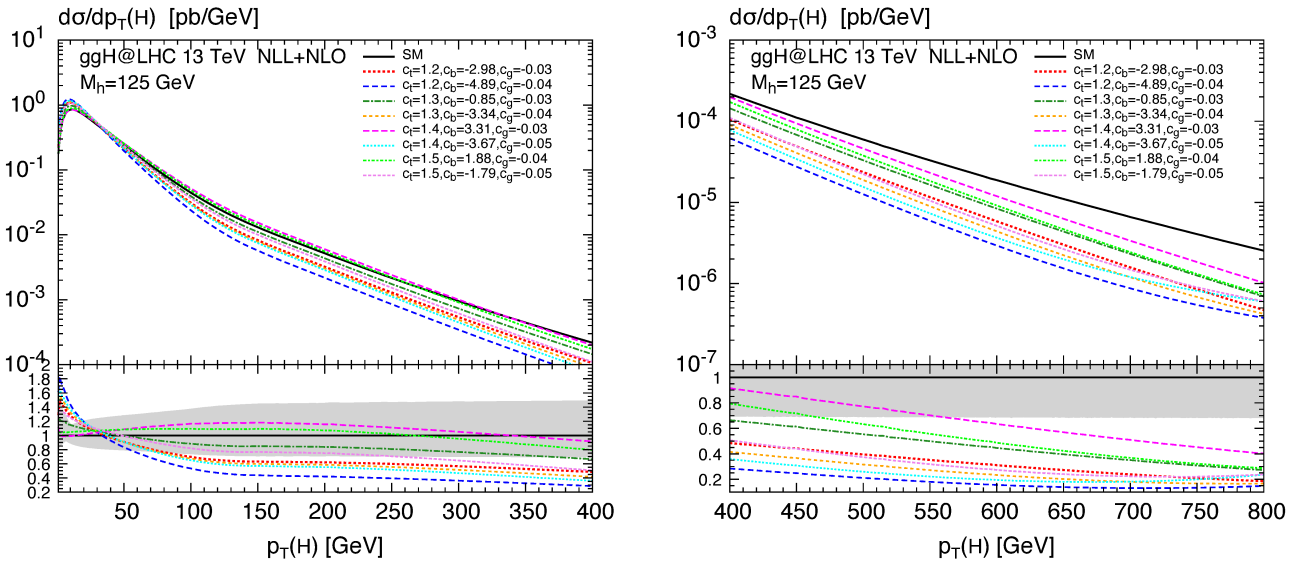

(a) (b)

Figure 5.6: Higgs transverse-momentum spectrum in the SM (black, solid) compared to simultaneous variations of c_t, c_g and c_b for (a) $p_T \leq 400\,\text{GeV}$ and (b) $400\,\text{GeV} \leq p_T \leq 800\,\text{GeV}$. The lower frame shows the ratio with respect to the SM prediction. The shaded band in the ratio indicates the uncertainty due to scale variations. See the text for more details.

By contrast, the simultaneous variation of more than a single coefficient, as considered in Figs. 5.3-5.6, gives rise to more significant effects. The c_g, c_t and c_b parameters are chosen in the ballpark suggested by the studies of Refs. [275–277], while still keeping the inclusive cross section within about 20% of its SM value. Indeed, many combinations of c_g, c_t and c_b can be found which mildly affect the total cross section, while significantly changing the shape of the spectrum.

In Fig. 5.3 we present the simultaneous variation of c_t and c_g. The general pattern of these figures follows the pattern of Fig. 5.2, but for the variations: $c_t = 0.1$, $c_g = 0.075$ (red, dotted); $c_t = 0.5$, $c_g = 0.042$ (blue, dashed); $c_t = 1.5$, $c_g = -0.042$ (green, dash-dotted) and $c_t = 2$ $c_g = -0.083$ (yellow, short-dashed). In this case, both the small and high-p_T behaviour of the spectrum is altered by the different combinations of c_t and c_g coefficients. It is clear that in particular the large-p_T region offers a good discrimination between the different structures of c_t and c_g in terms of shape. Again, negative (positive) c_g values will soften (harden) the spectrum. The effects are well beyond the theoretical uncertainties already at NLL+NLO. We note that the yellow, short-dashed curve corresponding to $c_t = 2$, $c_g = -0.083$ develops a minimum in the ratio to the SM around $\sim 650\,\text{GeV}$. This is due to a compensation between the negative interference between the $\mathcal{O}_1$ and $\mathcal{O}_2$ operators, which is proportional to $c_g c_t$ and the contribution of $\mathcal{O}_1$ itself, which is proportional to c_g^2 and tends to produce a harder spectrum with respect to the SM prediction. To validate this statement, in Fig. 5.4 we present the high-p_T behaviour of scenarios with different values of negative c_g. It is visible that the bend, caused by the dominance of the c_g^2 term, is moving toward the lower p_T with the growth of the $|c_g|$ value. The SMEFT predictions for these scenarios, even though below the SM total rate, tend to exceed the SM predictions for high enough p_T.

Fig. 5.5 shows spectra with modified top and bottom Yukawa couplings: $c_t = 0.5$, $c_b = -7.46$ (red, dotted); $c_t = 0.8$, $c_b = -3.67$ (blue, dashed); $c_t = 0.9$, $c_b = -1.79$ (green, dash-dotted); $c_t = 1.1$ $c_b = 3.79$ (yellow, short-dashed) and $c_t = 1.2$, $c_b = 4.67$ (magenta, long-dashed). In this case, the compensation of the BSM contributions is less straightforward, and it is difficult to compensate $c_t > 1$ without significantly affecting the inclusive cross section. For the magenta, long-dashed curve ($c_t = 1.2$, $c_b = 4.67$) we, thus, allow for a bigger change of the total cross section up to 30%. As pointed out before, the bottom-loop softens the spectrum and, since the variation of the bottom Yukawa coupling is rather large, the squared bottom-term is larger than the top-bottom interference term and the spectrum is softened also when negative c_b values are considered. The shape difference from the SM is very significant, but only in the small-p_T region, where the soft-gluon resummation is crucial to obtain a reliable prediction. Indeed, the contribution of the bottom loop decreases with growing p_T [278] and above 150 GeV the spectra have all very similar shapes, c_t driving their normalization.

Finally, we discuss spectra obtained by switching on all three SMEFT operators, as shown in Fig. 5.6: $c_t = 1.2$, $c_b = -2.98$, $c_g = -0.03$ (red, dotted), $c_t = 1.2$, $c_b = -4.89$, $c_g = -0.04$ (blue, dashed), $c_t = 1.3$, $c_b = -0.385$, $c_g = -0.03$ (green, dash-dotted), $c_t = 1.3$, $c_b = -3.34$, $c_g = -0.04$ (yellow, short-dashed), $c_t = 1.4$, $c_b = 3.31$, $c_g = -0.03$ (magenta, long-dashed); $c_t = 1.4$, $c_b = -3.67$, $c_g = -0.05$ (light-blue, short-dotted); $c_t = 1.5$, $c_b = 1.88$, $c_g = -0.04$ (light-green, short-dash-dotted) and $c_t = 1.5$, $c_b = -1.79$, $c_g = -0.05$ (violet, very-short-dashed). Our focus here is on scenarios with increased top-quark Yukawa coupling (up to $c_t = 1.5$). These scenarios would be of particular interest in the case in which the excess on the $t\bar{t}H$ rate over the SM prediction [154, 155] should be confirmed. In order to compensate the increase in the cross section driven by $c_t > 1$ a negative c_g has been chosen. We observe a general tendency of the BSM spectra to fall below the SM prediction in the intermediate and high transverse-momentum regions, which is due to the negative c_g contribution. The total rate is compensated by the enhancement in the low p_T region, due to a combination of the negative c_g coefficient with both negative and positive c_b modifications. Overall, we find sizable distortions of the p_T shapes due to the dimension-six operators far beyond the scale uncertainties of the NLL+NLO SM prediction, that exceed the previously considered scenarios with two simultaneous varied coefficients in both size and significance. Despite the similar overall behavior, the predictions for the various scenarios may differ significantly, which enables their discrimination when compared to data.

We conclude this Section with a comment on the validity of the EFT approach in the spirit of the Section 2.5.2.3. The computation we have performed is carried out under the assumption that we can consider the effects of higher-dimensional operators as a *small* perturbation with respect to the SM result. This implies in particular that the effect of dimension-eight operators can be neglected. This is not obvious, given that we are studying also the large transverse-momentum region.

To check the above assumption we have repeated our calculations by dropping the $\mathcal{O}(1/\Lambda^4)$ suppressed terms originating from the square of the dimension-six contributions—these scenarios are labelled "SILH" in the following Figures. In Fig. 5.7 we present the scenarios of separate variations of the dimension-six operators with and without the $\mathcal{O}(1/\Lambda^4)$ terms. We find that the differences between including and omitting the squared terms are very small, even at high transverse momenta. Only in the most extreme scenarios considered in Fig. 5.8 ($c_t = 0.1, c_g = 0.075$ and $c_t = 2, c_g = -0.083$) the $\mathcal{O}(1/\Lambda^4)$ effects are relevant. The yellow dashed line, corresponding

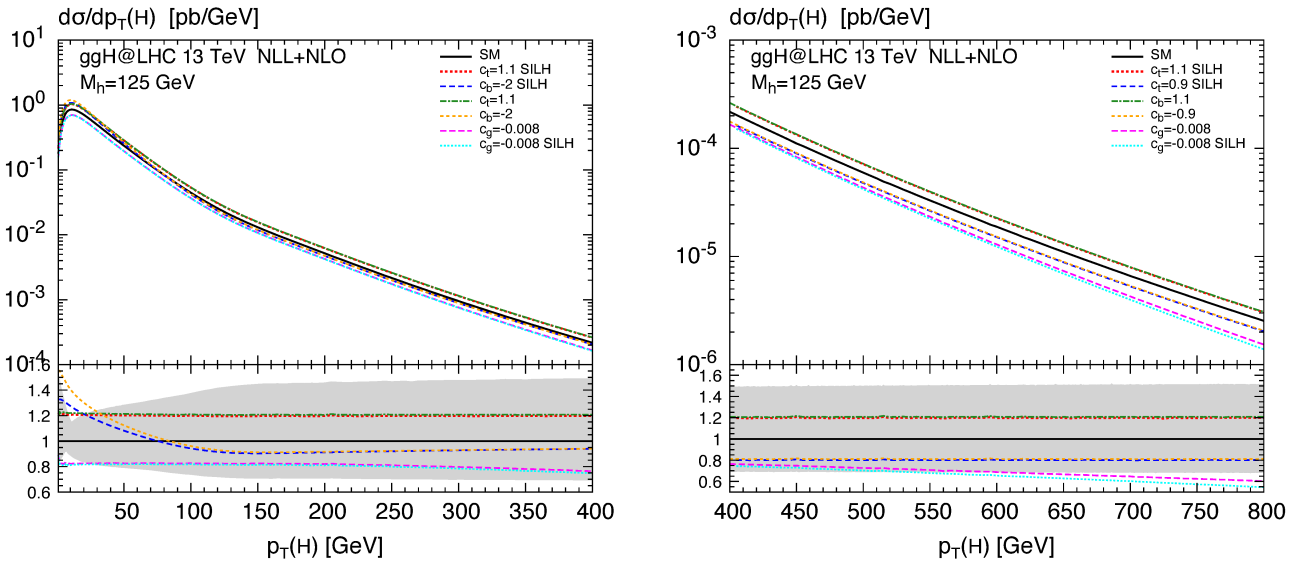

(a) (b)

Figure 5.7: Higgs transverse-momentum spectrum in the SM (black, solid) compared to separate variations of the dimension-six operators for (a) $p_T \leq 400\,\text{GeV}$ and (b) $400\,\text{GeV} \leq p_T \leq 800\,\text{GeV}$ including and omitting (SILH) the squared term. The lower frame shows the ratio with respect to the SM prediction. The shaded band in the ratio indicates the uncertainty due to scale variations. See the text for more details.

to the scenario $c_t = 2, c_g = -0.083$ with only the interference term included, drops abruptly at $p_T \approx 470$ GeV. This behaviour is cured by the addition of the squared term, causing the already described bending behaviour. The dependence of the prediction on the $\mathcal{O}(1/\Lambda^4)$ terms indicates that in this region of transverse momenta the results should be interpreted with care.

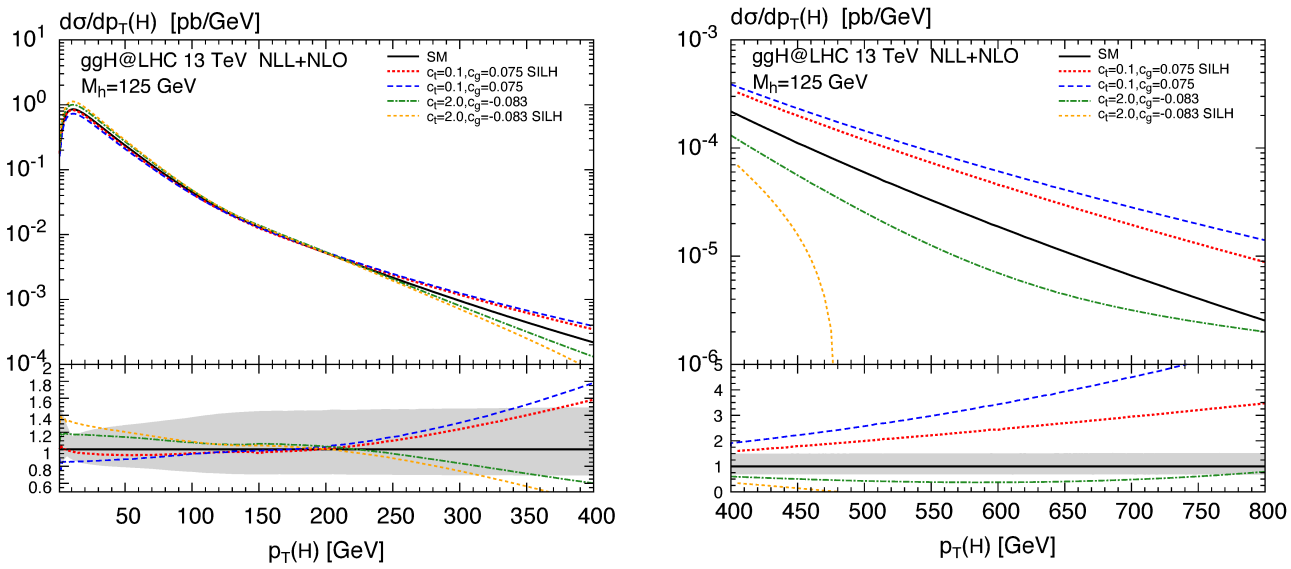

Figure 5.8: Higgs transverse-momentum spectrum in the SM (black, solid) compared to simultaneous variations of c_t and c_g for (a) $p_T \leq 400\,\text{GeV}$ and (b) $400\,\text{GeV} \leq p_T \leq 800\,\text{GeV}$ including and omitting (SILH) the squared term. The lower frame shows the ratio with respect to the SM prediction. The shaded band in the ratio indicates the uncertainty due to scale variations. See the text for more details.

5.2 Approximation at NNLL+NNLO[4]

The basis for the calculation presented here are the NLL+NLO spectra of Section 5.1. To provide the state-of-the-art NNLL+NNLO SMEFT calculations, we used the NNLL+NNLO SM predictions, and then scaled them with the NLL+NLO calculations including the SMEFT operators:

$$\left(\frac{d\sigma}{dp_t}\right)^{SMEFT}_{NNLL+NNLO}(p_T) = \frac{\left(\frac{d\sigma}{dp_t}\right)^{SMEFT}_{NLL+NLO}(p_T)}{\left(\frac{d\sigma}{dp_t}\right)^{SM}_{NLL+NLO}(p_T)} \cdot \left(\frac{d\sigma}{dp_t}\right)^{SM}_{NNLL+NNLO}(p_T) \tag{5.2}$$

This corresponds to the scaling of the NNLL+NNLO spectra by the lower panels of the spectra provided in Figs. 5.2-5.6. It is important to note here, that the NNLL+NNLO results [188–190] are known only in the heavy top limit, with just approximate inclusion of finite top mass effects. We used SM results obtained with the numerical code HRes [208, 279], and we ensured the set up as close as possible to the one used in the NLL+NLO calculations.

To estimate the uncertainties due to the renormalization and factorization scales we performed the customary seven-point μ_R, μ_F variation, i. e. we consider independent variations within the range $\mu_0/2 \leq \mu_F, \mu_R \leq 2\mu_0$ with $1/2 < \mu_R/\mu_F < 2$, where $\mu_0 = \sqrt{p_T^2 + m_h^2}/2$. We then varied also the two resummation scales by a factor of two[5].

We present the p_T spectra of the Higgs particle, including the modifications coming from the effective operators at the approximate NNLL+NNLO level. The values used for the Wilson coefficients correspond to Figures 5.2 and Fig. 5.6 in Section 5.1[6]. As a reference the NNLL+NNLO SM predictions are shown in the Figures as a solid black line, with the grey bands on the lower panel showing the perturbative uncertainties. The light grey band corresponds to the NLL+NLO uncertainty relative to the central scale NLL+NLO calculations, while the darker band corresponds to the NNLL+NNLO scale uncertainty relative to the NNLL+NNLO central scale calculation. This presentation allows us to observe the decrease of the uncertainty while going one order higher. It results in a decrease of the uncertainty by about a factor of two in the low and intermediate p_T range (up to around 250 GeV). In the higher p_T region, the uncertainties become more scattered due to statistical fluctuations.

In Figure 5.9 (a) we present the spectrum with the individual contributions of the operators. From the grey bands on the lower panel it can be noticed that at the NLL+NLO level all the curves are within the scale uncertainty, while in the NNLL+NNLO case the effects of higher dimension operators exceed the uncertainties.

The spectra presented in Figure 5.9 (b) correspond to switching on all three SMEFT operators, as shown previously in Fig. 5.6. As it was noticed also in the NLL+NLO case most of the scenarios distort the shape of the spectra beyond the scale uncertainty, but the further reduction of the scale uncertainty in the NNLL+NNLO case allows also for a better discrimination between different scenarios.

[4] All Figures presented here come from Ref. [3]

[5] Note that here only two resummation scales were used, corresponding to the top and interference ones (Q_t and Q_{int}) from the previous study.

[6] The procedure described above can be redone also for all the other operator combinations.

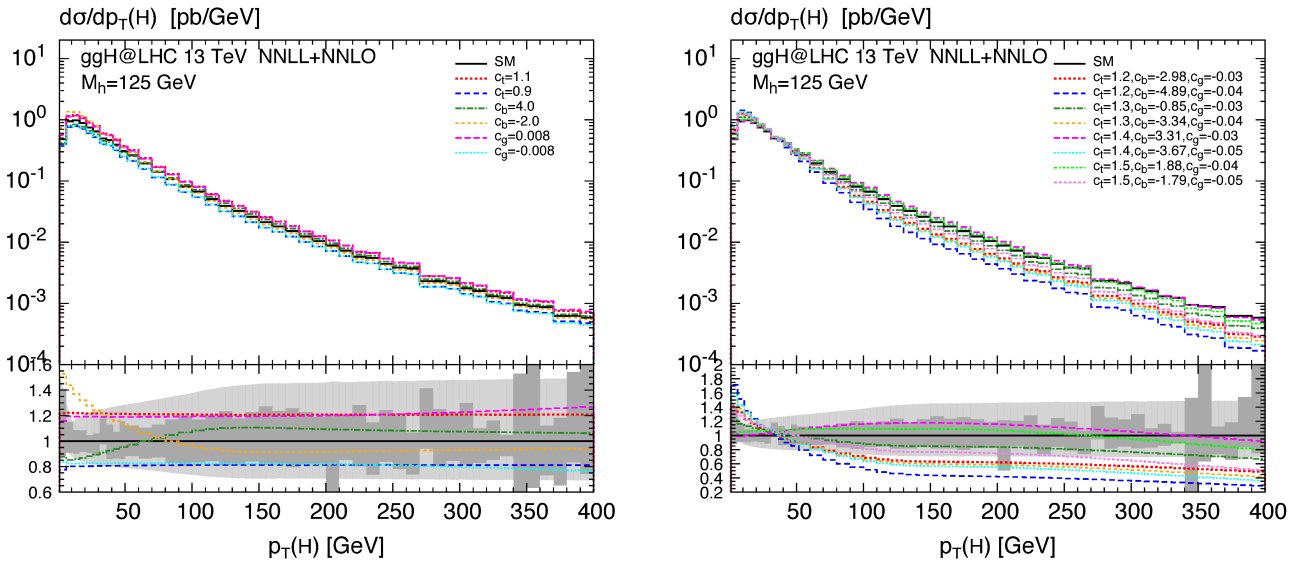

(a) (b)

Figure 5.9: Higgs transverse-momentum spectrum in the SM (black, solid) compared to (a) separate variations and (b) mixed contribution of the dimension-six operator for $0 \leq p_T \leq 400$ GeV. The lower frame shows the ratio with respect to the SM prediction. The shaded lighter and darker grey bands in the ratio indicate the uncertainty due to scale variations in the NLL+NLO and NNLL+NNLO case, respectively. See the text for more details.

Finally we mention the limitation of our study. The NNLL+NNLO SM predictions are known only in the heavy top limit, with just approximate inclusion of top mass effects, and thus the approach involving a scaling of the spectra was the only viable[7]. With the full top mass dependent results at NNLO it would be desirable to redo the analysis in the same spirit as the one done in Section 5.1 in the NLL+NLO case.

[7]Recent NLO Higgs+jet calculation [198] with full top-mass dependence provide a constant K-factor which can be used to rescale the spectra.

5.3 Effects of the chromomagnetic operator at high p_T

As discussed in the beginning of Section 5.1, the inclusion of low-p_T resummation requires not only the real-emission amplitudes, but also the virtual contributions. Since we did not evaluate the virtual corrections including the chromomagnetic operator[8] we can only predict the shape of the p_T spectrum in the high p_T range. The implementation was also carried out in the HQT program, and cross-checked with HIGLU. Agreement was also found with the results presented in Ref. [244].

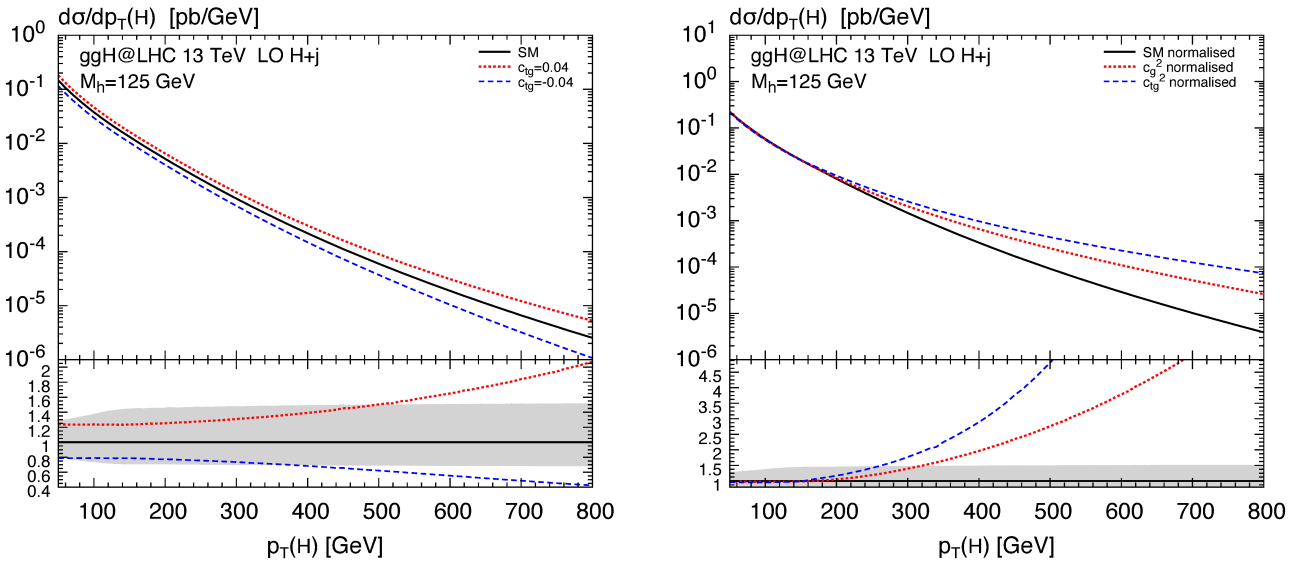

(a) (b)

Figure 5.10: (a) Higgs transverse-momentum spectrum in the SM (black, solid) compared to variations of the chromomagnetic operator for (a) 50 GeV$\leq p_T \leq$ 800 GeV in the experimentally allowed range. (b) The comparison of normalised spectra of the SM and spectra obtained with only the point-like Higgs gluon coupling operator ($\sim c_g^2$) and the chromomagnetic operator ($\sim c_{tg}^2$). See the text for more details.

In Fig. 5.10 we show the corresponding spectra, obtained with the same setup as in Section 5.1. Figure 5.10 (a) presents the spectrum with the inclusion of the chromomagnetic operator within the bounds coming from the top pair production measurements [251]. The spectra including the chromomagnetic operator diverge from the SM especially in the tail and start to exceed the SM scale uncertainty around $p_T \approx 400 - 500$ GeV.

It is visible, that the overall behaviour resembles the one of the point-like hgg coupling operator, as shown in Fig. 5.2. This is confirmed in Figure 5.10 (b), where the normalised SM spectrum is plotted along the spectra coming from these two operators. To obtain these spectra all other contributions, including SM loops are set to zero ($c_t = c_b = 0$), and only the square term of the c_g or c_{tg} operator contributes. For a better illustration of the impact on the shape the spectra are normalised to the total area below the spectra (in the range 50 GeV $\leq p_T \leq$ 800 GeV). It is visible

[8]The two-loop amplitudes including the chromomagnetic operator were recently obtained in Ref. [245].

that both operators produce harder spectra compared to the SM, and the difference between them and the SM grows with p_T. The effects originating from the chromomagnetic operator are even more sizable, roughly twice the size of the point-like hgg coupling operator contribution.

We conclude this Section by adding a few comments on the limitations of the approach we have been following. In Sections 4.1 and 4.2 we have mentioned that the chromomagnetic operator provides a contribution which is formally $\mathcal{O}(\lambda_t^2)$ with respect to the others, and that in a strict expansion in α_S it can be neglected and additionally it is a loop–generated operator whose Wilson coefficient should be additionally suppressed. This is the approach we followed in Sections 5.1 and 5.2, as well as in the current CMS analysis [43]. We have also seen that in this approach the dimension-six operators give rather different effects on the shape of the p_T spectrum. However, the impact of the chromomagnetic and hgg point-like operators on the shape of the spectrum is very similar, thereby making their separate study questionable. We have seen in Section 2.5.2.1 that the dimension-six operators contribute also to the associated production of the Higgs boson with a top-quark pair. A better approach would thus be to make a global analysis, and to include all the processes to which these operators contribute.

6

Conclusions and Outlook

New Physics might be not accessible through direct searches at the LHC, e.g. with the discovery of new resonances. In that case, it is crucial to fully exploit the data to study possible (small) deviations from the SM predictions. These deviations may become a long lasting legacy of the LHC. The SMEFT offers a formalism for the parametrisation of high-scale BSM effects, which can be used for this purpose, with the additional benefit of providing a well-defined procedure of translating them into the UV model's parameters via a top-down approach. In the SMEFT framework BSM effects are parametrised through appropriate higher-dimensional operators, and the bounds on the corresponding Wilson coefficients can be set by comparing to the experimental data.

In this thesis, we have presented a computation of the gluon fusion Higgs production cross section as well as its transverse-momentum spectrum, in which the SM prediction is supplemented by possible BSM effects. Such effects are modelled by augmenting the SM Lagrangian with appropriate dimension-six operators. We started by presenting the LO calculation including the impact of the relevant dimension-six operators:

- $\mathcal{O}_1$ of Eq. (4.3): the point-like Higgs coupling to gluons (characterised by the coefficient c_g),
- $\mathcal{O}_2$ of Eq. (4.4) and $\mathcal{O}_3$ of Eq. (4.5): the Yukawa coupling modificators (with the coefficients c_t and c_b for the interaction with top and bottom quark respectively),
- $\mathcal{O}_4$ of Eq. (4.6): the top-chromomagnetic dipole operator (characterised by the coefficient c_{tg}),

where the last had been previously addressed in the literature by different groups with contradicting results.

Then, the real contribution to the NLO corrections has been calculated analytically, to obtain a prediction for the transverse-momentum spectrum of the Higgs boson. In particular the analytical result of the chromomagnetic contribution is presented for the first time in this work. Additionally, the three dimension-six operators related to the modifications of top and bottom Yukawa couplings

and to the inclusion of a point-like ggh coupling were consistently included up to $\mathcal{O}(\alpha_S^3)$ accuracy and supplemented by a soft-gluon resummation at NLL accuracy, which is required to obtain reliable predictions at small transverse momenta.

We have constructed a tool to obtain reliable predictions for the Higgs p_T distribution including dimension-six operators and we have performed a comprehensive analysis of the possible effects due to the different dimension-six operators, by studying the impact of variations of c_t, c_b, c_g and c_{tg} on the transverse-momentum spectrum of the Higgs boson. We varied the above coefficients in the range suggested by recent global analyses and required the total cross section to meet the SM prediction at NLO within an $\mathcal{O}(20\%)$ experimental uncertainty. Our results can be summarized as follows:

- The effects of the different SMEFT operators manifest themselves in different regions of the Higgs p_T spectrum. A modification of the Higgs-bottom Yukawa coupling ($\mathcal{O}_3$) induces sizeable effects almost exclusively at small transverse momenta. A direct coupling of the Higgs boson to gluons ($\mathcal{O}_1$), as well as the chromomagnetic operator ($\mathcal{O}_4$), on the other hand, change the shape of the distribution most notably in the high-p_T tail. As expected, changes in the top-quark Yukawa coupling ($\mathcal{O}_2$) primarily affect the normalisation and approximately correspond to a simple rescaling of the SM spectrum.

- The shape of the transverse momentum distribution depends on the mass of the particle that mediates the Higgs-gluon coupling. The lower the mass of that particle, the softer is the resulting spectrum. Therefore, the p_T shape associated with the bottom loop is softer (thus affecting the region of small transverse momenta) than the SM one and, when increasing the absolute value of the bottom-quark Yukawa coupling, positive (negative) values soften (harden) the spectrum, if the top-bottom interference is dominant (small variations of c_b). In contrast the spectrum becomes always softer for $|c_b| \gg 1$, if the squared bottom-loop is dominant (large variations of c_b). Furthermore, a point-like coupling between gluons and the Higgs boson and the chromomagnetic operator both lead to a harder spectrum. More precisely a positive (negative) c_g or c_{tg} value hardens (softens) the shape as compared to a Higgs boson mediated by the SM loop.

- The similar sensitivity to the c_g and c_{tg} couplings in the high-p_T tail makes it difficult to disentangle these effects in one observable.

- While individual variations of the various Wilson coefficients produce effects that hardly exceed the (NLL+)NLO perturbative uncertainties, the simultaneous variation of two or more operators can significantly distort the spectrum, still keeping the total rate consistent with the NLO prediction within the current experimental uncertainties.

- Choosing combinations of c_t, c_b and c_g that compensate each other at the level of the total cross section makes possible to deform the shape of the Higgs p_T spectrum far beyond the uncertainties of our SM NLL+NLO prediction and thus will give sensitivity to these effects in future LHC analyses.

We have also presented an approximate extension of the Higgs p_T spectra augmented with the SMEFT operators to the NNLL+NNLO level of accuracy. We started with state-of-the-art

SM predictions and scaled them by the relative SMEFT/SM effects at the NLL+NLO level. The NNLL+NNLO SM predictions are currently known only in the heavy top limit, with just an approximate inclusion of top mass effects, and thus the approach involving scaling of the spectra was the best possibility. With the full top mass dependent results at NNLO, it would be desirable to repeat the analysis in the same spirit as the one done in the NLL+NLO case. It is evident that going one order higher in the perturbative expansion leads to a decrease of the scale uncertainty roughly by a factor of two. This provides a much better sensitivity to BSM effects.

We conclude our discussion by adding a few comments on the limitations of the results presented here, which may also be an outline for the continuation of this work. As mentioned, our study of the effects of the chromomagnetic operator was limited to moderate and high p_T, due to the lack of the NLO virtual part of the calculation which would be needed to include the full resummation at low p_T. This two loop calculation has recently been presented in Ref. [245], and could allow us to extend this study to the low-p_T region. Another issue is how to extract the Wilson coefficients explicitly. Since the effects of the point-like Higgs-gluon coupling and of the chromomagnetic operator manifest themselves in the same p_T region, it will probably not be possible to set separate bounds on them by just measuring the Higgs transverse momentum spectrum. As a first approximation the chromomagnetic operator can be omitted in the fit, due to the hierarchy of the operators discussed in Sect. 4.2. This is the approach currently used in the CMS analysis [43] based on the results obtained in the framework of this thesis. However, as our studies show, the effects of the chromomagnetic operator are not negligible compared to the other operators, and a more complete approach would be to perform a fit also to other observables sensitive to these operators, in particular for Higgs boson production associated with top quarks and top pair production. More generally, this calls for a global fit where the effects of the SMEFT operators are consistently included in all the relevant observables.

Acknowledgements

Firstly, I would like to express my gratitude to my supervisors, Massimiliano Grazzini and Michael Spira, for the opportunities, support and guidance. Thank you both for all the valuable discussions, advice, and time invested also in polishing this thesis. I would like to thank Marius Wiesemann as well, whose help in the beginning of this project was invaluable. I am also indebted to Günther Dissertori, who gave me the opportunity to be a part of the HiggsTools Initial Training Network.

Talking about HiggsTools, I am sincerely thankful to Nigel Glover, who not only agreed to be a referee of my thesis, but also was our HiggsTools boss, always full of enthusiasm and guidance. Thank you, together with Giampiero Passarino and Frank Krauss, for organising all the meetings and schools, and making this network function so well, both on the scientific and personal level. These thanks extend also to all my ESR fellows who contributed to so many good memories: Joosep, Giulia, Raquel, Shruti, Juan, Matias, Stephen, Tim, Hjalte, Davide M., Michele, Davide N., Theo, Giulio, Nicolas, Yacine, Zahari, Elisa, Marzieh, Cosimo - thanks, and *peace & love* :)

While working on my PhD I was delocalised between the theoretical particle physics groups of UZH and PSI, both of which were friendly and inspiring environments. Thanks to all of you for the lunch discussions, comments on my research and tips on living in Switzerland. To the UZH group also special thanks for the Christmas parties, boardgames evenings and weekend trips, and to the PSI group for organising two wonderful Zuoz schools I've participated in. It was fun working here.

Last, but not least I would like to thank two people whose importance to me, not only in the context of this thesis, is unmeasurable. This is to my Mom: for always supporting and believing in me and being the most reasonable person in the world. And for Leszek, my boyfriend, who is always there for me, no matter if it is a problem with configuring my computer, feeling blue, or climbing mountains, I can always count on him, and he is able to pull me out from many frustrations. Well, I cannot also skip the comforting fluffiness of our cat Szarutek, which is always helpful to brighten my world.

Finally, there are two people whom I want to thank, however I unfortunately no longer can: my Dad, who was always enthusiastic about my scientific pursuits; and Professor Maria Krawczyk, without whom, I have no doubt, I would not be where I am, and who was the kindest and most supportive person I have ever met on my scientific path.

Bibliography

[1] **HiggsTools Working Group** Collaboration, M. Boggia et al., *The HiggsTools Handbook: Concepts and observables for deciphering the Nature of the Higgs Sector*, arXiv:1711.09875.

[2] M. Grazzini, A. Ilnicka, M. Spira, and M. Wiesemann, *Modeling BSM effects on the Higgs transverse-momentum spectrum in an EFT approach*, JHEP **03** (2017) 115, [arXiv:1612.00283].

[3] M. Grazzini, A. Ilnicka, M. Spira, and M. Wiesemann, *Effective Field Theory for Higgs properties parametrisation: the transverse momentum spectrum case*, 52nd Rencontres de Moriond QCD 2017, La Thuile (2017) [arXiv:1705.05143].

[4] M. Grazzini, A. Ilnicka, and M. Spira, *Chromomagnetic operator in Higgs plus jet production*, in preparation, 2018.

[5] A. Ilnicka, M. Krawczyk, and T. Robens, *Inert Doublet Model in light of LHC Run I and astrophysical data*, Phys. Rev. **D93** (2016), no. 5 055026, [arXiv:1508.01671].

[6] **LHC Higgs Cross Section Working Group** Collaboration, D. de Florian et al., *Handbook of LHC Higgs Cross Sections: 4. Deciphering the Nature of the Higgs Sector*, arXiv:1610.07922.

[7] P. W. Higgs, *Broken symmetries, massless particles and gauge fields*, Phys. Lett. **12** (1964) 132–133.

[8] P. W. Higgs, *Broken Symmetries and the Masses of Gauge Bosons*, Phys. Rev. Lett. **13** (1964) 508–509.

[9] F. Englert and R. Brout, *Broken Symmetry and the Mass of Gauge Vector Mesons*, Phys. Rev. Lett. **13** (1964) 321–323.

[10] G. S. Guralnik, C. R. Hagen, and T. W. B. Kibble, *Global Conservation Laws and Massless Particles*, Phys. Rev. Lett. **13** (1964) 585–587.

[11] P. W. Higgs, *Spontaneous Symmetry Breakdown without Massless Bosons*, Phys. Rev. **145** (1966) 1156–1163.

[12] T. W. B. Kibble, *Symmetry breaking in nonAbelian gauge theories*, Phys. Rev. **155** (1967) 1554–1561.

[13] G. 't Hooft, *Renormalizable Lagrangians for Massive Yang-Mills Fields*, Nucl. Phys. **B35** (1971) 167–188.

[14] G. 't Hooft and M. J. G. Veltman, *Regularization and Renormalization of Gauge Fields*, Nucl. Phys. **B44** (1972) 189–213.

[15] **CMS** Collaboration, S. Chatrchyan et al., *Observation of a new boson at a mass of 125 GeV with the CMS experiment at the LHC*, Phys. Lett. **B716** (2012) 30–61, [arXiv:1207.7235].

[16] **ATLAS** Collaboration, G. Aad et al., *Observation of a new particle in the search for the Standard Model Higgs boson with the ATLAS detector at the LHC*, Phys. Lett. **B716** (2012) 1–29, [arXiv:1207.7214].

[17] **ATLAS, CMS** Collaboration, G. Aad et al., *Measurements of the Higgs boson production and decay rates and constraints on its couplings from a combined ATLAS and CMS analysis of the LHC pp collision data at $\sqrt{s} = 7$ and 8 TeV*, JHEP **08** (2016) 045, [arXiv:1606.02266].

[18] **Particle Data Group** Collaboration, C. Patrignani et al., *Review of Particle Physics*, Chin. Phys. **C40** (2016), no. 10 100001.

[19] J. de Swart, G. Bertone, and J. van Dongen, *How Dark Matter Came to Matter*, arXiv:1703.00013. [Nature Astron.1,0059(2017)].

[20] L. Canetti, M. Drewes, and M. Shaposhnikov, *Matter and Antimatter in the Universe*, New J. Phys. **14** (2012) 095012, [arXiv:1204.4186].

[21] E. Metral, *LHC: status, prospects and future challenges*, PoS **LHCP2016** (2016) 002.

[22] **LHC Higgs Cross Section Working Group** Collaboration, A. David, A. Denner, M. Duehrssen, M. Grazzini, C. Grojean, G. Passarino, M. Schumacher, M. Spira, G. Weiglein, and M. Zanetti, *LHC HXSWG interim recommendations to explore the coupling structure of a Higgs-like particle*, arXiv:1209.0040.

[23] **ATLAS** Collaboration, G. Aad et al., *Measurements of fiducial and differential cross sections for Higgs boson production in the diphoton decay channel at $\sqrt{s} = 8$ TeV with ATLAS*, JHEP **09** (2014) 112, [arXiv:1407.4222].

[24] **ATLAS** Collaboration, G. Aad et al., *Fiducial and differential cross sections of Higgs boson production measured in the four-lepton decay channel in pp collisions at $\sqrt{s}$=8 TeV with the ATLAS detector*, Phys. Lett. **B738** (2014) 234–253, [arXiv:1408.3226].

[25] **ATLAS** Collaboration, G. Aad et al., *Measurements of the Total and Differential Higgs Boson Production Cross Sections Combining the $H \to \gamma\gamma$ and $H \to ZZ^* \to 4l$ Decay Channels at $\sqrt{s}$=8??TeV with the ATLAS Detector*, Phys. Rev. Lett. **115** (2015), no. 9 091801, [arXiv:1504.05833].

[26] **ATLAS** Collaboration, G. Aad et al., *Measurement of fiducial differential cross sections of gluon-fusion production of Higgs bosons decaying to $WW^* \to e\nu\mu\nu$ with the ATLAS detector at $\sqrt{s} = 8$ TeV*, JHEP **08** (2016) 104, [arXiv:1604.02997].

[27] **CMS** Collaboration, S. Chatrchyan et al., *Measurement of differential cross sections for Higgs boson production in the diphoton decay channel in pp collisions at $\sqrt(s) = 8$ TeV*, arXiv:1508.07819 (2015) [arXiv:1508.07819].

[28] **CMS** Collaboration, V. Khachatryan et al., *Measurement of differential and integrated fiducial cross sections for Higgs boson production in the four-lepton decay channel in pp collisions at $\sqrt{s} = 7$ and 8 TeV*, JHEP **04** (2016) 005, [arXiv:1512.08377].

[29] **CMS** Collaboration, V. Khachatryan et al., *Measurement of the transverse momentum spectrum of the Higgs boson produced in pp collisions at $\sqrt{s} = 8$ TeV using $H \to WW$ decays*, JHEP **03** (2017) 032, [arXiv:1606.01522].

[30] **ATLAS** Collaboration, M. Aaboud et al., *Measurement of inclusive and differential cross sections in the $H \to ZZ^* \to 4\ell$ decay channel in pp collisions at $\sqrt{s} = 13$ TeV with the ATLAS detector*, JHEP **10** (2017) 132, [arXiv:1708.02810].

[31] **ATLAS** Collaboration, M. Aaboud et al., *Measurements of Higgs boson properties in the diphoton decay channel with 36 fb^{-1} of pp collision data at $\sqrt{s} = 13$ TeV with the ATLAS detector*, arXiv:1802.04146.

[32] **CMS** Collaboration, A. M. Sirunyan et al., *Inclusive search for a highly boosted Higgs boson decaying to a bottom quark-antiquark pair*, Phys. Rev. Lett. **120** (2018), no. 7 071802, [arXiv:1709.05543].

[33] **CMS** Collaboration, C. Vernieri, *Inclusive Search for Boosted Higgs Bosons Using $H\to \mathrm{b\bar{b}}$ Decays with the CMS Experiment*, in EPS-HEP 2017, p. 349, 2017. arXiv:1711.10508.

[34] C. J. C. Burges and H. J. Schnitzer, *Virtual Effects of Excited Quarks as Probes of a Possible New Hadronic Mass Scale*, Nucl. Phys. **B228** (1983) 464–500.

[35] C. N. Leung, S. T. Love, and S. Rao, *Low-Energy Manifestations of a New Interaction Scale: Operator Analysis*, Z. Phys. **C31** (1986) 433.

[36] W. Buchmuller and D. Wyler, *Effective Lagrangian Analysis of New Interactions and Flavor Conservation*, Nucl. Phys. **B268** (1986) 621–653.

[37] B. Grzadkowski, M. Iskrzynski, M. Misiak, and J. Rosiek, *Dimension-Six Terms in the Standard Model Lagrangian*, JHEP **10** (2010) 085, [arXiv:1008.4884].

[38] C. Anastasiou, C. Duhr, F. Dulat, F. Herzog, and B. Mistlberger, *Higgs Boson Gluon-Fusion Production in QCD at Three Loops*, Phys. Rev. Lett. **114** (2015) 212001, [arXiv:1503.06056].

[39] C. Anastasiou, C. Duhr, F. Dulat, E. Furlan, T. Gehrmann, F. Herzog, A. Lazopoulos, and B. Mistlberger, *High precision determination of the gluon fusion Higgs boson cross-section at the LHC*, JHEP **05** (2016) 058, [arXiv:1602.00695].

[40] B. Mistlberger, *Higgs Boson Production at Hadron Colliders at N3LO in QCD*, arXiv:1802.00833.

[41] F. A. Dreyer and A. Karlberg, *Vector-Boson Fusion Higgs Production at Three Loops in QCD*, Phys. Rev. Lett. **117** (2016), no. 7 072001, [arXiv:1606.00840].

[42] G. Passarino, *NLO Inspired Effective Lagrangians for Higgs Physics*, Nucl. Phys. **B868** (2013) 416–458, [arXiv:1209.5538].

[43] **CMS** Collaboration, V. Khachatryan et al., *Combination of Higgs differential observables from $h \to \gamma\gamma$ and $h \to 4l$ decays*, in preparation, private communication with T. Klijnsma, 2018.

[44] C. Mariotti and G. Passarino, *Higgs boson couplings: measurements and theoretical interpretation*, Int. J. Mod. Phys. **A32** (2017) 1730003, [arXiv:1612.00269].

[45] F. Boudjema et al., *On the presentation of the LHC Higgs Results*, in Workshop on Likelihoods for the LHC Searches, 2013. arXiv:1307.5865.

[46] D. Yu. Bardin and G. Passarino, *The standard model in the making: Precision study of the electroweak interactions*, . Oxford, UK: Clarendon, 1999.

[47] **The ALEPH, DELPHI, L3, OPAL, SLD, the LEP Electroweak Working Group, the SLD Electroweak and Heavy Flavour Groups** Collaboration, , *Precision Electroweak Measurements on the Z Resonance*, Phys. Rept. **427** (2006) 257, [hep-ex/0509008].

[48] M. Gonzalez-Alonso, A. Greljo, G. Isidori, and D. Marzocca, *Pseudo-observables in Higgs decays*, Eur. Phys. J. **C75** (2015) 128, [arXiv:1412.6038].

[49] A. Greljo, G. Isidori, J. M. Lindert, and D. Marzocca, *Pseudo-observables in electroweak Higgs production*, Eur. Phys. J. **C76** (2016) 158, [arXiv:1512.06135].

[50] E. E. Jenkins, A. V. Manohar, and M. Trott, *Renormalization Group Evolution of the Standard Model Dimension Six Operators I: Formalism and lambda Dependence*, JHEP **10** (2013) 087, [arXiv:1308.2627].

[51] E. E. Jenkins, A. V. Manohar, and M. Trott, *Renormalization Group Evolution of the Standard Model Dimension Six Operators II: Yukawa Dependence*, JHEP **01** (2014) 035, [arXiv:1310.4838].

[52] R. Alonso, E. E. Jenkins, A. V. Manohar, and M. Trott, *Renormalization Group Evolution of the Standard Model Dimension Six Operators III: Gauge Coupling Dependence and Phenomenology*, JHEP **04** (2014) 159, [arXiv:1312.2014].

[53] A. Celis, J. Fuentes-Martin, A. Vicente, and J. Virto, *DsixTools: The Standard Model Effective Field Theory Toolkit*, Eur. Phys. J. **C77** (2017), no. 6 405, [arXiv:1704.04504].

[54] J. Elias-Miro, C. Grojean, R. S. Gupta, and D. Marzocca, *Scaling and tuning of EW and Higgs observables*, JHEP **05** (2014) 019, [arXiv:1312.2928].

[55] F. del Aguila, M. Perez-Victoria, and J. Santiago, *Observable contributions of new exotic quarks to quark mixing*, JHEP **09** (2000) 011, [hep-ph/0007316].

[56] F. del Aguila, J. de Blas, and M. Perez-Victoria, *Effects of new leptons in Electroweak Precision Data*, Phys. Rev. **D78** (2008) 013010, [arXiv:0803.4008].

[57] F. del Aguila, J. de Blas, and M. Perez-Victoria, *Electroweak Limits on General New Vector Bosons*, JHEP **09** (2010) 033, [arXiv:1005.3998].

[58] M. Gorbahn, J. M. No, and V. Sanz, *Benchmarks for Higgs Effective Theory: Extended Higgs Sectors*, JHEP **10** (2015) 036, [arXiv:1502.07352].

[59] J. de Blas, M. Chala, M. Perez-Victoria, and J. Santiago, *Observable Effects of General New Scalar Particles*, JHEP **04** (2015) 078, [arXiv:1412.8480].

[60] C.-W. Chiang and R. Huo, *Standard Model Effective Field Theory: Integrating out a Generic Scalar*, JHEP **09** (2015) 152, [arXiv:1505.06334].

[61] J. de Blas, J. C. Criado, M. Perez-Victoria, and J. Santiago, *Effective description of general extensions of the Standard Model: the complete tree-level dictionary*, arXiv:1711.10391.

[62] C. Anastasiou, A. Carmona, A. Lazopoulos, and J. Santiago, *Automated one-loop matching with match maker*, in HEFT2017, 2017. see at: https://conference.ippp.dur.ac.uk/event/590/session/6/contribution/18/material/slides/0.pdf.

[63] M. K. Gaillard, *The Effective One Loop Lagrangian With Derivative Couplings*, Nucl. Phys. **B268** (1986) 669–692.

[64] B. Henning, X. Lu, and H. Murayama, *How to use the Standard Model effective field theory*, JHEP **01** (2016) 023, [arXiv:1412.1837].

[65] A. Drozd, J. Ellis, J. Quevillon, and T. You, *The Universal One-Loop Effective Action*, JHEP **03** (2016) 180, [arXiv:1512.03003].

[66] J. Fuentes-Martin, J. Portoles, and P. Ruiz-Femenia, *Integrating out heavy particles with functional methods: a simplified framework*, JHEP **09** (2016) 156, [arXiv:1607.02142].

[67] J. C. Criado, *MatchingTools: a Python library for symbolic effective field theory calculations*, arXiv:1710.06445.

[68] F. del Aguila, Z. Kunszt, and J. Santiago, *One-loop effective lagrangians after matching*, Eur. Phys. J. **C76** (2016) 244, [arXiv:1602.00126].

[69] M. Boggia, R. Gomez-Ambrosio, and G. Passarino, *Low energy behaviour of standard model extensions*, JHEP **05** (2016) 162, [arXiv:1603.03660].

[70] B. Henning, X. Lu, and H. Murayama, *One-loop Matching and Running with Covariant Derivative Expansion*, JHEP **01** (2018) 123, [arXiv:1604.01019].

[71] S. A. R. Ellis, J. Quevillon, T. You, and Z. Zhang, *Mixed heavy-light matching in the Universal One-Loop Effective Action*, Phys. Lett. **B762** (2016) 166–176, [arXiv:1604.02445].

[72] Z. Zhang, *Covariant diagrams for one-loop matching*, JHEP **05** (2017) 152, [arXiv:1610.00710].

[73] S. A. R. Ellis, J. Quevillon, T. You, and Z. Zhang, *Extending the Universal One-Loop Effective Action: Heavy-Light Coefficients*, JHEP **08** (2017) 054, [arXiv:1706.07765].

[74] I. Brivio and M. Trott, *The Standard Model as an Effective Field Theory*, arXiv:1706.08945.

[75] S. Weinberg, *Baryon and Lepton Nonconserving Processes*, Phys. Rev. Lett. **43** (1979) 1566–1570.

[76] L. Lehman, *Extending the Standard Model Effective Field Theory with the Complete Set of Dimension-7 Operators*, Phys. Rev. **D90** (2014) 125023, [arXiv:1410.4193].

[77] G. F. Giudice, C. Grojean, A. Pomarol, and R. Rattazzi, *The Strongly-Interacting Light Higgs*, JHEP **06** (2007) 045, [hep-ph/0703164].

[78] R. Contino, M. Ghezzi, C. Grojean, M. Muhlleitner, and M. Spira, *Effective Lagrangian for a light Higgs-like scalar*, JHEP **07** (2013) 035, [arXiv:1303.3876].

[79] R. S. Gupta, A. Pomarol, and F. Riva, *BSM Primary Effects*, Phys. Rev. **D91** (2015), no. 3 035001, [arXiv:1405.0181].

[80] A. Falkowski, B. Fuks, K. Mawatari, K. Mimasu, F. Riva, and V. Sanz, *Rosetta: an operator basis translator for Standard Model effective field theory*, Eur. Phys. J. **C75** (2015), no. 12 583, [arXiv:1508.05895]. see also http://feynrules.irmp.ucl.ac.be/wiki/BSMCharacterisation.

[81] P. Artoisenet et al., *A framework for Higgs characterisation*, JHEP **11** (2013) 043, [arXiv:1306.6464].

[82] R. Contino, M. Ghezzi, C. Grojean, M. Mühlleitner, and M. Spira, *eHDECAY: an Implementation of the Higgs Effective Lagrangian into HDECAY*, Comput. Phys. Commun. **185** (2014) 3412–3423, [arXiv:1403.3381].

[83] I. Brivio, Y. Jiang, and M. Trott, *The SMEFTsim package, theory and tools*, JHEP **12** (2017) 070, [arXiv:1709.06492].

[84] A. Dedes, W. Materkowska, M. Paraskevas, J. Rosiek, and K. Suxho, *Feynman rules for the Standard Model Effective Field Theory in R_ξ -gauges*, JHEP **06** (2017) 143, [arXiv:1704.03888].

[85] M. B. Einhorn and J. Wudka, *The Bases of Effective Field Theories*, Nucl. Phys. **B876** (2013) 556–574, [arXiv:1307.0478].

[86] J. Ellis, *TikZ-Feynman: Feynman diagrams with TikZ*, Comput. Phys. Commun. **210** (2017) 103–123, [arXiv:1601.05437].

[87] A. David and G. Passarino, *Through precision straits to next standard model heights*, Rev. Phys. **1** (2016) 13–28, [arXiv:1510.00414].

[88] J. Brehmer, A. Freitas, D. Lopez-Val, and T. Plehn, *Pushing Higgs Effective Theory to its Limits*, Phys. Rev. **D93** (2016) 075014, [arXiv:1510.03443].

[89] A. Crivellin, M. Ghezzi, and M. Procura, *Effective Field Theory with Two Higgs Doublets*, JHEP **09** (2016) 160, [arXiv:1608.00975].

[90] S. Karmakar and S. Rakshit, *Higher dimensional operators in 2HDM*, JHEP **10** (2017) 048, [arXiv:1707.00716].

[91] J. Rojo et al., *The PDF4LHC report on PDFs and LHC data: Results from Run I and preparation for Run II*, J. Phys. **G42** (2015) 103103, [arXiv:1507.00556].

[92] T. Kinoshita, *Mass singularities of Feynman amplitudes*, J. Math. Phys. **3** (1962) 650–677.

[93] T. D. Lee and M. Nauenberg, *Degenerate Systems and Mass Singularities*, Phys. Rev. **133** (1964) B1549–B1562.

[94] H. M. Georgi, S. L. Glashow, M. E. Machacek, and D. V. Nanopoulos, *Higgs Bosons from Two Gluon Annihilation in Proton Proton Collisions*, Phys. Rev. Lett. **40** (1978) 692.

[95] M. Spira, *Higgs Boson Production and Decay at Hadron Colliders*, Prog. Part. Nucl. Phys. **95** (2017) 98–159, [arXiv:1612.07651].

[96] D. Graudenz, M. Spira, and P. M. Zerwas, *QCD corrections to Higgs boson production at proton proton colliders*, Phys. Rev. Lett. **70** (1993) 1372–1375.

[97] M. Spira, A. Djouadi, D. Graudenz, and P. M. Zerwas, *Higgs boson production at the LHC*, Nucl. Phys. **B453** (1995) 17–82, [hep-ph/9504378].

[98] R. Harlander and P. Kant, *Higgs production and decay: Analytic results at next-to-leading order QCD*, JHEP **12** (2005) 015, [hep-ph/0509189].

[99] C. Anastasiou, S. Bucherer, and Z. Kunszt, *HPro: A NLO Monte-Carlo for Higgs production via gluon fusion with finite heavy quark masses*, JHEP **10** (2009) 068, [arXiv:0907.2362].

[100] S. Actis, G. Passarino, C. Sturm, and S. Uccirati, *NLO Electroweak Corrections to Higgs Boson Production at Hadron Colliders*, Phys. Lett. **B670** (2008) 12–17, [arXiv:0809.1301].

[101] S. Actis, G. Passarino, C. Sturm, and S. Uccirati, *NNLO Computational Techniques: The Cases H —> gamma gamma and H —> g g*, Nucl. Phys. **B811** (2009) 182–273, [arXiv:0809.3667].

[102] S. Catani, D. de Florian, and M. Grazzini, *Higgs production in hadron collisions: Soft and virtual QCD corrections at NNLO*, JHEP **05** (2001) 025, [hep-ph/0102227].

[103] R. V. Harlander and W. B. Kilgore, *Soft and virtual corrections to proton proton $\to H + X$ at NNLO*, Phys. Rev. **D64** (2001) 013015, [hep-ph/0102241].

[104] R. V. Harlander and W. B. Kilgore, *Next-to-next-to-leading order Higgs production at hadron colliders*, Phys. Rev. Lett. **88** (2002) 201801, [hep-ph/0201206].

[105] C. Anastasiou and K. Melnikov, *Higgs boson production at hadron colliders in NNLO QCD*, Nucl. Phys. **B646** (2002) 220–256, [hep-ph/0207004].

[106] V. Ravindran, J. Smith, and W. L. van Neerven, *NNLO corrections to the total cross-section for Higgs boson production in hadron hadron collisions*, Nucl. Phys. **B665** (2003) 325–366, [hep-ph/0302135].

[107] S. Marzani, R. D. Ball, V. Del Duca, S. Forte, and A. Vicini, *Higgs production via gluon-gluon fusion with finite top mass beyond next-to-leading order*, Nucl. Phys. **B800** (2008) 127–145, [arXiv:0801.2544].

[108] T. Gehrmann, M. Jaquier, E. W. N. Glover, and A. Koukoutsakis, *Two-Loop QCD Corrections to the Helicity Amplitudes for $H \to 3$ partons*, JHEP **02** (2012) 056, [arXiv:1112.3554].

[109] C. Anastasiou, C. Duhr, F. Dulat, and B. Mistlberger, *Soft triple-real radiation for Higgs production at N3LO*, JHEP **07** (2013) 003, [arXiv:1302.4379].

[110] C. Anastasiou, C. Duhr, F. Dulat, F. Herzog, and B. Mistlberger, *Real-virtual contributions to the inclusive Higgs cross-section at N^3LO*, JHEP **12** (2013) 088, [arXiv:1311.1425].

[111] W. B. Kilgore, *One-loop single-real-emission contributions to $pp \to H + X$ at next-to-next-to-next-to-leading order*, Phys. Rev. **D89** (2014), no. 7 073008, [arXiv:1312.1296].

[112] Y. Li, A. von Manteuffel, R. M. Schabinger, and H. X. Zhu, *Soft-virtual corrections to Higgs production at N^3LO*, Phys. Rev. **D91** (2015) 036008, [arXiv:1412.2771].

[113] C. Anastasiou, C. Duhr, F. Dulat, E. Furlan, T. Gehrmann, F. Herzog, and B. Mistlberger, *Higgs boson gluon-fusion production beyond threshold in N^3LO QCD*, JHEP **03** (2015) 091, [arXiv:1411.3584].

[114] R. V. Harlander and K. J. Ozeren, *Top mass effects in Higgs production at next-to-next-to-leading order QCD: Virtual corrections*, Phys. Lett. **B679** (2009) 467–472, [arXiv:0907.2997].

[115] A. Pak, M. Rogal, and M. Steinhauser, *Virtual three-loop corrections to Higgs boson production in gluon fusion for finite top quark mass*, Phys. Lett. **B679** (2009) 473–477, [arXiv:0907.2998].

[116] R. V. Harlander and K. J. Ozeren, *Finite top mass effects for hadronic Higgs production at next-to-next-to-leading order*, JHEP **11** (2009) 088, [arXiv:0909.3420].

[117] A. Pak, M. Rogal, and M. Steinhauser, *Finite top quark mass effects in NNLO Higgs boson production at LHC*, JHEP **02** (2010) 025, [arXiv:0911.4662].

[118] M. Kramer, E. Laenen, and M. Spira, *Soft gluon radiation in Higgs boson production at the LHC*, Nucl. Phys. **B511** (1998) 523–549, [hep-ph/9611272].

[119] M. Spira, *QCD effects in Higgs physics*, Fortsch. Phys. **46** (1998) 203–284, [hep-ph/9705337].

[120] S. Catani, D. de Florian, M. Grazzini, and P. Nason, *Soft gluon resummation for Higgs boson production at hadron colliders*, JHEP **07** (2003) 028, [hep-ph/0306211].

[121] S. Moch and A. Vogt, *Higher-order soft corrections to lepton pair and Higgs boson production*, Phys. Lett. **B631** (2005) 48–57, [hep-ph/0508265].

[122] V. Ravindran, *On Sudakov and soft resummations in QCD*, Nucl. Phys. **B746** (2006) 58–76, [hep-ph/0512249].

[123] V. Ravindran, *Higher-order threshold effects to inclusive processes in QCD*, Nucl. Phys. **B752** (2006) 173–196, [hep-ph/0603041].

[124] A. Idilbi, X.-d. Ji, J.-P. Ma, and F. Yuan, *Threshold resummation for Higgs production in effective field theory*, Phys. Rev. **D73** (2006) 077501, [hep-ph/0509294].

[125] V. Ahrens, T. Becher, M. Neubert, and L. L. Yang, *Renormalization-Group Improved Prediction for Higgs Production at Hadron Colliders*, Eur. Phys. J. **C62** (2009) 333–353, [arXiv:0809.4283].

[126] D. de Florian and M. Grazzini, *Higgs production through gluon fusion: Updated cross sections at the Tevatron and the LHC*, Phys. Lett. **B674** (2009) 291–294, [arXiv:0901.2427].

[127] D. de Florian, J. Mazzitelli, S. Moch, and A. Vogt, *Approximate N^3LO Higgs-boson production cross section using physical-kernel constraints*, JHEP **10** (2014) 176, [arXiv:1408.6277].

[128] S. Catani, L. Cieri, D. de Florian, G. Ferrera, and M. Grazzini, *Threshold resummation at N^3LL accuracy and soft-virtual cross sections at N^3LO*, Nucl. Phys. **B888** (2014) 75–91, [arXiv:1405.4827].

[129] M. Bonvini and L. Rottoli, *Three loop soft function for N^3LL' gluon fusion Higgs production in soft-collinear effective theory*, Phys. Rev. **D91** (2015), no. 5 051301, [arXiv:1412.3791].

[130] D. de Florian and M. Grazzini, *Higgs production at the LHC: updated cross sections at $\sqrt{s} = 8$ TeV*, Phys. Lett. **B718** (2012) 117–120, [arXiv:1206.4133].

[131] M. Bonvini and S. Marzani, *Resummed Higgs cross section at N^3LL*, JHEP **09** (2014) 007, [arXiv:1405.3654].

[132] T. Schmidt and M. Spira, *Higgs Boson Production via Gluon Fusion: Soft-Gluon Resummation including Mass Effects*, Phys. Rev. **D93** (2016), no. 1 014022, [arXiv:1509.00195].

[133] D. R. T. Jones and S. T. Petcov, *Heavy Higgs Bosons at LEP*, Phys. Lett. **84B** (1979) 440–444.

[134] R. N. Cahn and S. Dawson, *Production of Very Massive Higgs Bosons*, Phys. Lett. **136B** (1984) 196. [Erratum: Phys. Lett.**B 138**,(1984),464].

[135] K.-I. Hikasa, *Heavy Higgs Production in e^+e^- and e^-e^- Collisions*, Phys. Lett. **164B** (1985) 385. [Erratum: Phys. Lett.**B195**,(1987),623].

[136] G. Altarelli, B. Mele, and F. Pitolli, *Heavy Higgs Production at Future Colliders*, Nucl. Phys. **B287** (1987) 205–224.

[137] T. Han, G. Valencia, and S. Willenbrock, *Structure function approach to vector boson scattering in p p collisions*, Phys. Rev. Lett. **69** (1992) 3274–3277, [hep-ph/9206246].

[138] P. Bolzoni, F. Maltoni, S.-O. Moch, and M. Zaro, *Higgs production via vector-boson fusion at NNLO in QCD*, Phys. Rev. Lett. **105** (2010) 011801, [arXiv:1003.4451].

[139] P. Bolzoni, F. Maltoni, S.-O. Moch, and M. Zaro, *Vector boson fusion at NNLO in QCD: SM Higgs and beyond*, Phys. Rev. **D85** (2012) 035002, [arXiv:1109.3717].

[140] M. Cacciari, F. A. Dreyer, A. Karlberg, G. P. Salam, and G. Zanderighi, *Fully Differential Vector-Boson-Fusion Higgs Production at Next-to-Next-to-Leading Order*, Phys. Rev. Lett. **115** (2015), no. 8 082002, [arXiv:1506.02660].

[141] J. Cruz-Martinez, T. Gehrmann, E. W. N. Glover, and A. Huss, *Second-order QCD effects in Higgs boson production through vector boson fusion*, Submitted to: JHEP (2018) [arXiv:1802.02445].

[142] T. Figy, C. Oleari, and D. Zeppenfeld, *Next-to-leading order jet distributions for Higgs boson production via weak boson fusion*, Phys. Rev. **D68** (2003) 073005, [hep-ph/0306109].

[143] T. Figy and D. Zeppenfeld, *QCD corrections to jet correlations in weak boson fusion*, Phys. Lett. **B591** (2004) 297–303, [hep-ph/0403297].

[144] E. L. Berger and J. M. Campbell, *Higgs boson production in weak boson fusion at next-to-leading order*, Phys. Rev. **D70** (2004) 073011, [hep-ph/0403194].

[145] M. Ciccolini, A. Denner, and S. Dittmaier, *Strong and electroweak corrections to the production of Higgs + 2jets via weak interactions at the LHC*, Phys. Rev. Lett. **99** (2007) 161803, [arXiv:0707.0381].

[146] M. Ciccolini, A. Denner, and S. Dittmaier, *Electroweak and QCD corrections to Higgs production via vector-boson fusion at the LHC*, Phys. Rev. **D77** (2008) 013002, [arXiv:0710.4749].

[147] J. M. Butterworth, A. R. Davison, M. Rubin, and G. P. Salam, *Jet substructure as a new Higgs search channel at the LHC*, Phys. Rev. Lett. **100** (2008) 242001, [arXiv:0802.2470].

[148] S. L. Glashow, D. V. Nanopoulos, and A. Yildiz, *Associated Production of Higgs Bosons and Z Particles*, Phys. Rev. **D18** (1978) 1724–1727.

[149] Z. Kunszt, Z. Trocsanyi, and W. J. Stirling, *Clear signal of intermediate mass Higgs boson production at LHC and SSC*, Phys. Lett. **B271** (1991) 247–255.

[150] T. Han and S. Willenbrock, *QCD correction to the p p —> W H and Z H total cross-sections*, Phys. Lett. **B273** (1991) 167–172.

[151] O. Brein, A. Djouadi, and R. Harlander, *NNLO QCD corrections to the Higgs-strahlung processes at hadron colliders*, Phys. Lett. **B579** (2004) 149–156, [hep-ph/0307206].

[152] M. L. Ciccolini, S. Dittmaier, and M. Kramer, *Electroweak radiative corrections to associated WH and ZH production at hadron colliders*, Phys. Rev. **D68** (2003) 073003, [hep-ph/0306234].

[153] A. Denner, S. Dittmaier, S. Kallweit, and A. Muck, *Electroweak corrections to Higgs-strahlung off W/Z bosons at the Tevatron and the LHC with HAWK*, JHEP **03** (2012) 075, [arXiv:1112.5142].

[154] **ATLAS** Collaboration, G. Aad et al., *Search for the Standard Model Higgs boson produced in association with top quarks and decaying into $b\bar{b}$ in pp collisions at $\sqrt{s}$ = 13 TeV with the ATLAS detector*, ATLAS-CONF-2016-080.

[155] **CMS** Collaboration, S. Chatrchyan et al., *Search for associated production of Higgs bosons and top quarks in multilepton final states at $\sqrt{s} = 13$ TeV*, CMS-PAS-HIG-16-022.

[156] **CMS** Collaboration, V. Khachatryan et al., *Search for a Standard Model Higgs Boson Produced in Association with a Top-Quark Pair and Decaying to Bottom Quarks Using a Matrix Element Method*, Eur. Phys. J. **C75** (2015), no. 6 251, [arXiv:1502.02485].

[157] **ATLAS** Collaboration, M. Aaboud et al., *Search for the Standard Model Higgs boson produced in association with top quarks and decaying into a $b\bar{b}$ pair in pp collisions at $\sqrt{s}$ = 13 TeV with the ATLAS detector*, Submitted to: Phys. Rev. D (2017) [arXiv:1712.08895].

[158] R. Raitio and W. W. Wada, *Higgs Boson Production at Large Transverse Momentum in QCD*, Phys. Rev. **D19** (1979) 941.

[159] J. N. Ng and P. Zakarauskas, *A QCD Parton Calculation of Conjoined Production of Higgs Bosons and Heavy Flavors in $p\bar{p}$ Collision*, Phys. Rev. **D29** (1984) 876.

[160] Z. Kunszt, *Associated Production of Heavy Higgs Boson with Top Quarks*, Nucl. Phys. **B247** (1984) 339–359.

[161] J. F. Gunion, *Associated top anti-top Higgs production as a large source of W H events: Implications for Higgs detection in the lepton neutrino gamma gamma final state*, Phys. Lett. **B261** (1991) 510–517.

[162] W. J. Marciano and F. E. Paige, *Associated production of Higgs bosons with t anti-t pairs*, Phys. Rev. Lett. **66** (1991) 2433–2435.

[163] W. Beenakker, S. Dittmaier, M. Kramer, B. Plumper, M. Spira, and P. M. Zerwas, *Higgs radiation off top quarks at the Tevatron and the LHC*, Phys. Rev. Lett. **87** (2001) 201805, [hep-ph/0107081].

[164] W. Beenakker, S. Dittmaier, M. Kramer, B. Plumper, M. Spira, and P. M. Zerwas, *NLO QCD corrections to t anti-t H production in hadron collisions*, Nucl. Phys. **B653** (2003) 151–203, [hep-ph/0211352].

[165] L. Reina and S. Dawson, *Next-to-leading order results for t anti-t h production at the Tevatron*, Phys. Rev. Lett. **87** (2001) 201804, [hep-ph/0107101].

[166] S. Dawson, L. H. Orr, L. Reina, and D. Wackeroth, *Associated top quark Higgs boson production at the LHC*, Phys. Rev. **D67** (2003) 071503, [hep-ph/0211438].

[167] R. Frederix, S. Frixione, V. Hirschi, F. Maltoni, R. Pittau, and P. Torrielli, *Scalar and pseudoscalar Higgs production in association with a top-antitop pair*, Phys. Lett. **B701** (2011) 427–433, [arXiv:1104.5613].

[168] Y. Zhang, W.-G. Ma, R.-Y. Zhang, C. Chen, and L. Guo, *QCD NLO and EW NLO corrections to $t\bar{t}H$ production with top quark decays at hadron collider*, Phys. Lett. **B738** (2014) 1–5, [arXiv:1407.1110].

[169] S. Frixione, V. Hirschi, D. Pagani, H. S. Shao, and M. Zaro, *Weak corrections to Higgs hadroproduction in association with a top-quark pair*, JHEP **09** (2014) 065, [arXiv:1407.0823].

[170] S. Frixione, V. Hirschi, D. Pagani, H. S. Shao, and M. Zaro, *Electroweak and QCD corrections to top-pair hadroproduction in association with heavy bosons*, JHEP **06** (2015) 184, [arXiv:1504.03446].

[171] J. Baglio, A. Djouadi, R. Grober, M. M. Muhlleitner, J. Quevillon, and M. Spira, *The measurement of the Higgs self-coupling at the LHC: theoretical status*, JHEP **04** (2013) 151, [arXiv:1212.5581].

[172] E. W. N. Glover and J. J. van der Bij, *Higgs Boson pair production via gluon fusion*, Nucl. Phys. **B309** (1988) 282–294.

[173] T. Plehn, M. Spira, and P. M. Zerwas, *Pair production of neutral Higgs particles in gluon-gluon collisions*, Nucl. Phys. **B479** (1996) 46–64, [hep-ph/9603205]. [Erratum: Nucl. Phys.B531,655(1998)].

[174] S. Dawson, S. Dittmaier, and M. Spira, *Neutral Higgs boson pair production at hadron colliders: QCD corrections*, Phys. Rev. **D58** (1998) 115012, [hep-ph/9805244].

[175] G. Degrassi, P. P. Giardino, and R. Groeber, *On the two-loop virtual QCD corrections to Higgs boson pair production in the Standard Model*, Eur. Phys. J. **C76** (2016), no. 7 411, [arXiv:1603.00385].

[176] S. Borowka, N. Greiner, G. Heinrich, S. Jones, M. Kerner, J. Schlenk, U. Schubert, and T. Zirke, *Higgs Boson Pair Production in Gluon Fusion at Next-to-Leading Order with Full Top-Quark Mass Dependence*, Phys. Rev. Lett. **117** (2016), no. 1 012001, [arXiv:1604.06447]. [Erratum: Phys. Rev. Lett. **117**,(2016),no.7,079901].

[177] S. Borowka, N. Greiner, G. Heinrich, S. P. Jones, M. Kerner, J. Schlenk, and T. Zirke, *Full top quark mass dependence in Higgs boson pair production at NLO*, JHEP **10** (2016) 107, [arXiv:1608.04798].

[178] R. Frederix, S. Frixione, V. Hirschi, F. Maltoni, O. Mattelaer, P. Torrielli, E. Vryonidou, and M. Zaro, *Higgs pair production at the LHC with NLO and parton-shower effects*, Phys. Lett. **B732** (2014) 142–149, [arXiv:1401.7340].

[179] F. Maltoni, E. Vryonidou, and M. Zaro, *Top-quark mass effects in double and triple Higgs production in gluon-gluon fusion at NLO*, JHEP **11** (2014) 079, [arXiv:1408.6542].

[180] D. de Florian and J. Mazzitelli, *Two-loop virtual corrections to Higgs pair production*, Phys. Lett. **B724** (2013) 306–309, [arXiv:1305.5206].

[181] D. de Florian and J. Mazzitelli, *Higgs Boson Pair Production at Next-to-Next-to-Leading Order in QCD*, Phys. Rev. Lett. **111** (2013) 201801, [arXiv:1309.6594].

[182] J. Grigo, K. Melnikov, and M. Steinhauser, *Virtual corrections to Higgs boson pair production in the large top quark mass limit*, Nucl. Phys. **B888** (2014) 17–29, [arXiv:1408.2422].

[183] L.-S. Ling, R.-Y. Zhang, W.-G. Ma, L. Guo, W.-H. Li, and X.-Z. Li, *NNLO QCD corrections to Higgs pair production via vector boson fusion at hadron colliders*, Phys. Rev. **D89** (2014), no. 7 073001, [arXiv:1401.7754].

[184] H. T. Li and J. Wang, *Fully Differential Higgs Pair Production in Association With a W Boson at Next-to-Next-to-Leading Order in QCD*, Phys. Lett. **B765** (2017) 265–271, [arXiv:1607.06382].

[185] R. K. Ellis, I. Hinchliffe, M. Soldate, and J. J. van der Bij, *Higgs Decay to tau+ tau-: A Possible Signature of Intermediate Mass Higgs Bosons at the SSC*, Nucl. Phys. **B297** (1988) 221.

[186] U. Baur and E. W. N. Glover, *Higgs Boson Production at Large Transverse Momentum in Hadronic Collisions*, Nucl. Phys. **B339** (1990) 38–66.

[187] C. R. Schmidt, *H–>ggg(gqq) at Two Loops in the Large-Mt Limit*, Phys. Lett. **B413** (1997) 391.

[188] D. de Florian, M. Grazzini, and Z. Kunszt, *Higgs production with large transverse momentum in hadronic collisions at next-to-leading order*, Phys. Rev. Lett. **82** (1999) 5209–5212, [hep-ph/9902483].

[189] C. J. Glosser and C. R. Schmidt, *Next-to-leading corrections to the Higgs boson transverse momentum spectrum in gluon fusion*, JHEP **12** (2002) 016, [hep-ph/0209248].

[190] V. Ravindran, J. Smith, and W. L. Van Neerven, *Next-to-leading order QCD corrections to differential distributions of Higgs boson production in hadron hadron collisions*, Nucl. Phys. **B634** (2002) 247–290, [hep-ph/0201114].

[191] R. V. Harlander, T. Neumann, K. J. Ozeren, and M. Wiesemann, *Top-mass effects in differential Higgs production through gluon fusion at order α_s^4*, JHEP **08** (2012) 139, [arXiv:1206.0157].

[192] T. Neumann and M. Wiesemann, *Finite top-mass effects in gluon-induced Higgs production with a jet-veto at NNLO*, JHEP **11** (2014) 150, [arXiv:1408.6836].

[193] T. Neumann and C. Williams, *The Higgs boson at high p_T*, Phys. Rev. **D95** (2017), no. 1 014004, [arXiv:1609.00367].

[194] K. Kudashkin, K. Melnikov, and C. Wever, *Two-loop amplitudes for processes $gg \to Hg, qg \to Hq$ and $q\bar{q} \to Hg$ at large Higgs transverse momentum*, arXiv:1712.06549.

[195] J. M. Lindert, K. Kudashkin, K. Melnikov, and C. Wever, *Higgs bosons with large transverse momentum at the LHC*, arXiv:1801.08226.

[196] T. Neumann, *NLO Higgs+jet at large transverse momenta including top quark mass effects*, arXiv:1802.02981.

[197] R. Bonciani, V. Del Duca, H. Frellesvig, J. M. Henn, F. Moriello, and V. A. Smirnov, *Two-loop planar master integrals for Higgs→ 3 partons with full heavy-quark mass dependence*, JHEP **12** (2016) 096, [arXiv:1609.06685].

[198] S. P. Jones, M. Kerner, and G. Luisoni, *NLO QCD corrections to Higgs boson plus jet production with full top-quark mass dependence*, arXiv:1802.00349.

[199] R. Boughezal, F. Caola, K. Melnikov, F. Petriello, and M. Schulze, *Higgs boson production in association with a jet at next-to-next-to-leading order in perturbative QCD*, JHEP **06** (2013) 072, [arXiv:1302.6216].

[200] R. Boughezal, F. Caola, K. Melnikov, F. Petriello, and M. Schulze, *Higgs boson production in association with a jet at next-to-next-to-leading order*, Phys. Rev. Lett. **115** (2015), no. 8 082003, [arXiv:1504.07922].

[201] X. Chen, T. Gehrmann, E. W. N. Glover, and M. Jaquier, *Precise QCD predictions for the production of Higgs + jet final states*, Phys. Lett. **B740** (2015) 147–150, [arXiv:1408.5325].

[202] Y. L. Dokshitzer, D. Diakonov, and S. I. Troian, *Hard Processes in Quantum Chromodynamics*, Phys. Rept. **58** (1980) 269–395.

[203] G. Parisi and R. Petronzio, *Small Transverse Momentum Distributions in Hard Processes*, Nucl. Phys. **B154** (1979) 427–440.

[204] J. C. Collins, D. E. Soper, and G. F. Sterman, *Transverse Momentum Distribution in Drell-Yan Pair and W and Z Boson Production*, Nucl. Phys. **B250** (1985) 199–224.

[205] G. Bozzi, S. Catani, D. de Florian, and M. Grazzini, *Transverse-momentum resummation and the spectrum of the Higgs boson at the LHC*, Nucl. Phys. **B737** (2006) 73–120, [hep-ph/0508068].

[206] S. Catani and M. Grazzini, *QCD transverse-momentum resummation in gluon fusion processes*, Nucl. Phys. **B845** (2011) 297–323, [arXiv:1011.3918].

[207] H. Mantler and M. Wiesemann, *Top- and bottom-mass effects in hadronic Higgs production at small transverse momenta through LO+NLL*, Eur. Phys. J. **C73** (2013), no. 6 2467, [arXiv:1210.8263].

[208] M. Grazzini and H. Sargsyan, *Heavy-quark mass effects in Higgs boson production at the LHC*, JHEP **09** (2013) 129, [arXiv:1306.4581].

[209] Y. Li and H. X. Zhu, *Bootstrapping Rapidity Anomalous Dimensions for Transverse-Momentum Resummation*, Phys. Rev. Lett. **118** (2017), no. 2 022004, [arXiv:1604.01404].

[210] P. F. Monni, E. Re, and P. Torrielli, *Higgs Transverse-Momentum Resummation in Direct Space*, Phys. Rev. Lett. **116** (2016), no. 24 242001, [arXiv:1604.02191].

[211] G. Curci, M. Greco, and Y. Srivastava, *QCD Jets From Coherent States*, Nucl. Phys. **B159** (1979) 451–468.

[212] D. de Florian, G. Ferrera, M. Grazzini, and D. Tommasini, *Higgs boson production at the LHC: transverse momentum resummation effects in the $H \to 2gamma$, $H \to WW \to l\nu l\nu$ and $H \to ZZ \to 4l$ decay modes*, JHEP **06** (2012) 132, [arXiv:1203.6321].

[213] E. Bagnaschi, G. Degrassi, P. Slavich, and A. Vicini, *Higgs production via gluon fusion in the POWHEG approach in the SM and in the MSSM*, JHEP **02** (2012) 088, [arXiv:1111.2854].

[214] R. V. Harlander, H. Mantler, and M. Wiesemann, *Transverse momentum resummation for Higgs production via gluon fusion in the MSSM*, JHEP **11** (2014) 116, [arXiv:1409.0531].

[215] H. Mantler and M. Wiesemann, *Hadronic Higgs production through NLO+PS in the SM, the 2HDM and the MSSM*, Eur. Phys. J. **C75** (2015), no. 6 257, [arXiv:1504.06625].

[216] S. Liebler, H. Mantler, and M. Wiesemann, *Distributions for neutral Higgs production in the NMSSM*, arXiv:1608.02949.

[217] K. Melnikov and A. Penin, *On the light quark mass effects in Higgs boson production in gluon fusion*, JHEP **05** (2016) 172, [arXiv:1602.09020].

[218] K. Melnikov, L. Tancredi, and C. Wever, *Two-loop $gg \to Hg$ amplitude mediated by a nearly massless quark*, JHEP **11** (2016) 104, [arXiv:1610.03747].

[219] K. Melnikov, L. Tancredi, and C. Wever, *Two-loop amplitudes for $qg \to Hq$ and $q\bar{q} \to Hg$ mediated by a nearly massless quark*, Phys. Rev. **D95** (2017), no. 5 054012, [arXiv:1702.00426].

[220] J. M. Lindert, K. Melnikov, L. Tancredi, and C. Wever, *Top-bottom interference effects in Higgs plus jet production at the LHC*, Phys. Rev. Lett. **118** (2017), no. 25 252002, [arXiv:1703.03886].

[221] F. Maltoni, K. Mawatari, and M. Zaro, *Higgs characterisation via vector-boson fusion and associated production: NLO and parton-shower effects*, Eur. Phys. J. **C74** (2014), no. 1 2710, [arXiv:1311.1829].

[222] F. Demartin, F. Maltoni, K. Mawatari, B. Page, and M. Zaro, *Higgs characterisation at NLO in QCD: CP properties of the top-quark Yukawa interaction*, Eur. Phys. J. **C74** (2014), no. 9 3065, [arXiv:1407.5089].

[223] F. Demartin, F. Maltoni, K. Mawatari, and M. Zaro, *Higgs production in association with a single top quark at the LHC*, Eur. Phys. J. **C75** (2015), no. 6 267, [arXiv:1504.00611].

[224] F. Demartin, E. Vryonidou, K. Mawatari, and M. Zaro, *Higgs characterisation: NLO and parton-shower effects*, in HPNP2015, Japan, 2015, 2015. arXiv:1505.07081.

[225] **ATLAS, CMS** Collaboration, X. Chen, *Prospects for Higgs CP property measurements at the LHC*, in LCWS2016: Japan, December, 2016, 2017. arXiv:1703.07675.

[226] A. Alloul, N. D. Christensen, C. Degrande, C. Duhr, and B. Fuks, *FeynRules 2.0 - A complete toolbox for tree-level phenomenology*, Comput. Phys. Commun. **185** (2014) 2250–2300, [arXiv:1310.1921].

[227] A. Alloul, B. Fuks, and V. Sanz, *Phenomenology of the Higgs Effective Lagrangian via FEYNRULES*, JHEP **04** (2014) 110, [arXiv:1310.5150].

[228] K. Mimasu, V. Sanz, and C. Williams, *Higher Order QCD predictions for Associated Higgs production with anomalous couplings to gauge bosons*, JHEP **08** (2016) 039, [arXiv:1512.02572].

[229] C. Degrande, B. Fuks, K. Mawatari, K. Mimasu, and V. Sanz, *Electroweak Higgs boson production in the standard model effective field theory beyond leading order in QCD*, Eur. Phys. J. **C77** (2017), no. 4 262, [arXiv:1609.04833].

[230] C. Degrande, N. Greiner, W. Kilian, O. Mattelaer, H. Mebane, T. Stelzer, S. Willenbrock, and C. Zhang, *Effective Field Theory: A Modern Approach to Anomalous Couplings*, Annals Phys. **335** (2013) 21–32, [arXiv:1205.4231].

[231] R. Edezhath, *Dimension-6 Operator Constraints from Boosted VBF Higgs*, arXiv:1501.00992.

[232] G. Brooijmans et al., *Les Houches 2015: Physics at TeV colliders - new physics working group report*, arXiv:1605.02684.

[233] R. V. Harlander, S. Liebler, and H. Mantler, *SusHi Bento: Beyond NNLO and the heavy-top limit*, Comput. Phys. Commun. **212** (2017) 239–257, [arXiv:1605.03190].

[234] C. Anastasiou, C. Duhr, F. Dulat, E. Furlan, T. Gehrmann, F. Herzog, A. Lazopoulos, and B. Mistlberger, *CP-even scalar boson production via gluon fusion at the LHC*, JHEP **09** (2016) 037, [arXiv:1605.05761].

[235] C. Grojean, E. Salvioni, M. Schlaffer, and A. Weiler, *Very boosted Higgs in gluon fusion*, JHEP **05** (2014) 022, [arXiv:1312.3317].

[236] A. Azatov and A. Paul, *Probing Higgs couplings with high p_T Higgs production*, JHEP **01** (2014) 014, [arXiv:1309.5273].

[237] U. Langenegger, M. Spira, and I. Strebel, *Testing the Higgs Boson Coupling to Gluons*, arXiv:1507.01373 (2015) [arXiv:1507.01373].

[238] R. V. Harlander and T. Neumann, *Probing the nature of the Higgs-gluon coupling*, Phys. Rev. **D88** (2013) 074015, [arXiv:1308.2225].

[239] S. Dawson, I. M. Lewis, and M. Zeng, *Effective field theory for Higgs boson plus jet production*, Phys. Rev. **D90** (2014), no. 9 093007, [arXiv:1409.6299].

[240] A. Azatov, C. Grojean, A. Paul, and E. Salvioni, *Resolving gluon fusion loops at current and future hadron colliders*, JHEP **09** (2016) 123, [arXiv:1608.00977].

[241] D. Choudhury and P. Saha, *Higgs production as a probe of anomalous top couplings*, JHEP **08** (2012) 144, [arXiv:1201.4130].

[242] C. Degrande, J. M. Gerard, C. Grojean, F. Maltoni, and G. Servant, *Probing Top-Higgs Non-Standard Interactions at the LHC*, JHEP **07** (2012) 036, [arXiv:1205.1065]. [Erratum: JHEP03,032(2013)].

[243] C. Zhang, *Automating Predictions for Standard Model Effective Field Theory in MadGraph5 aMC@NLO*, PoS **RADCOR2015** (2016) 101, [arXiv:1601.03994].

[244] F. Maltoni, E. Vryonidou, and C. Zhang, *Higgs production in association with a top-antitop pair in the Standard Model Effective Field Theory at NLO in QCD*, JHEP **10** (2016) 123, [arXiv:1607.05330].

[245] N. Deutschmann, C. Duhr, F. Maltoni, and E. Vryonidou, *Gluon-fusion Higgs production in the Standard Model Effective Field Theory*, JHEP **12** (2017) 063, [arXiv:1708.00460].

[246] C. Zhang, *NLO predictions for SMEFT in the top-quark sector*, PoS **ICHEP2016** (2016) 659, [arXiv:1611.05091].

[247] A. Azatov, R. Contino, G. Panico, and M. Son, *Effective field theory analysis of double Higgs boson production via gluon fusion*, Phys. Rev. **D92** (2015), no. 3 035001, [arXiv:1502.00539].

[248] R. Grober, M. Muhlleitner, M. Spira, and J. Streicher, *NLO QCD Corrections to Higgs Pair Production including Dimension-6 Operators*, JHEP **09** (2015) 092, [arXiv:1504.06577].

[249] D. de Florian, I. Fabre, and J. Mazzitelli, *Higgs boson pair production at NNLO in QCD including dimension 6 operators*, JHEP **10** (2017) 215, [arXiv:1704.05700].

[250] Y. T. Chien, V. Cirigliano, W. Dekens, J. de Vries, and E. Mereghetti, *Direct and indirect constraints on CP-violating Higgs-quark and Higgs-gluon interactions*, JHEP **02** (2016) 011, [arXiv:1510.00725].

[251] D. Buarque Franzosi and C. Zhang, *Probing the top-quark chromomagnetic dipole moment at next-to-leading order in QCD*, Phys. Rev. **D91** (2015), no. 11 114010, [arXiv:1503.08841].

[252] G. Altarelli and G. Parisi, *Asymptotic Freedom in Parton Language*, Nucl. Phys. **B126** (1977) 298–318.

[253] P. Nogueira, *Automatic Feynman graph generation*, J. Comput. Phys. **105** (1993) 279–289.

[254] J. A. M. Vermaseren et al., FORM, , https://www.nikhef.nl/~form/maindir/maindir.html.

[255] Wolfram Research, MATHEMATICA, , https://www.wolfram.com/mathematica/.

[256] G. Passarino and M. J. G. Veltman, *One Loop Corrections for e+ e- Annihilation Into mu+ mu- in the Weinberg Model*, Nucl. Phys. **B160** (1979) 151–207.

[257] Maplesoft, MAPLE, , https://www.maplesoft.com/products/Maple/.

[258] R. Mertig, M. Bohm, and A. Denner, *FEYN CALC: Computer algebraic calculation of Feynman amplitudes*, Comput. Phys. Commun. **64** (1991) 345–359.

[259] V. Shtabovenko, R. Mertig, and F. Orellana, *New Developments in FeynCalc 9.0*, Comput. Phys. Commun. **207** (2016) 432–444, [arXiv:1601.01167].

[260] M. Spira, *Radiative QCD corrections to decay and production of Higgs bosons at e+e- and pp accelerators. (In German)*, , PhD thesis, Aachen, Tech. Hochsch., 1993.

[261] G. Bozzi, S. Catani, D. de Florian, and M. Grazzini, *The q(T) spectrum of the Higgs boson at the LHC in QCD perturbation theory*, Phys. Lett. **B564** (2003) 65–72, [hep-ph/0302104].

[262] D. de Florian, G. Ferrera, M. Grazzini, and D. Tommasini, *Transverse-momentum resummation: Higgs boson production at the Tevatron and the LHC*, JHEP **11** (2011) 064, [arXiv:1109.2109].

[263] M. Spira, *HIGLU: A program for the calculation of the total Higgs production cross-section at hadron colliders via gluon fusion including QCD corrections*, arXiv:hep-ph/9510347 (1995) [hep-ph/9510347].

[264] S. Catani and M. Grazzini, *An NNLO subtraction formalism in hadron collisions and its application to Higgs boson production at the LHC*, Phys. Rev. Lett. **98** (2007) 222002, [hep-ph/0703012].

[265] M. Grazzini, *NNLO predictions for the Higgs boson signal in the $H \to WW \to lnu\ lnu$ and $H \to ZZ \to 4l$ decay channels*, JHEP **02** (2008) 043, [arXiv:0801.3232].

[266] S. Catani, L. Cieri, D. de Florian, G. Ferrera, and M. Grazzini, *Universality of transverse-momentum resummation and hard factors at the NNLO*, Nucl. Phys. **B881** (2014) 414–443, [arXiv:1311.1654].

[267] J. Butterworth et al., *PDF4LHC recommendations for LHC Run II*, J. Phys. **G43** (2016) 023001, [arXiv:1510.03865].

[268] **NNPDF** Collaboration, R. D. Ball et al., *Parton distributions for the LHC Run II*, JHEP **04** (2015) 040, [arXiv:1410.8849].

[269] S. Dulat, T.-J. Hou, J. Gao, M. Guzzi, J. Huston, P. Nadolsky, J. Pumplin, C. Schmidt, D. Stump, and C. P. Yuan, *New parton distribution functions from a global analysis of quantum chromodynamics*, Phys. Rev. **D93** (2016), no. 3 033006, [arXiv:1506.07443].

[270] L. A. Harland-Lang, A. D. Martin, P. Motylinski, and R. S. Thorne, *Parton distributions in the LHC era: MMHT 2014 PDFs*, Eur. Phys. J. **C75** (2015), no. 5 204, [arXiv:1412.3989].

[271] J. Gao and P. Nadolsky, *A meta-analysis of parton distribution functions*, JHEP **07** (2014) 035, [arXiv:1401.0013].

[272] S. Carrazza, S. Forte, Z. Kassabov, J. I. Latorre, and J. Rojo, *An Unbiased Hessian Representation for Monte Carlo PDFs*, Eur. Phys. J. **C75** (2015), no. 8 369, [arXiv:1505.06736].

[273] E. Bagnaschi, R. V. Harlander, H. Mantler, A. Vicini, and M. Wiesemann, *Resummation ambiguities in the Higgs transverse-momentum spectrum in the Standard Model and beyond*, JHEP **01** (2016) 090, [arXiv:1510.08850].

[274] E. Bagnaschi and A. Vicini, *The Higgs transverse momentum distribution in gluon fusion as a multiscale problem*, JHEP **01** (2016) 056, [arXiv:1505.00735].

[275] B. Dumont, S. Fichet, and G. von Gersdorff, *A Bayesian view of the Higgs sector with higher dimensional operators*, JHEP **07** (2013) 065, [arXiv:1304.3369].

[276] A. Falkowski, *Effective field theory approach to LHC Higgs data*, Pramana **87** (2016), no. 3 39, [arXiv:1505.00046].

[277] A. Butter, O. J. P. Eboli, J. Gonzalez-Fraile, M. C. Gonzalez-Garcia, T. Plehn, and M. Rauch, *The Gauge-Higgs Legacy of the LHC Run I*, JHEP **07** (2016) 152, [arXiv:1604.03105].

[278] U. Langenegger, M. Spira, A. Starodumov, and P. Trueb, *SM and MSSM Higgs Boson Production: Spectra at large transverse Momentum*, JHEP **06** (2006) 035, [hep-ph/0604156].

[279] D. de Florian, G. Ferrera, M. Grazzini, and D. Tommasini, *Higgs boson production at the LHC: transverse momentum resummation effects in the H->2gamma, H->WW->lnu lnu and H->ZZ->4l decay modes*, JHEP **06** (2012) 132, [arXiv:1203.6321].